The effects of ultrasound on the cells of the vascular wall

Submitted by **Eleanor Martin**, to the University of Exeter as a thesis for the degree of Doctor of Philosophy in Physics, June 2010

I certify that all material in this thesis which is not my own work has been identified and that no material has been previously submitted and approved for the award of a degree by this or any other University.

(Signature) ………………………………………………………………………………………

Abstract

Investigations into the safety of diagnostic ultrasound and mechanisms of therapeutic ultrasound have provided evidence of a number of cellular responses to ultrasound. These studies have mainly concentrated on cells in culture, while work on intact tissue employed mainly kHz ultrasound fields, although diagnostic and many therapeutic procedures are performed using MHz ultrasound. Vascular tissue is known to respond to a variety of physical and chemical signals, and so arteries were used as a model system in this thesis to study the effects of MHz ultrasound *in vitro*.

Rings of equine carotid and lateral cecal mesenteric artery exhibited reversible, repeatable contraction on exposure to both pulsed and continuous wave 3.2 MHz ultrasound at acoustic powers up to 145 mW. Wall stress increased by up to 1.5% in carotid arteries and up to 2% in mesenteric arteries during exposure, and returned to basal levels after approximately 10 minutes. Contraction was endothelium independent, and was not affected by changes in the pulsing regime. The magnitude of contraction was dependent on the acoustic power, and the change in wall stress increased with increasing acoustic power in a linear fashion. The acoustic power dependence suggested the response was thermally mediated and this was confirmed by investigation of the response of arteries to non ultrasound generated heating, which also induced contraction. The effects of ultrasound and heating were also investigated in 1st order branches of the lateral cecal artery, as a model of a small artery. No response was observed in either case.

In order to determine the cellular basis of the response of carotid and mesenteric arteries, the involvement of potassium ion channels in the response was investigated using a potassium channel blocker. The response of arteries to ultrasound was increased by inhibition of inward-rectifier potassium channels, which would otherwise help to return the cell membrane potential to the normal level. The change in wall stress was increased by 42% on average, confirming the involvement of these channels in the response. Contraction of arteries is mediated by an increase in intracellular calcium. The ion channel activity during non ultrasound generated heating was examined further by observation of intracellular calcium concentration using a fluorescent calcium sensitive dye. Increases in intracellular calcium were observed in carotid and large mesenteric arteries, which confirmed the thermal influence on ion channel function in these vessels. No such effect was observed in the smaller vessels.

Acknowledgements

Throughout my PhD I have gratefully received the help and support of a number of people: colleagues, friends and family alike. Among those who have lent me such invaluable support, several deserve special mention. My supervisors, Peter Winlove here in Exeter and Francis Duck in Bath, deserve special thanks for all their enthusiasm and excellent guidance. Within the Biomedical Physics group of Exeter, the technical support staff have been a marvelous resource. Ellen Green has given me endless help with a huge range of things in the lab; none of us would get very far without her. Many thanks also go to Dick for the help he cheerfully gave in the earlier stages of this project. Dave Colridge deserves mention for lending me allsorts of bits and pieces without getting too annoyed, and for nursing my computer back to health. I would like to acknowledge Kenton Arkill for his help, discussion, hair and company at the abattoir, Hayley Kyte at the Peninsular Medical School for advice on myography systems and much else besides, and Jackie Whatmore for advice on buffer recipes.

Other marvelous members of the Physics department, such as Steve, Matt, Kevin, and Nick in the workshop deserve my everlasting gratitude for helping with the design and for building my equipment. John Meakin will always have my thanks for sorting out the abattoir bus, and being a source of everything. Thanks also to the men of Potter's abattoir in Taunton for making my frequent trips more pleasant, their knowledge of horse anatomy and skill with knives …. !

I would like to thank the other members of the biophysics group for being a supportive and enjoyable bunch of people to work with. There are too many to mention individually, but of the group Natalie and James in particular receive many thanks for fun and encouragement, and Jess and Rachel for making the abattoir trips more like a chance to gossip and less like a horror movie. I would also like to mention my flatmate and friend, Rachel, and Dan, Neda, Saminder and my family for constant moral support and relaxation.

I couldn't have done this without you all!

Table of Contents

List of figures

List of tables

Glossary of abbreviations

ΔT	Change in temperature
AIUM	American Institute of Ultrasound in Medicine
ATP	Adenosine triphosphate
$BaCl_2$	Barium chloride
CW	Continuous wave
DMSO	Dimethyl sulfoxide
EDHF	Endothelium derived hyperpolarising factor
FDA	Food and Drug Administration
I_{SPPA}	Spatial-peak pulse-average acoustic intensity
I_{SPTA}	Spatial-peak temporal-average acoustic intensity
LIPUS	Low intensity pulsed ultrasound
MI	Mechanical Index
NEMA	National Electrical Manufacturer's Association
NO	Nitric oxide
Np	Nepers
p_-	Peak negative acoustic pressure
p_+	Peak positive acoustic pressure
PVDF	Polyvinylidene fluoride
ROS	Reactive oxygen species
TI	Thermal Index
TPx	Polymethylpentene
TTO	Thermal Test Object
US	Ultrasound
VEGF	Vascular endothelial growth factor

1 Introduction

This thesis is concerned with the effects of ultrasound at low MHz frequency and at diagnostic acoustic intensity levels on large conducting and small resistance blood vessels *in vitro*. Preliminary results (R E Ellis, unpublished data, School of Physics, University of Exeter) showed evidence of ultrasound induced contraction in a carotid artery ring *in vitro*. The experiments described in this thesis were designed to investigate this effect further, aiming to establish the mechanism of interaction of the ultrasound with the tissue and the cellular mechanisms underlying the response. This involved investigation of the effects of varying ultrasound exposure parameters on the measured responses and investigations of the ion channel activity during the response. The responses of different types of blood vessels were investigated to determine the effects of ultrasound on different parts of the vascular system, where structure and function may vary. In this introduction, the relevance of this investigation is outlined in light of the current, widespread use of medical ultrasound for diagnostic purposes and the use of ultrasound for an increasing variety of therapeutic applications.

Ultrasound is employed widely for clinical diagnostic uses including obstetrics, cardiology and vascular studies and is generally accepted as a safe and versatile modality for medical imaging. It is also widely used for therapeutic applications such as physiotherapy. Extracorporeal shock-wave lithotripsy is often the treatment of choice for renal calculi, and the use of high intensity focused ultrasound (HIFU) is being developed in minimally invasive surgery and for cancer treatment. Ultrasound is increasingly used as an agent to accelerate bone, tendon and soft tissue healing. Efforts to assess the safety of these procedures and to understand the mechanisms responsible for therapeutic effects have demonstrated a number of non-lethal cellular responses to ultrasound in cells in culture, *ex vivo* tissue models, *in vivo* animal models and clinical models. At low intensities, these include increased proliferation of some cell types, altered gene expression, increased protein synthesis, changes related to cell signalling and changes in vascular tone (e.g. Korstjens et al. 2008; Lu et al. 2009). At

the higher acoustic intensities and pressures used for HIFU, sonoporation and drug delivery, changes in cell permeability and cell death can be induced (ter Haar 2007).

Relatively little is known about the effects of low-power ultrasound in intact tissues; most of the observations mentioned above have been made on cells in culture. The work presented in this thesis reports such investigations on arteries *in vitro*, chosen for study because the vascular system is known to be responsive to physical and chemical signals and is therefore likely to be sensitive to ultrasonic stimuli. Responses of the vascular system could lead directly to therapeutic or pathological effects as many processes are regulated by blood flow. A number of studies have shown that ultrasound at low frequencies can cause changes in vascular tone and whole tissue effects (e.g. Steffen et al. 1994; Suchkova et al. 2000).

The effective functioning of the circulation depends critically on changes in vascular tone which regulate local and systemic blood flow and tissue nutrition. Vascular tone is determined by a complex interplay between the endothelial cells lining the vessel wall and the smooth muscle cells of the underlying tissue that facilitate the response. The cellular interaction depends on a wide range of signals, including cytokines such as nitric oxide and free radicals that can be exchanged between the two cell populations, and also on mechanical and fluid mechanical forces that are transduced mainly by the endothelial cells. Studies on isolated cells have already demonstrated that ultrasound stimulates the release of cytokines (Saito et al. 2004; Lu et al. 2008). It is also possible that endothelial cells can sense directly the effects of ultrasound-induced cavitation and streaming and the resulting fluid shear stress (VanBavel 2007).

Ultrasound bioeffects are mainly classed as thermal (temperature rise $\Delta T > 1\text{-}2$ °C) or non-thermal ($\Delta T < 1\text{-}2$ °C). Most work on non-thermal bioeffects has focussed on cavitation and microbubbles and investigation of the significance of free radicals. However, there may also be other non-thermal bioeffects where cavitation is not present. Cells may respond directly to the mechanical forces produced by acoustic fields. Mechanical forces exerted on vascular cells are important in both the short term, in producing changes in vessel diameter that regulate blood flow, and the long term, in the growth and development of blood vessels and in the development of disease. The influence of small transient thermal changes on the function of cells and tissues has not been thoroughly investigated, and in many studies thermal

mechanisms are ignored when the temperature rise is less than 1 or 2 ℃. There is evidence that temperature changes of less than 1 ℃ can elicit a response in cells and tissues (e.g. Wang et al. 1991; Morrissey et al. 2009).

These findings suggest the need for further investigation of the bioeffects of ultrasound, especially the more subtle and transient effects, which may be associated with ultrasound intensities within the diagnostic range. The research presented here spans some of the areas discussed above, examining the transient effects of low acoustic intensity ultrasound at the tissue and cellular level.

In Chapter 2, the context of this research is described in terms of current literature on bioeffects of low acoustic intensity ultrasound for both therapeutic purposes and for safety. This chapter also reviews the theory and literature concerning the underlying physics, the mechanisms of interaction of ultrasound and resulting bioeffects and safety issues. Relevant literature and theory from the tissue and cellular perspective, which examines the structure and function of blood vessels and the cells within, their mechanical properties, and mechanisms of physical force sensing in these cells and the transduction of these signals is also reviewed. In Chapter 3, the experimental design process and development of equipment is described, and the ultrasound field characterisation and associated measurement techniques are presented. In Chapter 4, the results of the experiments are presented, beginning first with characterisation of the response in carotid and lateral cecal mesenteric arteries in terms of the acoustic power, pulse regime and endothelial dependence. The thermal interaction with the tissue is also studied. Chapter 5 describes similar experiments performed on first order branches from the lateral cecal artery as a model of a small artery. Chapter 6 describes experiments performed on both large and small arteries in order to investigate the involvement of ion channel activity in the cell membrane in the response to ultrasound. This is followed in Chapter 7 by a general discussion of all the results from this study and conclusions, together with suggestions for further work.

2 Background and supporting literature

In this chapter, the theory underlying the aspects of ultrasound and physiology relevant to this thesis is discussed. The literature concerning the bioeffects of ultrasound on tissues and cells is then reviewed, along with the cellular basis of the interaction between physical stimuli and cells.

2.1 Ultrasound and its interaction with soft tissue

Ultrasound is characterised as sound at frequencies above 20 kHz. Diagnostic ultrasound usually employs frequencies from 2 to 15 MHz and above depending on the depth of penetration and spatial resolution required. For therapeutic applications both kHz and MHz frequencies are employed. This chapter will focus on applications of MHz ultrasound with brief discussion of relevant literature concerning kHz ultrasound and its effects on the vasculature. First, the underlying physics of ultrasound as it relates to this thesis is outlined.

2.1.1 Physics of ultrasound

Ultrasound propagates through a medium such as soft tissue as longitudinal waves by the displacement of particles, u. The oscillations of the particles in the wave obey the wave equation

$$\frac{\partial^2 u}{\partial z^2} = \frac{1}{c^2}\frac{\partial^2 u}{\partial t^2},$$

2.1

where z is the distance in the direction of wave propagation and c is the wave velocity, i.e. the speed of sound. This has the general solution

$$u = u_0 \sin(\omega t - \phi)$$

2.2

$$= u_0 \sin\left[\frac{2\pi}{\lambda}(ct - z)\right].$$ 2.3

The displacement of the particles at time t is u, the maximum displacement of particles is u_0, the angular frequency $\omega = 2\pi f$, the phase angle $\phi = kz$, and the wave number $k = \frac{2\pi}{\lambda}$. During compressions and rarefactions, the particles oscillate about a fixed position, and so the pressure oscillates about the ambient pressure. This is the acoustic pressure, p which can be described by

$$p = -\rho c^2 \frac{\partial u}{\partial z},$$ 2.4

where ρ is the density of the medium. By differentiating Equation 2.3 with respect to z, and substituting into Equation 2.4, the acoustic pressure can be written as

$$p = \rho c v$$ 2.5

$$= \rho c\, u_0 \omega \cos(\omega t - \phi).$$ 2.6

A more complete derivation can be found in Wells (1977). The peak values of the acoustic pressure are of interest in acoustic output measurements and in the context of ultrasound safety. The peak rarefactional pressure or peak negative acoustic pressure is the greatest value of acoustic pressure below the ambient level. The peak compression pressure or peak positive pressure is the greatest value above the ambient pressure.

Where plane-wave conditions may be assumed, the acoustic intensity is proportional to the pressure squared and can be calculated from the acoustic pressure via the pulse intensity integral. The pulse intensity integral, Φ is calculated by integrating the square of the acoustic pressure, p, over a time which spans the whole pulse, T.

$$\Phi = \frac{1}{\rho c} \int_0^T p^2\, dt,$$ 2.7

where ρ is the density of the medium and c is speed of sound in the medium. For a continuous wave beam, the spatial-peak temporal-average intensity,

$$I_{SPTA} = \frac{p^2}{2\rho c}.$$ 2.8

For pulsed beams, I_{SPTA} is the pulse intensity integral divided by the pulse repetition period. The spatial-peak pulse-average intensity, I_{SPPA}, is calculated from the pulse intensity integral divided by the pulse duration, T, and

$$T = 1.25(t_2 - t_1), \qquad\qquad 2.9$$

where t_1 and t_2 are the times at which the pressure squared integral equals 10% and 90% of the total value.

Attenuation of ultrasound

As ultrasound propagates through tissue it is attenuated by absorption as well as scattering, depending on properties of the tissue and the frequency of the ultrasound. For a plane single frequency sound wave, the attenuation may also be given in terms of the change in acoustic pressure through a medium:

$$p_z = p_0 e^{-\alpha z}, \qquad\qquad 2.10$$

where p_0 is the initial acoustic pressure amplitude, p_z is the acoustic amplitude of the wave after it has travelled a distance z through the medium and α is the amplitude attenuation coefficient of the medium in Np cm^{-1}. Attenuation is described in terms of the acoustic intensity as

$$I = I_0 e^{-2\alpha z}, \qquad\qquad 2.11$$

where I_0 is the initial acoustic intensity and I is the acoustic intensity of the wave at distance z.

Attenuation occurs by both absorption of energy along the beam path and by scattering of energy out of the beam. The amplitude attenuation coefficient is the sum of the scattering coefficient, α_s and the absorption coefficient, α_a:

$$\alpha = \alpha_s + \alpha_a. \qquad\qquad 2.12$$

The attenuation in tissue depends on frequency in an approximately linear fashion and attenuation coefficients are often given in terms of dB cm^{-1} MHz^{-1} or in nepers cm^{-1} at a particular frequency. For soft tissue, the attenuation coefficient is often taken as 0.5 dB cm^{-1} MHz^{-1}. For soft tissue, evidence suggests that at frequencies in the low MHz range, attenuation is primarily due to absorption, and scattering accounts for a

relatively small proportion of the attenuation (Docker and Duck 1991). On a small scale, scatter occurs where reflectors are smaller than the wavelength of the ultrasound. Energy is scattered off the beam axis and the beam is attenuated. Absorption occurs by conversion of energy from the ultrasound beam into heat as it propagates through a medium. In fluids, there are frictional forces that act to oppose the motion of the particles in the medium due to the ultrasound wave. On a molecular scale, pressure fluctuations can affect tissue; the resulting compression and relaxation of molecular structures after the passage of an ultrasonic wave removes energy from the beam and converts it to heat.

The rate of energy deposition or heat production per unit volume is

$$\frac{dQ}{dt} = 2\alpha_a I \, , \qquad\qquad 2.13$$

where Q is the energy, t is time, α_a is the amplitude absorption coefficient and I is the acoustic intensity. The rate of energy deposition will vary spatially. The absorption coefficient will vary with the tissue properties and with inhomogeneities within tissues, ranging from approximately 0.1 nepers cm^{-1} at 5 MHz in blood, and 0.17 to 0.57 nepers cm^{-1} in the liver at 5 MHz (Duck 1990). The pattern of energy deposition also depends on the acoustic intensity profile of the beam; for a tightly focused beam with a small, high acoustic intensity focus, energy deposition may be quite localised.

The acoustic dose rate, i.e. the rate of energy absorption per unit mass of a medium has been defined by Duck (2009) as

$$Q_m = \frac{2\alpha_a I}{\rho_0} \, , \qquad\qquad 2.14$$

where ρ_0 is the density of the medium. Therefore, the total energy deposited per unit mass of a medium in a given time, t, is

$$\Phi = \frac{2\alpha_a I t}{\rho_0} \, . \qquad\qquad 2.15$$

The acoustic dose rate is then analogous to the Specific Absorption Rate used to quantify exposure to non ionising electromagnetic radiation, and the acoustic dose is analogous to radiation dose used for ionising radiation.

The initial rate of temperature increase is dependent only on the heat capacity of the medium, C and the acoustic dose rate:

$$\frac{dT}{dt} = \frac{2\alpha_a I}{\rho_0 C} = \frac{Q_m}{C}.$$

2.16

After the initial temperature rise, the heating depends on the beam width; for a given acoustic intensity, the rate of heating will be greater in a broader beam. The steady state temperature that is reached depends on the thermal conductivity of the tissue and on heat loss due to blood flow, which can have a significant effect on the temperature. The Thermal Index discussed later gives an indication of this temperature increase.

Nonlinear propagation

In part of this study, relatively high acoustic pressures are employed. For this reason it is important to consider nonlinear effects when discussing ultrasound propagation through a medium. In the range of acoustic pressures encountered in diagnostic ultrasound, as a sinusoidal wave propagates through a medium, its shape changes possibly producing shock fronts (Duck and Starritt 1984). The compressions catch up with the rarefactions travelling in front of them, eventually forming a shock front or discontinuity in acoustic pressure. Thus, whilst a pulse near to the transducer will have sinusoidal type oscillations, as the pulse travels further from the transducer, the pulse shape will be distorted and the increases in acoustic pressure will become more rapid, eventually forming a discontinuity. The degree of nonlinearity depends on several factors and is described by the nonlinear propagation or shock factor:

$$\sigma = \varepsilon \kappa \beta z,$$

2.17

where β is the coefficient of nonlinearity of the medium and z is the distance travelled through the medium. The acoustic Mach number, $\varepsilon = \frac{v_0}{c_0}$ where v_0 is particle velocity at the source and c_0 is the wave speed. Equation 2.5 showed that acoustic pressure is proportional to particle velocity, so this term gives a linear dependence of nonlinearity on acoustic pressure. The wave number, $\kappa = \frac{2\pi}{\lambda} = \frac{2\pi f}{c_0}$ so there is also a linear dependence on the frequency of the ultrasound wave (Duck 2002).

Nonlinear propagation causes a change in the frequency content of the ultrasound as energy is transferred to the harmonic frequencies. Absorption of the ultrasound energy increases with frequency so the harmonic components will be more strongly absorbed as they propagate through the medium. This change in absorption has two consequences: the amount of energy deposited in the tissue will increase due to absorption of the higher frequency components and more energy will be deposited along the beam path. In a situation such as that in this study, where a section of tissue is placed in liquid at the focal region, the energy deposited in the water path due to nonlinearity will result in a lower acoustic intensity at the tissue. It is not known exactly how these factors will affect the acoustic dose rate; the two effects may cancel each other out to a degree.

2.1.2 Mechanisms of ultrasound interaction

In this section, the mechanisms of interaction of ultrasound with tissue are outlined. They will be discussed in relation to the results of this study and their involvement in the responses measured here will be investigated.

The mechanisms of ultrasound interaction with tissue can be thermal or mechanical in nature. Thermal interaction depends on the acoustic power in the beam, as well as acoustic properties of the tissue. Mechanical interaction depends on acoustic pressure. The principles of these interaction mechanisms are described here. Interaction mechanisms classed as non-thermal and non-cavitational are also described.

Thermal effects

Heating caused by absorption of ultrasound in soft tissue and bone, and the resulting thermal bioeffects, are related to the acoustic power and beam width. The potential for thermal bioeffects is represented by the Thermal Index,

$$TI = \frac{W_p}{W_{deg}},$$

2.18

where W_p is the beam power and W_{deg} is the estimated acoustic power needed to raise the temperature of the tissue by 1°C under steady state worst case conditions (NCRP 1992). The quantity W_{deg} depends on acoustic properties of the tissue at a particular frequency and the ultrasonic beam structure. Cell death is likely above 43°C, a temperature increase of 6°C above core body temperature (O'Brien 2007). Increases

in temperature will affect cellular biochemistry, causing increased reaction rates. When the temperature rise is sufficient, enzymes will begin to break down, proteins in the cell will denature and the cell will cease to function normally. Damage to cells has been observed after prolonged periods at temperatures of 39 to 43 ℃. Above this temperature the time taken to cause damage halves for every degree of temperature rise. Lower temperature rises for sustained periods can also cause damage, especially to sensitive tissues such as foetal tissue. It is possible that smaller temperature rises for short periods may cause transient effects in cells and tissues; this possibility will be explored further later in this chapter.

On a larger scale, increases in the core body temperature by several degrees in several species of pregnant animals induced brain disorders among other defects in the foetus (Miller and Ziskin 1989). Users of diagnostic ultrasound equipment are provided with the Thermal Index as an indicator of the possible temperature rise during exposure. The Food and Drug Administration (FDA) (1997) states that a Thermal Index of 6 must not be exceeded without justification. This suggests that diagnostic ultrasound equipment may be being used in a way that could produce temperature rises of up to 6°C.

Mechanical effects

Where a medium is subjected to high acoustic pressures, large mechanical forces act on particles in the beam. The potential for mechanical bioeffects mediated by cavitation may be estimated by the Mechanical Index, *MI*, which is defined as:

$$MI = \frac{p_{-(derated)}}{\sqrt{f}}, \qquad\qquad 2.19$$

where $p_{-(derated)}$ is the value of the peak negative acoustic pressure attenuated from values measured in water to represent *in situ* levels and f is the centre frequency of the transducer (Apfel and Holland 1991). This quantity is most relevant where there is gas present in the field, making cavitation likely, for example when contrast agents are used. Cavitation is unlikely under diagnostic exposure conditions when there is no gas present. The FDA (1997) places a limit of 1.9 on the Mechanical Index for medical diagnostic equipment except for ophthalmology where the limit is 0.23.

The presence of gas bubbles and high acoustic pressures can lead to cavitation and the generation of free radicals due to bubble collapse (Edmonds and Sancier 1983; Takahashi et al. 2007). The peak rarefactional pressure threshold for inertial cavitation with spontaneous nucleation in tissue, i.e. with no bubbles present, is of the order of 4 MPa (Church 2002). There are two types of cavitation; inertial (collapse) and non-inertial (stable) cavitation. Non-inertial cavitation is the stable oscillation of microbubbles in an acoustic field where the inertia is not high enough to cause bubble collapse. Inertial cavitation is the growth and collapse of bubbles within a few cycles of an acoustic wave, where the bubbles are short lived and collapse is violent. Under these conditions, encapsulated microbubble contrast agents and free gas bubbles can expand and then collapse, generating high temperatures and free radicals.

Bioeffects attributed to cavitation have been observed in cells and tissues. Ultrasound exposure in the presence of a microbubble contrast agent caused cell membrane damage, which increased with increasing acoustic pressure amplitude (Miller 1998). It has been shown by Miller and Qudus (2000) that ultrasound exposure in the presence of contrast agents induces petechial haemorrhages (capillary rupture) in mouse intestine and abdominal muscle. It has been observed that the increase in extracellular reactive oxygen species production associated with collapse cavitiation, caused by exposure to 1.6 MHz ultrasound can lead to DNA laddering i.e. cell damage and ultimately cell death (Basta et al. 2003). There is also evidence that inertial cavitation causes damage to vascular endothelial cells (Hwang et al. 2006).

Non-thermal non-cavitational effects

Radiation stress is classed as a non-thermal, non-cavitational interaction mechanism exerted when an ultrasound beam passes through a medium. The resulting forces can be observed through acoustic streaming. When an ultrasound beam is incident on an absorbing or reflecting solid surface, a force is exerted on that surface. The magnitude of this force depends on the properties of both the surface and the beam. The local stresses depend on the ratio of the acoustic intensity in the beam to the velocity of the sound in the medium, i.e. the energy density, $\frac{I}{c}$.

In a three dimensional medium, a force in the direction of propagation of the ultrasound wave is generated as energy is deposited in the medium by absorption. Radiation stress is the force per unit area acting at a point in a plane. For a plane

wave, the local radiation stress gradient is $\frac{2\alpha I}{c}$, where α is the absorption coefficient, I is the acoustic intensity at the point and c is the speed of sound in the medium. Therefore, the local radiation stress gradient varies with these quantities throughout the medium. If the surface is perfectly absorbing then the radiation pressure at a point is the ratio of acoustic intensity at that point to the speed of sound in the medium.

Acoustic streaming is a bulk movement of fluid in the direction of propagation of the beam. It can be generated due to the stress field produced in water as an ultrasound beam passes through. The flow velocity of the stream is proportional to the acoustic intensity and radius of the beam and the amplitude attenuation coefficient of the fluid. The maximum velocity of the stream is limited by viscous forces in the fluid and by the geometrical constraints of the containing vessel. At the boundary of a fluid stream, shear stress will be exerted. Streaming will be enhanced where there is strong nonlinear propagation due to increased absorption of the higher frequency components. Streaming has been observed in water insonated with pulsed diagnostic ultrasound fields (ter Haar and Duck 2000).

In tissue, radiation stresses are exerted by the propagation of an ultrasound beam, but streaming is not set up as in fluid. Radiation stress is likely to be the mechanism by which mechanical forces are applied to cell and tissue systems resulting from ultrasound exposure (when cavitation is not present). In terms of the bioeffects of radiation stress, these will depend on pulse average intensity and amplitude as forces are exerted only during the pulse. Bioeffects could also be dependent on the application of the stress over time so the time averaged acoustic intensity would be important as with thermal effects. These factors cross the divide between the factors influencing thermal and mechanical effects.

2.2 Ultrasound exposure parameters for diagnosis and therapy

In diagnostic systems, exposure parameters vary according to the ultrasound mode used. The lowest temporal average intensities are used during B-mode imaging, with higher intensities typically found during pulsed Doppler studies. User controlled settings such as the acoustic output power, field of view and focus depth also alter the

Table 2.1 Ultrasound exposure parameters for different diagnostic and therapeutic applications. Exposure parameters taken from Hoskins, Thrush et al. (2003), Duck and Martin (1991), Davros, Garra et al. (1991), ter Haar (2007).

Mode of ultrasound	Frequency range (MHz)	Peak negative acoustic pressure range (MPa)	I_{spta} range (W/cm^2)	Acoustic power range (W)
B - mode	1.5 - 15 – 40	0.45 – 5.54	3×10^{-4} – 0.991	3×10^{-4} – 0.285
Spectral pulsed Doppler	1.5 - 15	0.67 – 5.32	0.173 – 9.080	0.010 – 0.440
Doppler imaging	1.5 – 15	0.46 – 4.25	.021 – 2.050	0.015 – 0.440
Physiotherapy	1 - 3	~1	~ 10	Up to 12
Lithotripsy	0.1 - 1	~ 10 - 100	~ 100 – 500	
Bone healing	1		Low intensity (I_{satp} 0.03 - 0.5)	~ 0.020
HIFU	MHz		1300 – 6500	
Sonophoresis	kHz, MHz		~0.2	

beam output characteristics. Therapeutic ultrasound uses different values for these parameters, in order to elicit a particular effect. For example, physiotherapy ultrasound uses much higher acoustic power than diagnostic imaging and may have some thermal effect on tissue, however, the mechanisms are not clear. Lithotripsy uses high acoustic pressures to destroy calcifications, but the time averaged acoustic intensity is relatively low compared to pulsed Doppler, for example. Pulse length may also vary between applications; short pulse lengths (μs) are employed in ultrasound imaging in order to obtain good spatial resolution and longer pulses (ms) are used in pulsed therapy beams where this is not important. Pulse length may still be important for other reasons, possibly where cavitation is involved. High intensity focused ultrasound (HIFU) is used to heat and thermally ablate tissue such as uterine fibroids and cancerous tumours. The beam is focused on a small area of tissue within a target area and the tissue is heated to at least 56°C for a few seconds bringing about cell death and necrosis. Other therapeutic ultrasound applications may depend in non-thermal effects such as cavitation and streaming. They include wound healing in both soft tissue and bone, and sonophoresis – the use of ultrasound to increase the penetration of drugs through the skin. The therapeutic applications of ultrasound are reviewed by ter Haar (2007).

A summary of exposure parameters for different applications is given in Table 2.1. There is considerable variation between applications; peak negative acoustic pressures are in the range of 0.5 to 5 MPa for all diagnostic imaging modes and physiotherapy and many times greater for lithotripsy. Spatial-peak time-averaged intensities are low for B mode imaging but can be much higher, up to several W/cm^2 in Doppler imaging applications, while for bone healing low intensities are used. Data is quoted in the table where it is available; different parameters are recorded in the literature for different uses, so a complete description cannot be given.

Safety guidelines

The thermal and mechanical mechanisms of interaction of ultrasound with tissue have been discussed, and it must be noted that there is a possibility of bioeffects under diagnostic ultrasound conditions. Streaming and small temperature rises have been observed in diagnostic fields (Starritt et al. 1989) and cavitation is important where

ultrasound contrast agents are employed. Although ultrasound is seen as a safe imaging modality, safety is still important. In diagnostic ultrasound it is good practice to keep exposure times and acoustic output as low as possible while obtaining images of a high enough quality to facilitate correct diagnosis (BMUS 2009). Safety recommendations are discussed briefly here as the exposure parameters employed and the outcomes of this study will be discussed in this context in later chapters.

The manufacturers of medical ultrasound equipment are required to design and build systems that conform to international regulations and standards. In Europe, manufacturers must demonstrate that their equipment meets the requirements for safety and performance of the Medical Devices Directive. Manufacturers refer to IEC standards to demonstrate that their products meet the regulatory requirements. In the USA, manufacturers must demonstrate to the FDA that their equipment is safe.

The FDA requires that values of mechanical and thermal indices are displayed to the user during scanning to comply with the Output Display standard set out by AIUM/NEMA (American Institute of Ultrasound in Medicine with the National Electrical Manufacturers' Association) (1992). The upper limits set by the FDA (1997) are 720 mW cm^{-2} for estimated *in situ*, or derated I_{SPTA}, 190 W cm^{-2} for derated I_{SPPA}, 1.9 for Mechanical Index and a value of 6 for Thermal Index that should not be exceeded without justification. These limits prevent manufacturers from making it possible to increase acoustic output to potentially harmful levels in order to produce better images, which may not be necessary for correct diagnosis. Other British and European standards exist which apply to the general safety of medical electrical equipment. A more comprehensive review of ultrasound safety can be found in ter Haar and Duck (2000).

By the nature of therapeutic ultrasound, exposure is intended to elicit a bioeffect of the exposed tissue. It is important that exposure protocols are optimised and that efforts are made to understand the mechanisms involved so that these procedures can also be performed safely and effectively. The IEC standards and European directives that apply to medical electrical equipment obviously also apply to therapeutic ultrasound systems. IEC 60601-2-5 (IEC 2009), which applies to physiotherapy ultrasound equipment, sets limits on the variation of acoustic output parameters from the

nominal values. It seems reasonable to suggest that this requirement should extend to other therapeutic equipment to ensure the safe and effective delivery of treatment.

2.3 The vascular system

This section provides some background on the structure, function and biomechanical properties of arteries and the cells that form them. This section will discuss ultrasound bioeffects, in many cases where the mechanisms are unknown, of cells and tissues and the processes involved at the tissue and cellular level.

2.3.1 Vascular structure and function

Arteries throughout the circulation have the same basic structure composed of three layers; the intima, media and adventitia; this arrangement is illustrated in Figure 2.1. The intima is made up of the glycocalyx, the endothelium, which sits on the collagenous basement membrane, and the internal elastic lamella which separates this layer from the media. In large vessels there may be some cells separating the basement membrane and internal elastic lamellae, especially in aging or diseased tissue. The media contains layers of smooth muscle cells, elastic lamellae and collagen fibres. The adventitia is the outer layer of the artery which is formed mainly of elastin and collagen. This layer of connective tissue anchors the blood vessel to surrounding tissue. In thicker walled vessels, this layer also contains lymphatic vessels and capillaries that supply nutrients to the medial cells.

The mechanical properties of blood vessels are determined by the composition of the media. Therefore, the size and relative proportions of the different components vary from place to place in the circulation, depending on the mechanical stresses placed on the vessels by blood flow. Typical diameters and wall thicknesses for vessels throughout the circulation are shown in Figure 2.2. Elastic arteries are the largest diameter arteries, also known as the conducting arteries. They have a high proportion of elastin in the media and their walls are relatively thin compared to their overall diameter. These arteries are found close to the heart where flow is pulsatile; their elasticity helps the movement of blood along the vessel, as the walls are stretched and then relax. The media of muscular arteries contains a higher proportion of smooth
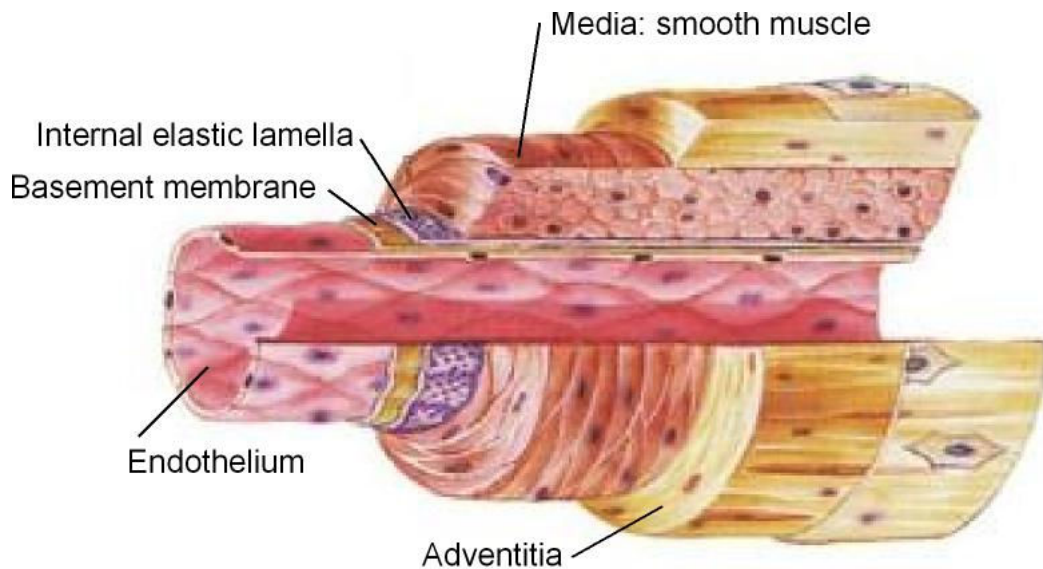
Figure 2.1 Structure of an artery illustrating the intimal region formed of endothelium surrounded by basement membrane, elastic lamellae, the medial region formed of smooth muscle, and the adventitial region formed of connective tissue. (adapted from diagram http://www.sci.sdsu.edu/class/bio590/pictures/lect5/artery-vein.jpeg.)

muscle and less elastin than elastic arteries. They have smaller diameters and have a greater range of vasoconstriction and dilatation, important for controlling vessel diameter and thereby blood flow. Their function is to distribute blood to parts of the body, such as the hand and arm via the brachial and radial arteries. Arterioles are smaller vessels which have a muscular media layer with little elastin. The wall thickness decreases as the vessels make the transition from artery-like arteriole to capillary-like arteriole. Arterioles are the main source of vascular resistance and determinants of tissue perfusion, controlling blood flow into the capillaries. The capillaries make up the microcirculation which has a large surface area with which to deliver nutrients to tissues and organs in the body and remove their waste products. They are composed of a single layer of endothelial cells which allow substances to pass through from the blood to the tissue and vice versa. The proportion of the capillary network in which blood flows is dependent on the metabolic activity of the tissue at a particular time. This flow is regulated by contraction of metarterioles at the arteriole end of the microcirculation, and by precapillary sphincters which either relax to allow blood to flow into the capillary bed, or contract to stop it. At the end of the capillary bed, capillaries join to form venules, which are small veins. This is the beginning of the

venous return system. The venules drain into veins which eventually drain into the vena cava and back into the heart. Veins have the same intima, media and adventitia structure as arteries, but the components are present in different proportions. The intimal region is thinner, as is the media, which contains relatively little smooth muscle and elastin. The adventitia is the thickest layer, formed of collagen and elastin fibres. Blood pressure drops through the circulation, beginning at about 120 mmHg during systole and 80 mmHg during diastole in the large arteries, and dropping to about 5 mmHg in the veins. Veins are not designed to withstand high pressures as the arteries are; they contain valves to prevent reverse flow of the blood travelling back to the heart at these low pressures.
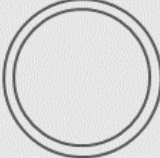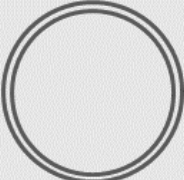
	Aorta	Artery	Arteriole	Capillary	Venule	Vein	Vena Cava
Lumen diameter	25 mm	4 mm	20 μm	5 μm	20 μm	5 mm	30 mm
Wall thickness	2 mm	1 mm	15 μm	1 μm	2 μm	0.5 mm	1.5 mm

Figure 2.2 Typical dimensions for vessels throughout the vascular system, adapted from Aaronson et al (2004).

2.3.2 Mechanical properties of arteries

The mechanical properties of arteries enable them to cope with changes in pressure during the cardiac cycle, without being damaged. During the cardiac cycle, large arteries experience diameter oscillations of up to 8% (Dobrin 1978), while the diameter of small arteries and arterioles changes much less. The mechanical properties of arteries are determined by the passive and active components of the vascular wall. The active components such as the smooth muscle play a role alongside the collagenous and elastic components. At low pressures arteries are compliant and the properties of their elastic components are dominant. At higher pressures arteries become stiffer as the load is transferred to the inelastic collagen fibres. These properties are discussed further by Winlove, Bishop et al. (1995). The adventitia,

which is rich in collagen, gives vessels stiffness and strength, especially at large distensions. At physiological pressures, some arterial stiffness is contributed by stretched elastic lamellae and collagen fibres in the media.

Arteries are viscoelastic; the elastic components of the vessel exhibit strain as soon as stress is applied, and the viscous component, in this case the smooth muscle, resists strain when stress is applied. Smooth muscle can contract even when stretched, so after stretching, the fibres contract before beginning to relax. Tension in the smooth muscle initially increases after stretching and is followed by a slow decrease. The variation of tension with time after sudden loading and the resultant lengthening of segments of artery is termed stress relaxation. After a large increase in tension there is a steep decrease to begin with, followed by a slower decline. Stress relaxation curves for arterial tissue samples were plotted by Zatzman et al. (1954) for dog carotid arteries and Speden (1960) for sheep mesenteric arteries. Both sets of data show that the behaviour is linear over a couple of orders of magnitude in time. The timescale of stress relaxation to approximately 20% of the maximum for sheep mesenteric and canine carotid arteries is 10 to 30s.

The contribution of smooth muscle to the mechanical properties of arteries is to increase circumferential stiffness and resist stretching, and to create active tension to constrict arteries. The mechanics and physiology of smooth muscle is a very wide field, a thorough discussion is given in The Handbook of Physiology (Bohr et al. 1980). The creation of active tension is especially important in small arteries and arterioles, where muscle cells are spontaneously active in vasomotion. For a given strain, a high stress is generated, and they resist distension better than large arteries. Changes in smooth muscle tone can be induced by a wide range of pharmacological agents, such as noradrenaline and potassium ions (Aziba and Okpako 2003); this will be discussed further later in this Chapter.

Small arteries respond differently to changes in stretch, pressure and flow. Increased flow induces vasodilatation; stretching opens stretch-dependent ion channels which affect muscle tone. Increases in pressure stimulate the endothelium to secrete a vasoconstrictor. Mulvany and Aalkjaer (1990) reported that observations of arterioles showed that an increase in pressure stimulated a reduction in diameter sufficient to

maintain a constant wall tension. We can see from Laplace's law, assuming a thin walled vessel, that tension, T, varies with pressure, P, and radius, R:

$$T = PR .$$

2.20

Under isobaric conditions, contraction of the vessel (a decrease in R) by activation of the smooth muscle causes a reduction in wall tension, by decreasing passive tension (tension in the elastic and collagenous components). In a thin walled vessel, this decrease compensates for the increase in active tension in the smooth muscle.

Fluid mechanics of blood flow

Making many assumptions, blood flow, Q, can be described by Poiseuille's law

$$Q = \frac{\pi}{8\mu} R^4 \frac{\Delta P}{L} ,$$

2.21

where μ is viscosity, R is vessel radius, $\frac{\Delta P}{L}$ is the pressure gradient. Poiseuille's law applies to steady laminar flow of a Newtonian fluid in a long straight rigid tube. These assumptions do not hold for blood, which is a non Newtonian fluid. Furthermore blood vessels branch after short distances and are distensible. At high flow rates, such as those experienced in the aorta, flow is not steady; it is disturbed by the pulsatile nature of the flow. However, as a simple approximation, flow is proportional to the fourth power of the radius of the blood vessel. So it can be seen that small changes to the radius of a blood vessel will have a larger effect on blood flow; for a 10% decrease in radius, a 35% reduction in flow would be induced. Shear stresses are exerted by blood flowing through a vessel. The peak shear stresses are exerted at the vessel wall; this maximum shear stress, τ_{max} is described by

$$\tau_{max} = -\frac{4\mu Q}{\pi R^3} .$$

2.22

From this it can also be seen that small changes in vessel diameter also have a larger effect on the level of shear stress experienced by the endothelium of a blood vessel.

2.3.3 Cells of the vascular system

The main functional components of blood vessels are the endothelial and smooth muscle cells. In order to understand how physical and chemical stimuli can influence arterial function we must first understand the physiology of these cells. We begin with a brief general overview of the cell, concentrating on the components important in the context of this research. A more comprehensive description can be found in Tortora and Grabowski (2000).

The Cell

Cells are formed of a nucleus, plasma membrane and cytoplasm. The cytoplasm contains organelles such as the cytoskeleton, mitochondria and endoplasmic reticulum floating in the cytosol. For the purposes of this thesis we are mainly interested in vascular smooth muscle and endothelial cells. Here the main components common to animal cells are described; later more detail is given concerning structures and functions of the cells important to this investigation.
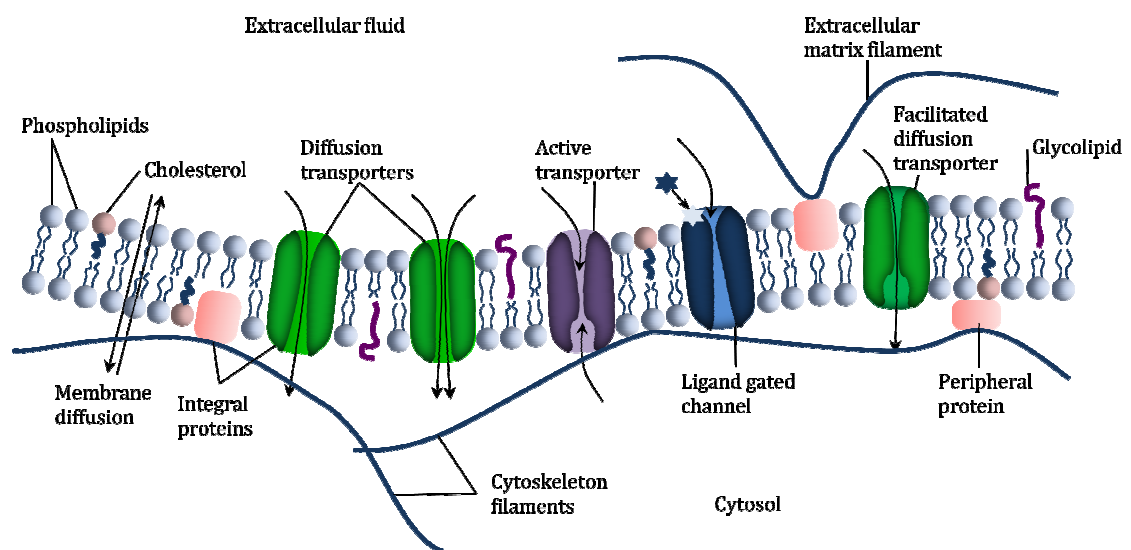
Figure 2.3 Schematic diagram of the cell membrane; transmembrane lipids acting as ion channels float within the lipid bilayer formed of phospholipids, cholesterol and glycolipids. Cytoskeleton and extracellular matrix filaments are anchored to proteins and the membrane. The processes of diffusion through the membrane, through passive and facilitated diffusion channels, active transporters and gated channels are shown.

The plasma membrane

Cells are bordered by the plasma membrane, a lipid bilayer with proteins floating within, which are either anchored or free to diffuse through the membrane. The membrane prevents charged or polar substances from passing in and out of the cell. These substances can instead pass selectively through channels formed by the floating proteins (see Figure 2.3). The lipid bilayer is permeable to most uncharged non-polar molecules and water passes through aquapores. The bilayer lipids are arranged with their polar heads on the outside, forming a hydrophobic central region which excludes the extracellular fluid on one side and the cytosol on the other. The majority of the lipids are phospholipids, with smaller proportions of cholesterol and glycolipid molecules. The bilayer is a fluid structure, allowing the lipid and non anchored proteins to rotate and move past each other. The stiffness is affected by the proportions of the different lipids; increased amounts of cholesterol leads to a stiffer membrane. Membrane proteins float in the lipid bilayer, either spanning the entire thickness (transmembrane proteins), or reaching halfway across the bilayer. There are also peripheral proteins which attach to lipids or other proteins at the surface of the membrane. The proteins found in the plasma membrane can vary greatly between one cell type and another; it is these proteins that determine many of the functions that can be performed by the cell membrane. Some common functions of the membrane proteins are as channels, transporters, receptors and linkers. Channels are formed by proteins that have a pore running through them, which allows a specific substance, for example, a particular ion, to flow in and out of the cell. Transporters are proteins that have binding sites for polar substances, which they move through the membrane by conformational changes. Receptor proteins bind to specific molecules which affect cellular function, such as hormones or nutrients. Both integral and peripheral proteins can also act as linkers; they attach to proteins in membranes of nearby cells, and to internal and external filaments in the extracellular matrix.

For a cell to function correctly it must maintain a balance between concentration gradients of different substances and electrical gradients due to charged ions and molecules. The selective permeability of the membrane makes this possible and different concentrations of substances can be maintained inside and outside the cell. For example, sodium ions have a higher concentration outside the cell than inside,

while potassium ions have a higher concentration inside. The concentration gradients also create electrical gradients due to the distribution of charged ions and molecules. The interior of the cell is more negatively charged when the cell is in a resting state.

Ions and molecules can diffuse down a concentration gradient by passive transport through the lipid bilayer, either directly or via a channel, or by facilitated diffusion through other channels which mediate the process. Substances can move against a concentration gradient by active transport through a transporter protein, a process which requires energy. Transporters may move a single substance or two substances either in the same direction or in opposite directions depending on the type of transporter and its intended function.

Molecules that can diffuse through the lipid bilayer are nonpolar and hydrophobic such as oxygen and carbon dioxide. Molecules that cannot pass through the bilayer must instead diffuse through ion channels in the membrane. Molecules can only move through channels that specifically allow them to pass. The most common ion channels are potassium ion channels and chloride ion channels, with smaller numbers of sodium and calcium ion channels. Some of these channels are gated and so can be either open or closed depending on chemical gradients or cell potential. Others are opened and closed in response to chemical (ligand gated) and mechanical (stretch, shear activated) stimuli. Different cell types may have different ion channel populations, resulting in the cell having different permeability to different ions.

Facilitated diffusion occurs when substances such as glucose, which are too large to fit through ion channels, are transported down the concentration gradient by binding to a transporter protein, which then undergoes a conformational change. Once equilibrium has been reached, transport takes place in each direction at the same rate so there is no net movement.

Substances including sodium, potassium and calcium ions, that must move across the membrane against a concentration gradient, do so by active transport which uses energy from one of two sources. The first of these is primary active transport, which derives its energy from the hydrolysis of adenosine triphosphate (ATP). The energy is used to induce a conformational change in a transporter protein, which pumps an ion

or molecule across the membrane. The most common active transport protein is the Na^+/K^+ ATPase, or the Na^+/K^+ pump, which moves sodium ions out of the cell and brings potassium ions in to maintain a low intracellular Na^+ concentration and a high intracellular K^+ concentration. These ions will slowly diffuse back across the membrane through other ion channels, so this pump works continuously to keep the cell in a steady state. Secondary active transport makes use of energy stored in the concentration gradient of sodium and hydrogen ions. Secondary active transport proteins allow sodium ions to enter the cell by moving down their concentration gradient. The channel simultaneously binds another substance and transports it using the energy released from movement of a Na^+ ion down the concentration gradient. This energy source drives many biological functions in the cell.

Cytoplasm

The cytoplasm contains the cytosol and organelles. The cytosol is mainly water with ions, lipids, proteins, amino acids and other substances, both dissolved and suspended in it. The organelles sit within the cytosol; they are the sites of cellular growth, maintenance and reproduction. Some of the structures most relevant to the background of this study are described here.

The cytoskeleton forms a sort of scaffolding inside the cell made up of protein filaments that stretch through the cytosol. The cytoskeleton helps to shape the cell and is involved in cell movements. The cytoskeleton is formed of three types of structure: microfilaments, intermediate filaments and microtubules. Microfilaments are thin strands of the protein actin, found mainly around the edge of the cell. They provide mechanical support to the cell, attach the cytoskeleton to membrane proteins and are involved in cell functions such as muscle contraction, cell division and movement. The intermediate filaments are made of different proteins. They provide strength to parts of the cell which are placed under mechanical stress. The microtubules are hollow structures formed of the protein tubulin; it is the microtubules that help to form the shape of the cell. The cytoskeleton can play a part in the transduction of physical forces by the cell.

The ribosomes are the sites of protein synthesis within the cell. Some ribosomes manufacture proteins for use within the cell; this type of ribosome normally floats

within the cytosol. Other ribosomes manufacture proteins which are used in the cell membrane or exported from the cell. These are bound to either the cell membrane or the membrane of the endoplasmic reticulum.

The endoplasmic reticulum is made up of a network of membranes forming flat sac-like structures around the nucleus of the cell. There are two types of endoplasmic reticulum, rough and smooth. The rough endoplasmic reticulum is where ribosomes attach and the proteins manufactured there are processed further. The proteins are used to form glycoproteins, or attached to phospholipids, for example. The smooth endoplasmic reticulum is an extension of the rough endoplasmic reticulum; it synthesises phospholipids, fats and steroids. It also performs other functions such as the storage of calcium ions released from the sarcoplasmic reticulum, a form of the endoplasmic reticulum. In muscle cells the release of calcium ions from this site starts the process of muscle contraction.

The nucleus

The cell nucleus contains most of the cell's genes, which control the structure and function of the cell. The genes are arranged along chromosomes which are each formed of a long DNA molecule. The nucleus is spherical or ovoid in shape and is surrounded by the nuclear envelope. This structure contains pores, through which proteins are selectively transported from the cytosol to the nucleus, and RNAs are transported in the other direction. The RNA molecules contain a copy of information contained within the nuclear DNA which instructs protein synthesis.

Physiology of the cell

Cells such as muscle fibres, which can be electrically excited, normally exist in a resting state that depends on a balance between electrical and chemical gradients. In this resting state, the interior of the cell is negatively charged. In smooth muscle, contraction can be stimulated by an action potential in the muscle or a local graded potential. When an action potential is stimulated, the membrane becomes depolarised, i.e. the interior becomes more positive before returning to a negative potential, overshooting the resting potential before returning to the rest state. An action potential always has the same amplitude, as long as the initial depolarisation is large enough to stimulate the action potential; once it reaches the threshold, then

depolarisation will always be to the same degree. A graded potential is a small depolarisation, or a small hyperpolarisation of the membrane potential, the magnitude and direction depend on the strength of the stimulus and the resulting ion channel activity.

The changes in membrane potential described are caused by the action of ion channels in response to nerve, neurotransmitter or hormonal stimulation. During an action potential, voltage gated Na^+ channels begin to open once the threshold has been reached. The resting concentration of Na^+ in the cell is low and the cell interior is negative, so when the channels open, sodium ions flow in causing depolarisation. These channels remain open for a few hundred microseconds before they are inactivated and the constant action of the Na^+/K^+ pump expels the sodium ions. Depolarisation also causes voltage-gated potassium channels to open; these open more slowly and begin to take effect as the sodium channels are inactivated. Potassium ions flow out of the cell as the rate of flow of sodium ions into the cell slows, inducing repolarisation. As potassium ions continue to flow out of the cell, the membrane potential becomes hyperpolarised (more negative than the resting potential). The K^+ channels begin to close and the potential returns to the resting level (Tortora and Grabowski 2000).

There are different types of ion channels, which are either always open (leakage channels) or can be opened or closed by electrical, chemical or mechanical stimuli. Voltage-gated ion channels open and close in response to changes in the membrane potential of the cell; these channels are important in the generation and propagation of action potentials and graded potentials. Ligand-gated ion channels open and close in response to chemical stimuli, or ligands, such as neurotransmitters, hormones and other ions. The ligand may bind directly to the channel in order to open or close it, or may operate indirectly through a second messenger pathway, by binding to a membrane protein to activate another molecule. Mechanically-gated ion channels open or close due to mechanical stimulation such as stretching, vibration or pressure. When a force acts on the channel it is physically distorted, opening the channel.

Smooth muscle

Smooth muscle is non-striated involuntary muscle, and as such is different from skeletal muscle. The function of this type of muscle is regulated by the autonomic nervous system, by chemical stimuli and by mechanical forces. The muscle cells can function when stretched and have elastic properties so they can return to their original length after contraction or stretching. The diameter of blood vessels, and therefore the blood pressure, is determined by contraction and relaxation of smooth muscle in the vessel wall.

There are two types of smooth muscle, visceral and multiunit. In visceral tissue, the fibres are joined in such a way that action potentials generated in one fibre spread to neighbouring fibres, so they all contract as one. In multiunit tissue, an action potential will cause contraction of the fibre in which it was generated only; each fibre has its own nerve terminals. In the vascular system, visceral smooth muscle is found in the walls of small arteries and veins, while multiunit smooth muscle is found in the walls of large arteries. Most smooth muscle fibres are controlled by the autonomic nervous system, but many can also respond to stimuli such as hormones, stretching and local changes in pH, ion concentrations, temperature, and carbon dioxide and oxygen levels. The type of smooth muscle found in the vasculature is tonic; it contracts slowly for prolonged periods in contrast to the phasic smooth muscle found in the gastrointestinal tract, which contracts quickly and rhythmically to perform peristalsis. Tonic smooth muscle usually responds to stimuli by graded potential rather than by generating an action potential (Somlyo and Somlyo 1994).

The mechanism of contraction of smooth muscle involves the contractile proteins actin and myosin, as in skeletal muscle. Thick filaments are formed of many myosin molecules, each with two myosin head groups. The myosin head groups can attach to binding sites on thin filaments, which are formed of actin. To achieve contraction of the muscle fibre, the myosin head groups bind to the actin and the head moves pulling the thin filament along. The myosin head then binds ATP and detaches from the actin, the ATP is hydrolysed and the process can be repeated (Figure 2.5).

In striated muscle, the thick and thin filaments are arranged in a regular pattern which produces striations; there is no such regular arrangement in smooth muscle. The

Intermediate filaments

Nucleus

Cytoplasm

Dense bodies

Plasma membrane

Relaxed fibre   Contracted fibre
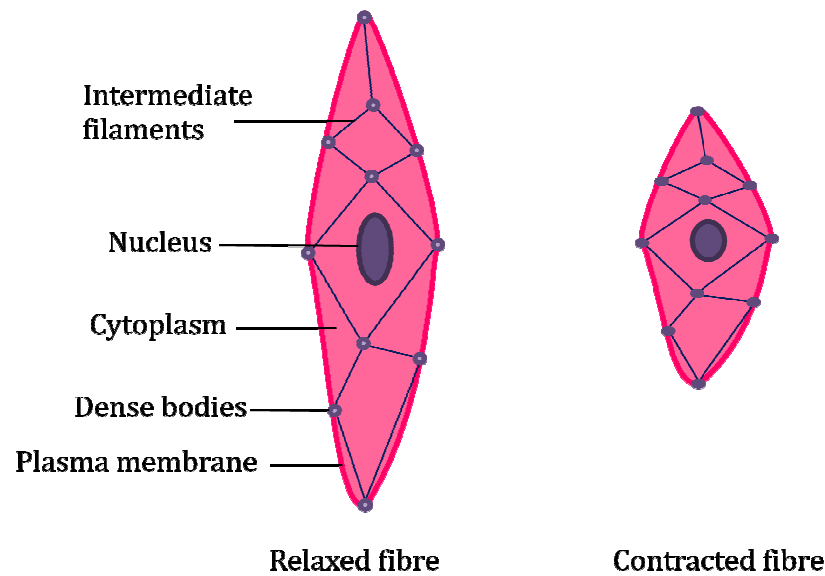
Figure 2.4 Diagram of a smooth muscle in the relaxed and contracted state, showing the structural components of the cell with network of filaments connected to dense bodies, which act as fixed points which are pulled together during contraction.

force generated by movement of the thick and thin filaments is transferred to intermediate filaments, which form a network joined by structures called dense bodies, distributed through the cytoplasm and plasma membrane of the fibre. The force transferred to the intermediate filaments acts to pull together the dense bodies, causing contraction of the fibre (see Figure 2.4).

As in other types of muscle, contraction is stimulated by an increase in the intracellular calcium concentration. Calcium ions enter the cell from the extracellular fluid and from the sarcoplasmic reticulum within the cell (of which there is much less in smooth muscle than in striated muscle). Because of differences in the signalling pathways and structure of smooth muscle cells compared to striated muscle cells, contraction happens more slowly and is more prolonged. Once the calcium ions have entered the cell, it takes longer for them to reach the muscle filaments and trigger contraction. This is also the reason for prolonged contraction as the calcium ions also leave the cell slowly. Following an increase in intracellular calcium concentration, the calcium binds to the protein calmodulin. After binding, this then activates an enzyme called myosin light chain kinase, which phosphorylates part of the myosin head group. Once this has taken place the myosin can bind to actin and contraction can begin (Figure 2.5).
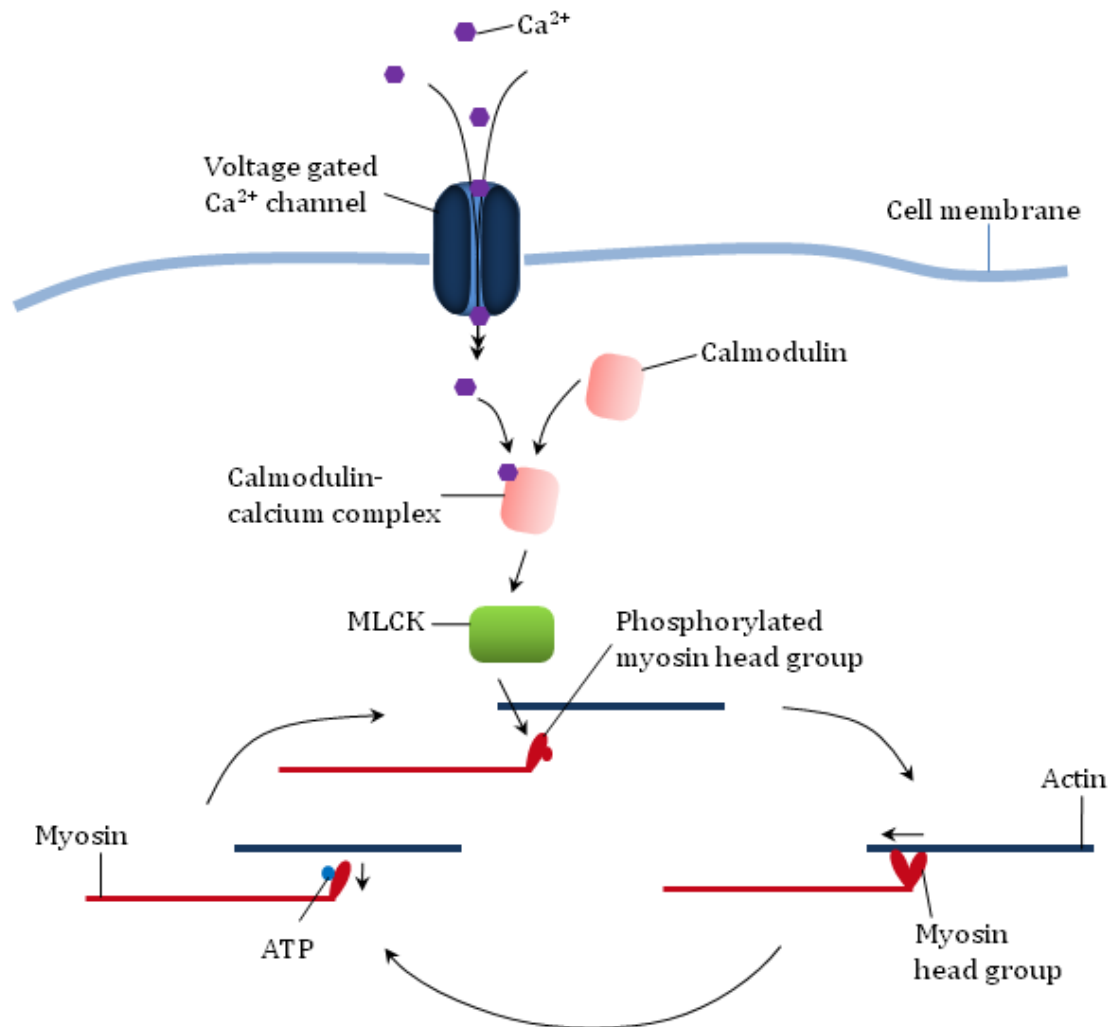
Figure 2.5 Diagram of the pathway leading to smooth muscle contraction: during membrane depolarisation calcium ions enter through voltage-gated channels, and bind to calmodulin creating a complex, which activates the enzyme myosin light chain kinase (MLCK). The enzyme phosphorylates the myosin head group enabling binding to actin, the head group moves, pulling along the actin filament, it then binds to ATP and releases from the actin, the ATP hydrolyses and the process can begin again.

Smooth muscles can maintain tone in the long term; this is possible because of the balance between entry and exit of calcium ions. Transmural pressure in arteries has the effect of depolarising the membrane potential slightly. This increases the probability of voltage-dependent calcium channels being in the open state, so more Ca^{2+} can flow in to the cell. A small number of open voltage-dependent calcium channels is sufficient to maintain steady contraction or tone. From this state, small

hyperpolarisations of the membrane potential act to decrease tone, and small depolarisations act to increase tone. This may be due to the action of neurotransmitters, which can act on voltage-independent calcium channels in the membrane or sarcoplasmic reticulum to increase $[Ca^{2+}]_i$. Release of calcium from the sarcoplasmic reticulum can also be stimulated by the increased $[Ca^{2+}]_i$, termed calcium-induced calcium release. Some agents for example, may cause contraction by decreasing the rate at which Ca^{2+} is pumped out of the cell by Na^+/Ca^{2+} exchange, and by increasing entry, which will depolarise the membrane potential further, increasing the number of open voltage-dependent channels. Dilation can also be stimulated by inhibition of voltage-dependent calcium channels, and for example by stimulation of the pump that transports Ca^{2+} into the sarcoplasmic reticulum for storage. Potassium channels may also be opened by chemical stimuli, allowing potassium ions to flow out of the cell, causing hyperpolarisation and relaxation. Other potassium channels will open due to membrane depolarisation, returning the membrane potential back towards the rest state, and others are activated by $[Ca^{2+}]_i$. These processes are discussed in further detail by (Nelson et al. 1990).

Four types of potassium channel have been found in smooth muscle: voltage-gated channels, Ca^{2+}-activated channels, ATP-sensitive channels and inward rectifier channels (Nelson and Quayle 1995). Voltage-gated potassium channels open during depolarisation and allow K^+ to flow out of the cell, causing repolarisation and return to the rest potential. They help to maintain resting tone, but deactivate due to prolonged depolarisation. Calcium-activated potassium channels open due to increased $[Ca^{2+}]_i$ and depolarisation; they counteract this and the resulting vasoconstriction. ATP-sensitive potassium channels are associated with pathophysiological responses; inhibition leads to depolarisation and vasoconstriction. Inward rectifier potassium channels allow small outward potassium currents and help to maintain resting tone. Some vasoconstricting agonists function by inhibiting potassium ion channels, causing depolarisation of the membrane. The membrane also contains the Na^+/K^+ ATPase pump and calcium-gated chloride channels, the opening of which can cause depolarisation.

There are many different types of ion channels that can be found in the membranes of smooth muscle, with varying distributions and properties. The ion channel population varies between different tissues, such as large and small blood vessels (Somlyo and Somlyo 1994).

The role of smooth muscle in contraction has been investigated using drugs to induce vasodilatation or constriction (Dobrin and Rovick 1969; Dobrin 1973). Data of this sort are useful in establishing the properties of the blood vessels under normal physiological conditions, at extremes and under conditions which may simulate disease. These may include loss of elasticity due to atherosclerosis, or the effects of high blood pressure due to diabetes or other disease.

Vascular endothelial cells

All blood vessels are lined with a layer of endothelial cells. These are normally the only part of the vessel which comes into contact with the blood. They are involved in several processes including control of blood pressure by vasomotion, blood clotting, inflammation, barrier function and formation of new blood vessels.

The endothelium forms a barrier between the blood and underlying tissue, controlling the passage of molecules and white blood cells into tissue. It also influences the underlying smooth muscle cells, as well as elements of the blood by secreting hormones and vasoactive chemicals such as prostacyclin and nitric oxide. These agonists act on the smooth muscle to alter vessel tone and inhibit platelet aggregation, which would cause clotting. Endothelial cells can be stimulated to release these substances by mechanical stimuli, such as changes in blood pressure, as well as chemical stimuli. Other agonists can stimulate the endothelial cells to produce substances which promote clotting, by inducing adhesion of platelets and white blood cells to the endothelium. Endothelial cells also release vascular endothelial growth factor to promote growth and formation of new blood vessels. Endothelial cell dysfunction is a factor in many pathologies, such as atherosclerosis, sepsis and congestive heart failure. These cells therefore play a very important role in the function of the vascular system.

As already discussed, vascular tone can be controlled either by direct interaction with the smooth muscle cells of the vascular wall, or by endothelium dependent means. For instance, blood vessels can be stimulated to relax by acetylcholine, providing that the endothelial layer is intact; in the absence of endothelium, contraction is instead induced. Acetylcholine binds to receptors on the endothelial cell surface, which initiates a signal pathway that stimulates release of Ca^{2+} from the endoplasmic reticulum. The Ca^{2+} binds to calmodulin, then this complex stimulates the enzyme nitric oxide synthase to produce nitric oxide (NO) (Zecchin et al. 2007). The NO diffuses through the plasma membrane into the smooth muscle cells, where it initiates a second messenger pathway, which induces muscle relaxation by catalysing phosphorylation of the contractile proteins. Substances such as the endothelium-dependent vasodilator, bradykinin, can induce the release of NO and prostacyclin, and cause hyperpolarisation of the smooth muscle cells, causing vasodilation (Selemidis and Cocks 2007). Other substances that can induce endothelium-dependent relaxation include histamine and insulin. Changes in shear stress that occur during increases in blood flow also induce endothelium-dependent relaxation.

2.4 Biological effects of ultrasound in cells and tissues

Further to the initial discussion of ultrasound bioeffects of thermal, mechanical and non-thermal, non-cavitational nature, evidence of bioeffects specific to the vascular system is now discussed. In many cases, bioeffects have been observed but the physical mechanisms are not known. As important as discovering the physical mechanisms of ultrasound bioeffects, is discovering the associated cellular mechanisms. The experiments presented in this thesis employ MHz ultrasound at relatively low acoustic powers and mainly at low acoustic pressures. Many bioeffects associated with techniques such as HIFU and physiotherapy are therefore unlikely. In this context, the bioeffects of low intensity ultrasound at a cellular level are discussed, including many cell types, in order to build a general picture.

2.4.1 Bioeffects on the vasculature

In vascular tissue, important bioeffects would be those changes that affect blood flow, such as changes in smooth muscle tone with changes in diameter or blood pressure.

As outlined previously, these effects could operate directly on the smooth muscle or take effect via the endothelium. Other more long term effects may include changes in growth and proliferation of cells; this type of effect will be discussed later. Here the short term effects of ultrasound on the vasculature are concentrated upon. A summary of the effects is presented in Table 2.2.

Several research groups have demonstrated that dilation of blood vessels can be induced with kHz ultrasound by both endothelium dependent and independent mechanisms. Catheter delivered high acoustic power (25 W), low frequency (19.5 kHz) pulsed ultrasound was found to cause reversible endothelium-independent vasodilatation in canine coronary arteries and human femoropopliteal arteries (Steffen et al. 1994). Vessel diameter increased by an average of 20% in canine arteries and by an average of 14% in human arteries after exposure to ultrasound. The investigators discussed the possibility of disruption of actin-actin bonds in the smooth muscle, which can realign after exposure causing recontraction, and the involvement of NO produced by the smooth muscle cells. Fischell et al. (1991) demonstrated that exposure of sections of rabbit aorta to 20 kHz ultrasound from a ball tipped probe (0.7 to 5.5 W for 60 s) induced dose-dependent relaxation of the vessels when precontracted by phenylephrine and by KCl, also by an endothelium-independent mechanism. Similar relaxation was observed in canine internal mammary arteries on exposure to an ultrasonic scalpel at 55 kHz (p₋ 4 kPa at 10 cm) (Maruo, et al., 2004). This time the response was increased in samples with intact endothelium (50.4% cf. 10.5% relaxation for denuded samples). The response was shown to be caused by a combination of NO release during the initial response and prostacyclin release during the longer term response over a 5 minute period after exposure.

Similar effects have also been demonstrated *in vivo*. Iida et al. (2006) showed that 29 kHz transcutaneous ultrasound (1.4 W cm^{-2}, 2-5 min) caused vasodilation in human brachial arteries, as measured by ultrasound in the range of 5-12 MHz. Vasodilatation continued to increase 5 minutes after exposure was ceased, returning to normal after 21 minutes. Vasodilation was also induced in canine coronary arteries, due to NO release by exposure to 27 kHz ultrasound (Miyamoto et al. 2003). After 5 minute

Table 2.2 Summary of conditions and results from the reported studies on bioeffects of the vasculature. Duty cycle = ratio of the pulse duration to the pulse period

Tissue type and preparation	Exposure	Process observed and proposed mechanism	Reference
Rabbit aorta *in vitro*	20 kHz, 50% duty cycle, 30 ms pulse, 0.7-5.5 W, 60s, ball tipped probe	Endothelium independent, dose dependent relaxation in precontracted vessels, $\Delta T < 1°C$, imaged with 10 MHz ultrasound	Fischell at al. 1991
Canine mammary artery *in vitro*	55 kHz, p_- 40 kPa at tissue, 50 mWcm^{-2}, 3s	Partially endothelium dependent relaxation, enhanced in intact vessels (50% vs. 10.5%); initial response – NO, longer term response – prostaglandin, $\Delta T = 0.3$-0.4 °C	Maruo et al. 2004
Canine coronary artery, human femoropopliteal artery *in vivo*	19.5 kHz, 50% duty cycle, 30ms pulse, 25 W, catheter delivered	Endothelium independent vasodilatation, NO related; diameter increase 21% canine, 14% human	Steffen et al. 1994
Human brachial artery *in vivo*	29 kHz, I_{max} 1.4 W/cm^2, I_{SATA} 0.12 W/cm^2, 30% duty cycle, 25 Hz, 1-5 min	Vasodilatation with 2-5 min exposure, for 5 mins after, diameter increase 6% max, returned to baseline after 20 mins, measured by 12 MHz ultrasound, skin $\Delta T = 0.2$ °C	Iida et al. 2006
Canine coronary artery *in vivo*	27 kHz, 30% duty cycle, 1.4 W/cm^2, 170kPa at 4cm, 5,-90 min	Vasodilatation, luminal area increase 21% after 5 min exposure, returned to baseline during longer exposures, NO release, measured with 30 or 40 MHz ultrasound	Miyamoto et al. 2003
Rabbit gracilis muscle ischemic muscle tissue model	40 kHz, 0.75 w/cm^2, CW	Improved perfusion, increased flow measured with laser Doppler, capillaries more prominent in histological analysis, NO dependent, $\Delta T = 0.9$ °C	Suchkova et al. 2002
Hamster arterioles *in vivo*	2.5 MHz, 0.4µs pulse, p_- 2 MPa, MI 1.3, 15 min	Vasodilatation, increased permeability, reduction in production of ROS after ischemic period	Bertuglia et al. 2004
Human forearm clinical	1 MHz, 1.5 W/cm^2, 5 min, physiotherapy	No effect on blood flow in muscle, skin, forearm measured with laser Doppler	Robinson and Buono 1995
Human skin clinical	3 MHz, 1 W/cm^2, Pulsed and CW physiotherapy, 6 min	Increases in cutaneous blood flow at 2, 4, 6 min	Noble et al. 2007
Frog heart	1.2 MHz, 5 ms pulse, I_{SPPA} 390-2400 W/cm^2, p_- 2.7-5.1 MPa	Altered cardiac rhythm – premature ventricular contraction, decrease in aortic pressure above p_+ 10 MPa (p_- 4.4MPa), ultrasonic pacing	Dalecki et al. 1993
Rat heart	1.2 MHz, 5 ms pulse. I_{SPPA} 25-800 W/cm^2, p_- 0.9-3 MPa	Altered cardiac rhythm for 2+ MPa with 5 ms pulse, for 10 MPa with 1-2 ms pulse	McRobbie et al. 1997
Human heart	Diagnostic cardiac US, MI 1.1, 1.5	Premature ventricular contraction in presence of UCA with MI 1.5 with end systolic triggered imaging	Van der Wouw et al. 2000

exposures, vessel diameter increased by 21% and returned to baseline after 60 minutes. Longer exposure periods of 30 and 60 minutes did not induce as much vasodilatation. The diameter returned to baseline during exposure, suggesting that the vasodilatory effect decreased over time.

In a clinical application, exposure to low acoustic intensity 40 kHz ultrasound was found to improve perfusion in ischemic muscle tissue, by a nitric oxide dependent mechanism. Capillaries appeared more prominent in exposed tissue under histological analysis and increased flow was measured with laser doppler (Suchkova et al. 2002). Exposure to ultrasound with cardiac imaging parameters (2.5 MHz, MI 1.3, p. 2 MPa) induced vasodilatation in hamster arterioles *in vivo*, acompanied by a reduction in the production of reactive oxygen species (ROS) under normal conditions and following a period of ischemia (Bertuglia et al. 2004). The investigations just discussed are mainly concerned with kHz ultrasound; there is less evidence of effects of MHz ultrasound on blood vessels.

The effects of physiotherapy ultrasound on the vasculature have also been examined *in vivo*. Continuous wave 1 MHz ultrasound at an acoustic intensity of 1.5 W cm^{-2}, applied to the forearm for 5 minutes, was found to have no effect on blood flow in the muscle, skin and forearm, measured using laser Doppler flowmetry (Robinson and Buono 1995). This evidence suggests that increased blood flow is not the primary mechanism involved with physiotherapy ultrasound, but another group (Noble et al. 2007) found that pulsed and continuous wave therapeutic ultrasound did stimulate blood flow in the skin. These studies demonstrate that bioeffects and mechanisms linked with physiotherapy ultrasound are not well defined or understood and further work is required in this area.

The effect of MHz ultrasound observed by Bertuglia et al. (2004) seemed similar to the effects of kHz ultrasound in the other studies, but the mechanisms are likely to be different. No thorough investigation of the effect of ultrasound exposure parameters on the response of blood vessels was conducted during any of these investigations. Between these studies there were variations in frequency, acoustic power, acoustic intensity and peak acoustic pressure. This may account for the different magnitudes and signal pathways reported, as the magnitude and type of bioeffect may depend on these quantities.

Other effects of ultrasound related to the vascular system have been observed. Exposure to 1.2 MHz (5 ms pulse) ultrasound altered cardiac rhythm in frogs above a threshold of 10 MPa peak negative acoustic pressure (Dalecki et al. 1993). A similar effect was observed in rats, also using 1.2 MHz (5 ms pulse) ultrasound; this time with a lower acoustic pressure threshold of 2 MPa (MacRobbie et al. 1997). It has also been reported that in some cases premature ventricular contraction can occur in humans as a result of diagnostic cardiac ultrasound in the presence of contrast agents (van der Wouw et al. 2000).

2.5 Bioeffects on the cellular level

It has been observed that ultrasound exposure has effects on many cell types, ranging from subtle, transient modification of metabolic patterns, to cell death. Efforts have been made to understand these, both in order to minimise side effects of ultrasonography and to exploit them therapeutically and even surgically. Research in this area will also help to inform the cellular mechanisms of tissue bioeffects, which may be induced during diagnostic exposures. In this section we focus on the non-lethal cellular effects of low acoustic intensity (30 – 1000 mW cm^{-2}) ultrasound, where it is probable that the mechanisms are non cavitational and where the processes involved are not well understood.

The effects of low acoustic intensity exposures have been studied *in vivo*, on *ex vivo* preparations and on cells in culture. These studies have revealed a wide range of responses at the whole tissue and cellular level. The outcomes of these studies and their limitations are discussed first, followed by a summary of the current understanding of the processes involved in the interaction between cells and ultrasound, in the light of recent work on mechanical and thermal effects and cell signal transduction undertaken in other contexts.

2.5.1 Effects on cells in culture and animal models

Studies have been performed on a range of cell types, usually employing cultures of a single cell type taken to be representative of those involved in soft tissue and bone healing processes. A summary of the exposure parameters and findings for each of the reported studies is given in Table 2.3. Many of these studies have used very similar

exposure parameters and experimental designs, incorporating 'low intensity pulsed ultrasound' (LIPUS) systems, either adapted from clinical bone and tissue healing systems, or specially designed to be used with cell culture plates. The frequency and pulse regime in most of these LIPUS studies is very similar, usually employing 1 or 1.5 MHz ultrasound with a 200μs pulse duration, pulse repetition frequency of 1 kHz and free-field spatial-average temporal-average intensities (I_{SATA}) ranging from 30 mW cm^{-2} to about 100 mW cm^{-2}, delivered with a transducer of a few cm in diameter with a non-scanned beam.

The experimental set up in cell culture studies is extremely different from clinical therapy delivery. Ultrasound transducers are coupled directly to the bottom of cell culture plates, or sometimes with a water filled gap of up to 15cm to place the cells just in the far field of the ultrasound beam. In most cases a layer of cells and medium a few millimetres thick is the target, sometimes with an absorber placed on top of the cells to stop reflections. These arrangements make heating of the transducer, petri dish and cells likely in many cases. However, hardly any of the studies include estimates of possible temperature rises during exposure. Few groups made independent acoustic output measurements in the beam, or tried to quantify losses through the culture plates. Most of those that did, found significantly lower intensities at the position of the cells than in the open field. Standing waves are also likely, making it difficult to predict the acoustic intensity distribution at the target. Temperature rises of a similar magnitude and standing waves are less likely in animal models and clinical treatment, where the transducer is coupled to the skin and there is blood flow in the tissue. The ultrasound set up and lack of independent acoustic output measurement in some of the cell culture studies, creates difficulties in relating effects measured in cells in culture, to those observed in animal models and in a clinical setting. This limitation also creates problems in determining the mechanism of ultrasound interaction. In general, the cell functions used as indicators of the effects of ultrasound on cells, and of healing processes, are not the same in the two types of studies.

Given these caveats, LIPUS exposure has been found to influence osteoblasts, fibroblasts, chondrocytes and a number of other cell types in culture. Iwabuchi et al. (2005) found that LIPUS increased resorption of herniated rat intervertebral discs co-cultured with activated peritoneal macrophages, believed to be associated with disc resorption processes. Increases in proteoglycan and DNA synthesis were recorded in

human intervertebral disc cells, after exposure with a similar US regime (Kobayashi et al. 2009). LIPUS exposure increased proliferation and migration (Raz et al. 2005; Mizrahi et al. 2007) of aortic endothelial cells, and increased leukocyte adhesion when they were incubated together after exposure (Maxwell et al. 1994). Increased proliferation of Schwann cells (the coating of nerve axons) was reported after 4 to 10 days of exposure (Zhang et al. 2009), and there is further evidence that ultrasound enhances nerve regeneration (Crisci and Ferreira 2002; Raso et al. 2005). In an *in vivo* LIPUS exposed rabbit skin graft model, an increase in cell proliferation and formation of new blood vessels in the dermis were observed (da Costa Gonçalves et al. 2007).

Fibroblasts are a primitive and ubiquitous cell type found in connective tissue; their function is to produce components of the extracellular matrix such as collagen. They have been used as a cell type representative of bone and connective tissue cells in many ultrasound studies. Increases in alkaline phosphatase, an enzyme involved in bone mineralisation, were measured in human gingival fibroblasts after exposure to ultrasound (LIPUS) (Mostafa et al. 2009). Responses were more significant in the group treated with 5 minute exposures. Osteopontin, an extracellular matrix protein involved in the early stages of mineralisation was also increased in this group. It has also been found that ultrasound can increase DNA synthesis at lower intensities compared to higher intensities (Kondo and Yoshii 1985), possibly due to stable cavitation, and can increase intracellular calcium levels in fibroblasts (Mortimer and Dyson 1988). In this study, calcium levels returned to normal about 10 minutes after exposure, showing that calcium pumps were still functioning and that no permanent membrane damage was caused. It has also been observed that continuous wave ultrasound exposure increases proliferation in fibroblasts, as observed in other cell types (Ramirez et al. 1997). This has been linked to integrins (Zhou et al. 2004), which act as mechanosensors in cells and also couple cells to the extracellular matrix. *In vivo*, ultrasound treatment for tendon repair increased mean collagen fibril diameter relative to a control group (Ng and Fung 2007); varying the beam intensity had no significant effect.

Chondrocytes are the cells of cartilage, producing type II collagen and proteoglycans, which form the cartilaginous matrix. Increases in aggrecan expression and type II collagen synthesis have been observed after daily 10 or 20 minute LIPUS exposures

Table 2.3 Summary of conditions and results from the reported studies on cellular bioeffects of low intensity ultrasound. Intensities are spatial-average temporal-average unless otherwise specified. τ = pulse duration. Duty cycle = ratio of the pulse duration to the pulse period.

Cell type and preparation	Exposure	Process observed and proposed mechanism	Reference
Co cultured herniated rat intervertebral disk/ peritoneal macrophages	1.5 MHz, τ = 200μs at 1kHz, 30 mW cm^{-2}, 20 min, 4 days	Increased disc resorption	Iwabuchi et al. 2005
Human intervertebral disc cells alginate bead culture	1.5 MHz, τ =200μs at 1kHz, 7.5-120 mW cm^{-2}, 20 min, 5 or 12 days	Increased DNA synthesis after 5 days at 60 or 120 mW cm^{-2}; increased proteoglycan synthesis max at 30 mW cm^{-2}.	Kobayashi et al. 2009
Bovine aortic endothelial monolayer culture	0.5-5MHz, τ = 0.1-5 ms, 10-100% duty cycle, 0.8-2 W cm^{-2}, 0.5-30 min	Increased proliferation, greater for CW exposure and at 1MHz Increased migration, greater at 1MHz than 3.5MHz, and for CW exposure; not thermal or cavitational, transmission of acoustic pressure	Raz et al. 2005
Bovine aortic endothelial cells monolayer and 3D culture	1 MHz, 20% duty cycle, up to 2.2 W cm^{-2}, 15/30 min	Increased proliferation, migration, promotion of angiogenesis.	Mizrahi et al. 2007
Bovine aortic endothelial cells monolayer culture	1MHz CW, up to 1.6 W cm^{-2}, 15 min	Increase in leucocyte adhesion on incubation after exposure, morphological changes; possibly thermal	Maxwell et al. 1994
Rat sciatic nerve Schwann cells in suspension	1 MHz, τ = 200μs at 1.5kHz, 100 mW cm^{-2}, 5 min, 14 days	Increased proliferation	Zhang et al. 2009
Rat sciatic nerve injury	1 MHz, 20% duty cycle, 0.4W cm^{-2}, 10 min, 10 days	Improved function after 2 or 3 weeks, higher number of Schwann cells in treated group	Raso et al. 2005
Rat sciatic nerve injury	1.5 MHz, τ = 200 μs, 1 kHz, 16 mW cm^{-2}, 20 min, 12 days	More myelin fibres, thicker myelin sheath, larger axon area after US	Crisci and Ferreira 2002
Rabbit skin graft *in vivo*	3 MHz, 50% duty cycle, 500 mW cm^{-2}, 5 min, 7 days	Increased cell proliferation, new blood vessels	da Costa Gonçalves et al. 2007
Human gingival fibroblasts in layer culture	1.5 MHz pulsed, 30 mW cm^{-2}, 5 or 10 min, 28 days	Increased alkaline phosphatase, greater for 5min than 10 min exposures after 21 days, increased osteopontin	Mostafa et al. 2009
Mouse L cells (fibroblasts) monolayer culture	1.2 MHz CW, 0.5-3.1W cm^{-2}	Increased DNA synthesis at lower intensities; stable cavitation	Kondo and Yoshi 1985
3T3 fibroblasts in suspension	1MHz, τ = 2ms, 2:8 duty cycle, 0.25-1.5W cm^{-2} I_{SPPA}, 1-20 min	Increased intracellular Ca^{2+}, max at 0.75 W/cm^2; no cavitation, fluid motion at cell surface	Mortimer and Dyson 1988

Rat Achilles tendon fibroblasts monolayer culture	1MHz CW or τ = 2ms at 100 Hz, 400 mW cm^{-2}, 3 min, 1-9 days	PW: matrix damage. CW: Increased proliferation after 3,5 days, increased collagen synthesis after collagenase digestion of matrix	Ramirez et al. 1997
Human foreskin fibroblast culture	1.5 MHz, τ = 200μs at 1kHz, 30 mW cm^{-2}, 6 or 11 min, 7 days	Increased DNA synthesis and cell proliferation, mediated by integrins - mechanosensors	Zhou et al. 2004
Rat Achilles tendon *in vivo*	1MHz CW, 0.5-2 W/cm², 4 min, 30 days	Increase mean collagen fibril diameter, intensity had no effect	Ng and Fung 2007
Rat chondrocytes in culture	1 MHz, τ = 200μs at 1kHz, 50 or 100 mW cm^{-2}, 10 min	Aggrecan expression increase; mechanical, possibly cavitation or streaming, pressure at membrane mechanoreceptors	Parvizi et al. 1999
Human articular chondrocytes 3D Agarose gel culture	1 MHz, τ = 200μs at 1kHz, 18-98mW cm^{-2}, 20 min, 14 days	Aggrecan expression increase, collagen synthesis increase; greater at 48 mW cm^{-2}	Tien et al. 2008
Murine chondrocytes culture	1 MHz, τ = 200μs at 1kHz, 50 mW cm^{-2}, 10 min, 3 days	Increased intracellular Ca^{2+}, increased proteoglycan synthesis, inhibited by depletion of extracellular Ca^{2+}, internal Ca^{2+} stores; mechanical	Parvizi et al. 2002
Human articular chondrocytes monolayer culture, explants culture	1.5 MHz, 30 mW cm^{-2}, 20 min, 6 days	Increased proliferation and matrix production	Korstjens et al. 2008
Porcine articular cartilage 3D sponge/gel culture	1.5 MHz, τ = 200μs at 1kHz, 30 mW cm^{-2}, 20 min, 14 days	Increased proliferation and collagen accumulation; mechanical signal transduction	Takeuchi et al. 2008
Human articular chondrocytes alginate bead culture	1 MHz CW, 100-300mW cm^{-2}, 10 min, 2, 7 or 15 days	Increased type II collagen & proteoglycan synthesis, max at 200 mW cm^{-2}, no change in proliferation	Choi et al. 2006
Rabbit shoulder joint chondrocytes atelecollagen gel culture	1.5 MHz, τ = 200μs at 1kHz, 30mW cm^{-2}, 20 min, 6 days out of 21	Increased chondroitin sulphate content, increased stiffness of culture composite, no change in proliferation	Nishikori et al. 2002
Rat bone marrow stromal cell (osteoblasts) culture	1.5 MHz, τ = 200μs at 1kHz, 30 mW cm^{-2}, 20 min	Altered expression of early response and bone differentiation genes, peak at 3hrs after exposure	Sena et al. 2005
Murine bone marrow stromal cell culture	1.5 MHz, pulsed, 20 min	Osteocalcin increase and early gene expression	Naruse et al. 2003
Human osteoblastic osteocarcoma culture	1.5 MHz, τ = 200μs at 1kHz, 30 mW cm^{-2}, 20 min	Regulation of 165 genes; many related to sensing of mechanical signals	Lu et al. 2009
MC3T3-E1 subclone 14 cells (osteoblasts) Culture	1.5 MHz, 1kHz, 20% duty cycle, 30 mW cm^{-2}, 20 min, 10 days	Increased alkaline phosphatase and mineralization	Unsworth et al. 2007
Murine MC3T3-E1 osteoblasts multilayer culture with type 1 collagen	1.5 MHz, τ = 200μs at 1kHz, 30 or 120 mW cm^{-2}, 20 min, 4 days	Increased prostaglandin, cylooxygenase-2, lysil oxidase expression and no. of cross links, significant at low intensity	Saito et al. 2004

Rat femora bone defect tissue culture	1.5MHz, τ = 2 ms at 250Hz, 320 or 770mW cm^{-2}, 15 min, 7 or 14 days	Increased speed of defect healing, trabecular regeneration, decreased PGE$_2$ secretion after 2 weeks; not thermal, non cavitational mechanical	Sun et al. 1999
Murine tibia *in vivo* bone injury	1.5 MHz, τ = 200µs at 1kHz, 30mW cm^{-2}, 20 min, 3-14 days	Healing delayed by cyclooxygenase inhibition	Huang et al. 2008
MG63 osteoblasts, human periodontal ligament cells culture	3MHz CW, 125-1000mW cm^{-2}, 5 min	Increased fibronectin at 140 mW cm^{-2} in MG63, decreased in PDL, changes in osteopontin, osteonectin etc, no change in proliferation; non thermal	Korstjens et al. 2004
Cultured mouse embryonic bone rudiments	1.5MHz, 30mW cm^{-2}, 20 min, 3 or 6 days	Increased calcified cartilage, osteoblast differentiation, matrix production, no increase in proliferation	Harle et al. 2001
Human fibula *in vivo* delayed union (biopsy)	1.5 MHz, τ = 200µs at 1kHz, 30 mW cm^{-2}, 20 min, 87 days	Increased bone volume and mineralized volume in bony callus and trabecular bone	Rutten et al. 2008
Rabbit chondrocytes, osteoblasts, *in vivo* bone-tendon junction	1.5 MHz, τ = 200µs, 30 mW cm^{-2}, 20 min, 5 days/week, 2-16 weeks	Increased expression of VEGF (2-4 wks) and cartilage formation, remodeling Non thermal,	Lu et al. 2008
Rabbit fibula *in vivo* bone injury	1.5MHz, τ = 2ms at 250Hz, 500mW cm^{-2}, 15 min	Increased bone formation, increased tortional stiffness with US not with equivalent temp rise (~10 °C) delivered by microwave exposure; probably not thermal	Chang et al. 2002
Frog skin *ex vivo*	1MHz, CW or τ = 2ms at 100Hz, 60-2000mW cm^{-2} nominal, up to 20 min	Decreased membrane potential and resistance with intensity, reversible. Increased ionic conductance greater with pulsed than continuous exposure; non thermal, cavitation	Dinno et al. 1989
Frog skin *ex vivo*	1MHz CW, 300mW cm^{-2} nominal, 10 min	Increased ionic conductance with US in presence of Ca^{2+} ions; cavitation	Al-Karmi et al. 1994
Human hepatocarcinoma cells suspension	0.4-1.7 MHz CW or pulsed 10-90% duty cycle, 170-430mW cm^{-2}	Increased rhodamine 123 uptake and retention, max with 0.8 MHz, increased with increasing energy density, max at 60% duty cycle	Zhai et al. 2008
Human metastatic lung carcinoma, epidermoid carcinoma and MDR variants culture	1MHz, 50-100% duty cycle, 400mW cm^{-2}, 20 min	US and non US induced hyperthermia (41 °C, 20 min) increased cellular rhodamine 123 and DOX accumulation; thermal	Liu et al. 2001
HeLa cells in suspension	0.8 MHz CW, 50-500 mW cm^{-2} (SA), 5 or 10 min	Inhibited proliferation, cells in M and S phases of cell cycle	Hrazdira et al. 1998
SaOS-2 osteoblasts, HUVEC monocultures, co-culture	1.5 MHz, τ = 200µs at 1kHz, 30 mW cm^{-2}, 20 min	Increase in PDGF secretion in co-culture, not seen/significant in monocultures; mechanical	Ito et al. 2000

(Parvizi et al. 1999; Tien et al. 2008). Aggrecan expression and collagen synthesis were higher at an acoustic intensity of 48 mW cm^{-2} than at lesser or greater intensities (in the range 18 – 98 mW cm^{-2}). Increased proteoglycan synthesis was inhibited by depleting extracellular calcium or internal cellular calcium stores (Parvizi et al. 2002). Increases in chondrocyte proliferation after LIPUS exposure were also observed in some studies (Korstjens et al. 2008; Takeuchi et al. 2008), but not in others (Nishikori et al. 2002; Choi et al. 2006).

Osteoblasts are bone forming cells, which synthesise type I collagen and other components of bone matrix and initiate calcification. Exposure of osteoblasts to ultrasound alters expression of early response genes, bone differentiation genes (Sena et al. 2005) and osteocalcin, a protein involved in bone mineralisation (Naruse et al. 2003). Another study found that ultrasound exposure regulated 165 genes, including those involved in sensing mechanical forces, inhibition of osteoblast proliferation, extracellular matrix production and bone remodelling (Lu et al. 2009). Ultrasound exposure also increased expression and activity of alkaline phosphatase (Unsworth et al. 2007), as noted above for fibroblasts. Levels of prostaglandin and cyclooxygenase-2, which is involved in production of prostaglandin, were increased in murine osteoblasts after ultrasound exposure (Saito et al. 2004). Levels of prostaglandin-E2, a chemical messenger involved in inflammation, were also found to accumulate with increasing ultrasound intensity. Decreases in prostaglandin-E2 secretion, compared to control levels in a bone defect model, were observed after exposure to ultrasound at a higher acoustic intensity (300 or 770 mW cm^{-2}) (Sun et al. 1999). The biological effect of prostaglandin-E2 is biphasic; low concentrations increase mineralisation, while high concentrations decrease it. This may explain why studies on intact bone showed that lower intensity ultrasound treatment proved to be more beneficial to bone healing. When cyclooxygenase-2 was inhibited in an *in vivo* bone healing model, ultrasound induced healing was delayed, but not totally stopped (Huang et al. 2008).

Low intensity ultrasound is used for bone healing treatment clinically; it has been reviewed in detail by e.g. Claes and Willie (2007) and Malizos (2006). Many studies have been performed to clarify the processes involved. Studies have recorded that ultrasound exposure increased osteoblast differentiation and matrix production

(Korstjens et al. 2004), but did not affect osteoblast proliferation (Harle et al. 2001; Korstjens et al. 2004); this is contrary to observations of other cell types. Rutten et al. (2008) found that exposure of human fibula *in vivo*, increased bone volume and mineralised volume in newly formed bony callus and trabecular bone. No differences were observed in cortical bone. The study found that bone healing was accelerated by increased osteoblastic activity. This study investigated differences in the bone matrix after treatment, but other studies provide more of a link between cell culture and *in vivo* studies by examining messenger responses in diverse cell populations. Ultrasound exposure was found to increase the rate of cartilage formation, remodelling and expression of vascular endothelial growth factor (VEGF) in chondrocytes and osteoblasts in a rabbit bone-tendon junction model (Lu et al. 2008). There is some evidence that non-thermal mechanisms are involved in bone healing. Ultrasound exposure was found to increase torsional bone stiffness, which was not observed after an equal non-ultrasound-induced temperature rise ($\Delta T \sim 10$ °C) (Chang et al. 2002).

One consistent conclusion from these studies is that ultrasound produces some effect at lower intensities, which is not seen at higher intensities. This indicates a need for exploration of exposure parameters to optimise treatments. It is also apparent that ultrasound can accelerate processes involved in the early stages of healing, so the timing of application of these therapies should also be optimised.

2.5.2 Cellular mechanisms of sensing external forces

An important part of understanding physiological responses to ultrasound is establishing how the cell senses ultrasound and how this is transduced into a metabolic response. It is likely that the process of signal transduction starts at the cell membrane. As set out earlier, there are many proteins in the lipid membrane of a cell that transport ions and signal molecules across the cell membrane, or act as binding sites for chemical messengers, provoking a response inside the cell.

Ion channels are vital in maintaining the electrical potential across the cell membrane, the cell volume and other parameters important in cell homeostasis. There is evidence that ion channel activity is sensitive to ultrasound. The effect of 1 MHz ultrasound

(0.06-2 W/cm^2, pulsed, up to 20 min) on ionic conductance has been investigated using frog skin as a biological model (Dinno et al. 1989). The role of calcium ions in the response of cells to ultrasound was also investigated using this model (Al-Karmi et al. 1994). Exposure to ultrasound was shown to reversibly increase ionic conductance; the mechanism in this case was thought to involve cavitation and microstreaming. As mentioned previously, calcium uptake in fibroblasts was increased by exposure to ultrasound (Mortimer and Dyson 1988). No significant increase in temperature was measured, but the authors suggested that small temperature changes at the cell surface could be responsible, as these ion channels are known to be temperature sensitive (Schatzmann and Vincenzi 1969). Changes in intracellular calcium levels lead to a variety of cellular responses, such as changes in smooth muscle tone and the processes of cell growth, proliferation and differentiation.

Exposure to ultrasound can alter the permeability of the cell to drugs, which is exploited in combatting multidrug resistance (MDR) in cancer cells, which is a major limitation in chemotherapy. This concept has been demonstrated by a study showing that cellular retention of rhodamine 123 in human hepatocarcinoma cells in suspension was increased by exposure to ultrasound (Zhai et al. 2008). Uptake was maximised in samples exposed to 0.8 MHz ultrasound and also increased with increasing acoustic intensity while the energy density was kept constant (exposure duration and duty cycle, and intensity were varied). Retention increased with increasing % duty cycle until 60%, then began to decline. Another study found that the mechanism for ultrasound induced drug uptake changes in human metastatic lung carcinoma and MDR variant in culture, and human epidermoid carcinoma and MDR variant in culture was thermal. Similar benefits were produced by non-ultrasound induced hyperthermia (41 °C, 20 min) (Liu et al. 2001).

2.5.3 Ultrasound interaction mechanisms

In this section, studies on the influence of thermal and non-cavitational mechanical effects of ultrasound on cells are outlined. Thermal effects, as a mechanism of ultrasound interaction, are often dismissed when the temperature rise is known to be small ($\Delta T < 1\text{-}2$ °C). In many of the studies mentioned above, heating was not measured, although the experimental design makes it likely that some temperature

elevation did occur. Temperatures of 56°C or more are employed to kill cells. As temperature increases, cell death by apoptosis becomes likely at about 43°C, proteins begin to denature, and above this temperature, the exposure time needed to induce thermal death halves for each degree the temperature is increased (Miller and Ziskin 1989). Non-lethal cellular effects can occur at lower temperatures. For example, temperature elevations of 1 or 2 °C can influence the growth of cells (Morrissey et al. 2009) and cause heat shock proteins to be released (Park et al. 2005). Mild hyperthermia is used in combination with chemotherapy or radiotherapy in cancer treatment, as it can increase the effectiveness of treatment by increasing tumour oxygenation (Song et al. 2009).

More transient effects of mild hyperthermia of a fraction of a degree have also been noted at the cellular level, such as in the sensitivity of ion channels (Schatzmann and Vincenzi 1969) and whole-tissue level effects such as artery constriction, mediated by potassium ion channel activation, leading to changes in intracellular calcium (Mustafa and Thulesius 2005; Mustafa et al. 2007). Potassium channels are universal in cell membranes, so if vascular smooth muscle cells are affected, then heating could elicit similar responses in other cell types. Other groups have investigated the effect of cooling on vascular tone, Herrera et al (2000) reported opposite effects due to cooling in two vessel types. Cooling induced relaxation in rat aorta, while inducing contraction in pig renal artery. Contraction was inhibited by calcium depletion; it was therefore proposed to be related to intracellular calcium stores and was associated with a metabolic mechanism. Relaxation was independent of calcium levels, and was associated with structural factors. Another group (Oo et al. 2007) reported differences between the effects of rapid and slow cooling on tone in human radial artery sections. Rapid cooling induced rapid transient contraction, with an accompanying increase in intracellular calcium, due to release of calcium from intracellular stores. Slow cooling over a period of 20 to 30 minutes induced relaxation and a corresponding reduction in intracellular calcium. Re-warming of these artery rings after cooling, stimulated contraction and increased intracellular calcium. This was partly due to activity of L-type calcium ion channels in the cell membrane. Wang et al (1991) explored the temperature dependence of this type of calcium channel, reporting that the calcium current increased as temperature increased from 22 ℃, peaking at 35 ℃ before

decreasing slowly by a small fraction of the increase. The timescale of activation and inactivation of the channels was also shortened by increased temperature. These studies suggest that temperature changes may affect different parts of the cell differently and that the time course of temperature change may be important in producing these varied outcomes. It is also clear from these studies that temperature affects the function of vascular smooth muscle. The cellular effects of hyperthermia are reviewed by Hildebrant et al. (2002). Sensing of thermal signals by the cell membrane and related intracellular signal pathways are reviewed by e.g. Park et al. (2005).

The mechanisms responsible for changes in protein function and therefore ion channel activity are not clear. However, it is becoming apparent that membrane protein function depends on the physical state of the surrounding phospholipid molecules. Membrane lipids are in a state very close to phase transition, and as such they are very sensitive to temperature. Small changes in temperature could therefore have a large effect on membrane function. Mechanical effects such as cavitation and microstreaming could interact with the cell membrane via the lipid bilayer or by exerting forces directly on membrane proteins, altering their function. Both thermal and mechanical bioeffects mechanisms are discussed in more detail by O'Brien (2007).

On present evidence, it seems possible that non-lethal cellular responses to ultrasound may depend on both mechanical and thermal effects. To determine the relative importance of interactions, exploration of the effect of ultrasound exposure parameters on cellular effects is needed. There are a limited number of studies which address this need thoroughly and systematically.

2.5.4 Physical mediators of vascular tone

It is known that fluid shear stress affects endothelial cells and that ultrasound is capable of generating shear stresses. The source of fluid shear stress generated by ultrasound is acoustic streaming, which is more substantial when propagation of ultrasound is nonlinear and harmonics are generated. For a 3.5 MHz ultrasound beam with an acoustic intensity of 1 W/cm^2, a pressure gradient of 4 Pa/mm was predicted (Starritt et al. 1991) if propagation of the wave in water was linear, and a pressure

gradient of 700 Pa/mm if propagation was nonlinear. Van Bavel (2007) calculated from this that transient shear stresses of 8 Pa and 1500 Pa could be generated in a vessel of 8mm diameter in the direction of the beam, with linear propagation and with nonlinear propagation respectively. The real level is likely to be much lower in smaller vessels at other angles of insonation. However, both of these estimates are above normal physiological levels of steady shear stress, which are of the order of 2-4 Pa in large arteries away from bifurcations.

Shear stress alters many aspects of endothelial function including the release of nitric oxide, a smooth muscle relaxant, causing flow dependent dilatation on the scale of minutes. The mechanisms responsible for sensing physiological shear stresses may be the same as the mechanisms related to the higher levels, associated with the stresses created by ultrasound exposure. There may also be some further mechanisms that sense these higher levels. It is suggested that some ion channels act as stress sensors. For example, the opening of potassium channels in the endothelial cell membrane due to stress, causes calcium channels to open, causing an influx of calcium, which activates nitric oxide synthase, causing the production of nitric oxide (Geiger et al. 1992; e.g. James et al. 1995). Nitric oxide can also be produced without the involvement of calcium.

The time-course of the shear stress can also affect the release of vasoactive substances. Frangos et al. (1996) demonstrated that nitric oxide production occurs in response to shear stress by two independent mechanisms, depending on the nature of the shear stress. Cells were exposed to shear stress that was either stepped or ramped from 0 to 2 Pa and followed by steady flow for several hours. The increase in NO production due to stepped shear stress was greater than that due to ramped shear stress. The rate of production then decreased during the period of steady flow. These levels were several times higher than those measured in the control. Cells were also exposed to a pulse of shear stress, which caused a high rate of NO production straight away, but not in the long term. This response to a change in shear stress was shown to be G protein-dependent, while the NO production produced by steady flow occurred through a G protein-independent mechanism.

Nitric oxide and endothelin-1 production in response to steady laminar shear stresses, periodic step changes (square wave), oscillating (sinusoidal) and turbulent shear stresses has also been investigated (Noris et al. 1995). Periodic shear stresses caused large increases in NO production, while oscillating shear stresses caused smaller increases. Turbulent flow had no significant effect on NO production. Turbulent flow occurs around sights of vessel narrowing and occlusion, so NO production may be decreased in these areas. This fact seems to agree with evidence suggesting that NO has a protective effect against atherosclerotic plaque formation. Periodic shear stress caused a slight increase in the release of the vasoconstrictor endothelin-1 and there was a decrease in its release under the other conditions. A decrease in the production of endothelin-1 was also measured by Malek and Izumo (1992) in response to pulsatile and turbulent shear stress. This complex pattern will require careful consideration in establishing the transduction mechanisms for ultrasound.

The dependence of shear stress induced vascular constrictions on the endothelium was investigated by Bryan et al. (2001), in rat cerebral arteries with and without intact endothelium. Arteries with intact endothelium showed a smaller response to shear stress, which was not due to release of NO, prostacyclin or EDHF from endothelial cells. They claim that the reduction in response may therefore be due an unknown dilating mechanism involving the endothelium or by attenuation of mechanical forces across the endothelium. Reactive oxygen species (ROS) generated by smooth muscle seemed to be involved in the response; scavengers of ROS attenuated the constrictions.

Shear stresses acting on the cell membrane due to oscillation of microbubbles in an acoustic field and microstreaming around them, is thought to be the mechanism by which changes in cell permeability are induced in sonoporation (Wu and Nyborg 2008). Shear stress can also affect endothelial cell viability. It has been shown (Dunn, 1985) that shear stresses equivalent to those generated by acoustic streaming in a beam with an acoustic intensity of 3 W cm^{-2}, decreased the time taken for the cell population to fall to a survivng fraction of $\frac{1}{10}$ in a temperature dependent manner. At 37 °C shear stress did not affect the cell survival curve. At 41.5°C the surviving fraction was not decreased by heat only, but the addition of shear stress did decrease

the surviving fraction. The experiment was performed using a cell suspension so it is difficult to relate the results to *in vivo* conditions.

2.5.5 Mechanotransduction in cells

The ability of cells to sense and respond to mechanical forces is essential to normal growth and development. Impaired responses are implicated in diseases ranging from atherosclerosis to arthritis. Recognition of this importance has stimulated increasing efforts to establish the underlying mechanisms. For example, endothelial cells act as sensors of pressure and shear stress from blood flow (Dunn 1985; Bryan et al. 2001). These forces are sensed at the cell membrane by shear-activated potassium channels and stretch-activated channels. Other cells, such as those in soft tissue and bones, may sense forces transmitted from deformation of proteins in the extracellular matrix, for example, bone cells sense flow in the canaliculi. These strains are transduced by the cell membrane and coupled into the cell cytoskeleton and cytoplasm, where they initiate intracellular signalling cascades. These signal cascades can in turn influence cell functions, such as proliferation and gene expression, which are the type of responses initiated by exposure to ultrasound. These signal transduction mechanisms, and the resulting intracellular signals, are reviewed in more detail by Lehoux and Tedgui (2003) and Huang et al. (2004).

Clearly, cells can respond to physical forces by producing chemical signals. The forces must therefore interact with some structure in the cells in order to produce a response. Current thinking on mechanotransduction in cells is reviewed by Huang et al. (2004). Transducers of mechanical forces in cells include mechanosensitive ion channels, which may be controlled by membrane tension transmitted by the extracellular matrix or cell cytoskeleton. Mechanosensitive ion channels and signalling in endothelial cells related to the response to shear stress, have been studied by Malek and Izumo (1996). Membrane and intracellular signal transduction in vascular cells is also discussed by Lehoux and Tedgui (2003). Force transduction in vascular endothelial cells and related vascular responses are reviewed by Davies (1995) and also discussed by VanBavel (2007).

Other proteins within cells may also act as mechanosensors, undergoing conformational changes caused by forces transduced through the cytoskeleton. Effects on gene expression may be caused by forces transmitted through the cytoskeleton to the nucleus of the cell (Lehoux and Tedgui 2003). In the long run it will be necessary to investigate the effects of ultrasound at this level.

2.5.6 Discussion and Conclusions

The literature concerning cellular bioeffects reviewed here demonstrates a wide variety of cellular responses to ultrasound. A summary is provided in Table 2.3. An increase in cell proliferation after ultrasound exposure was measured in several cell types, but other than this, few recurring observations were noted. A systematic investigation of cellular effects and dose response is needed. The radiobiology of cells is known to be different throughout the cell cycle; it may therefore be likely that cells in different states will respond differently to ultrasound. This has been briefly discussed by Hrazdira et al. (1998).

Cell culture conditions are far from the normal environment of the cell. Physiological and pathological processes of growth and remodelling result from symbioses between different cell types and interactions with the extracellular matrix, that depend on the exchange of a variety of chemical and physical signals. The studies reported here employ only monoculture cells. Co-culture systems, in which these interactions can be simulated, are only slowly being developed and few have been applied to ultrasound studies. Differences were found in one such study between the response to ultrasound of monoculture osteoblasts and endothelial cells and those in co-culture (Ito et al. 2000), demonstrating that interactions between cell types are important. Cells in suspension, or in culture plates will be metabolically abnormal and feel many more fluid mechanical forces than they would *in vivo*, in contact with the extracellular matrix and other cells. These problems are not unique to ultrasound studies, but are a problem in all cell culture studies. Cells grown in more tissue like structures such as gels or cartilaginous matrices, may prove a more realistic model and may enable the use of improved ultrasound exposure conditions. Combined with improved acoustic output measurement, it should then be possible to link cell culture and *in vivo* studies. There is also some gap between conditions in *in vitro* tissue studies and *in vivo* models.

In vitro tissue samples are not connected to nervous feedback systems and there is the possibility of damage on excision. There are other differences, such as lack of perfusion and surrounding tissue, which would dissipate heat *in vivo*. These factors mean that even in tissue models, we must be careful in extrapolating effects measured *in vitro* to *in vivo* models. However, this review has presented some cases where similar effects were observed in both *in vitro* and *in vivo* studies.

There is also a lack of systematic investigation of the effects of ultrasound exposure parameters on cell function and also on *in vitro* tissue and *in vivo* bioeffects. This is essential in order to determine mechanisms of ultrasound interaction. A few of the reported studies mention processes involved in inflammation, but further work is needed to clarify the effects of ultrasound in this context with relevance to physiotherapy. Further work is essential in order to optimise treatment protocols for the therapeutic applications discussed here, and may produce evidence for new applications in therapeutic ultrasound.

3 Experimental design

The first section of this chapter gives a description of the ultrasound equipment, force measurement system, perfusion myograph and the experimental design process. The second half of this chapter gives details of the measurements and processes used to characterise the acoustic field.

3.1 Ultrasound system description

This section describes the ultrasound system used throughout this study. The transducer was a nominal 3 MHz narrow bandwidth transducer, with a single circular damped lead zirconate titanate (PZT) element, and was weakly focused. The transducer was manufactured by Diagnostic Sonar, Livingston, UK, model number MD3483. The radiating area was 3.8 cm^2 and the diameter was 2.2 cm. Further details of the acoustic field are given in the following sections.

The input signal was generated by an Agilent 33220A signal generator (Agilent, Wokingham, UK). This was used to create continuous wave and pulsed wave input signals of variable amplitude, pulse length and pulse repetition frequency. The signal was amplified by a 150A100B radio frequency power amplifier (Amplifier Research, Souderton, PA, USA), before being fed to the transducer.

For measurement of the acoustic field and positioning of tissue samples, a Precision Acoustics 0.2 mm PVDF (polyvinylidene fluoride) needle hydrophone and preamplifier was used; this is described in more detail in Section 3.6.2. The signal from the hydrophone was visualised on a Hameg HM504-2 oscilloscope (Hameg, Mainhausen, Germany) for positioning and peak acoustic pressure measurement. A PicoLog ADC-20 High Resolution Data Logger unit (Pico Technology, Cambridgeshire, UK) and PicoScope PC oscilloscope software were used for acoustic intensity calculation.

3.2 Isometric force measurement system

A high sensitivity FORT25 force transducer (World Precision Instruments Inc., Sarasota, FL, USA) was used to make isometric force measurements up to 25g. A stainless steel hook was attached to the force transducer. The tissue was mounted between this and another stainless steel rod, the position of which could be fixed. The stainless steel rods were cushioned with PVC tubing to reduce damage to the endothelium of the tissue sections. The force transducer was connected to a WPI TBM4M bridge amplifier (World Precision Instruments Inc, as previously). This signal was detected by an ADC-20 High Resolution Data Logger connected to a computer and displayed in real time using PicoLog Data Acquisition software (Pico Technology). The signal was sampled at 1 second intervals; this provided adequate temporal resolution for measurement of tension changes and enabled data acquisition over long time periods. The data files were saved and exported to Microsoft excel for processing.

3.3 Design of apparatus – stage 1

A system was designed to incorporate the elements and requirements of the ultrasound system with the isometric force measurement system and the tissue support system. This section details the considerations of different aspects of the design process. The complete initial set up is shown in Figure 3.1.

Coupling of the transducer

The ultrasound transducer was coupled with ultrasound gel to the bath via a TPx (polymethylpentene) membrane window (Goodfellow, Huntingdon, UK) in the side of the tank. The acoustic properties of TPx provide good coupling of the beam with the water tank; the acoustic impedance is well matched so that there was very little disturbance of the field. The transducer was held using a clamp stand and coupled to the side of the tank so that the beam axis was horizontal and perpendicular to the tissue supports. The use of an acoustic window enabled easy removal and positioning of the transducer. This allowed the transducer to be removed and coupled to the power balance so that measurements could be made before each set of experiments. However, coupling the transducer in this way may have increased positioning errors.

To minimise these errors, hydrophone measurements were used to determine the position and amplitude of the focal region for positioning of the tissue. The transducer was not moved once the system had been set up for each set of experiments.

Absorber

The acoustic impedance of materials along the beam path must be considered during the experimental design process. The transducer was coupled either to a TPx membrane or directly into the solution. Under later experimental conditions there was an additional thin polythene membrane. These barriers along the path of the beam between the transducer and tissue must be closely matched in terms of impedance to avoid reflections of the beam which would cause difficulty in establishing the properties of the acoustic field at the point of interest. Another major consideration is the reduction of reflections. This is important at the end of the beam path and around the sides of the ultrasonic bath, so that consistent measurements can be performed, and in order to simulate free-field conditions.

Reflections from impedance mismatches at the tank boundaries could give rise to interference effects and produce areas of high acoustic intensity and elevated heating. To eliminate these problems the tank was lined with Aptflex 28 acoustic absorber obtained from Precision Acoustic Ltd., Dorchester, UK. The absorber consists of a single homogeneous layer of a polyurethane rubber type material. The density is 1.01 kg m^{-3} which is well matched to the density of water.

Ultrasound bath dimensions

Because of the requirements of the tissue support system, it was advantageous to create a bath in which experiments could be performed that was of a relatively small size. In order to determine the minimum size of the ultrasound bath, the following considerations were made. The focal depth of the transducer was approximately 8.5cm. The needle hydrophone would be placed with its tip at this point during measurements. The hydrophone is 10 cm in length in total including the needle and preamplifier. A further 3.5 cm was added to allow for the hydrophone cable, for movement and for measurement of points in the field beyond the focal region; this amounted to a length of 22 cm in total. The width of the tank had to be enough to

allow several cm on either side of the tissue, which was 7cm in total. The depth of the tank had to be enough so that the focal region was a few cm from the bottom of the tank and several cm deep in the water to reduce reflections from the water surface; at least 7 cm. The tank would be lined on all sides with the acoustic absorber which is acquired in 1cm thick tiles, which were cut into sections to fit the bath. An extra 2 cm was added to the width and length of the tank and 1 cm to the depth to accommodate this. In the event, a Perspex tank of a greater depth and slightly larger area was acquired. This was cut down to size in the workshop and a circular window was cut into one end. The internal dimensions were 12 cm x 24 cm x 13.5cm. A mechanism was manufactured with which to clamp a disc of TPx across the window. This consisted of two Perspex rings, one of which was bonded to the tank and contained a circular groove in which a rubber 'O' ring as placed. The second ring was screwed into the first ring with 6 Perspex thumb screws, clamping the TPX disc in between. This method provided a secure watertight seal and easy removal of the membrane for cleaning and replacement.

Ultrasound bath fluid

A volume of fluid is required for propagation of the ultrasound beam because the impedance of the transducer is matched to that of soft tissue/water. Ideally, for measurement purposes this would be filtered degassed deionised water. In this system, this was not possible as the tissue was immersed in the water bath; the fluid had to be a buffer which supported the function of the tissue. Krebs-Ringer buffer was used as the tissue support medium. Originally a commercially available bicarbonate Krebs-Ringer buffer solution was used (in g/L: 0.1 $MgCl_2 \cdot 6H_2O$, 0.34 KCl, 7.0 NaCl, 0.1 Na_2HPO_4 (anhyd), 0.18 NaH_2PO_4 (anhyd), 1.8 D-glucose, plus 1.26 $NaHCO_3$) (Sigma Aldrich). To achieve the correct pH, the solution was bubbled with a 95% O_2 5% CO_2 mixture. This was impractical during experiments and the introduction of gas into the solution in this way was undesirable in the context of ideal ultrasound measurement conditions. Another formulation was obtained for a buffer solution containing HEPES which did not require bubbling with O_2/CO_2 mixture during experiments. The formula was as follows: 119 mM NaCl, 5 mM HEPES, 2.3 mM $CaCl_2$, 5 mM KCl, 1 mM KH_2PO_4, 25 mM $NaHCO_3$, 5 mM D-Glucose. This buffer was made up the day before experiments, stirred and stored at 4 °C until used. The pH of the solution was measured and

adjusted to pH 7.4 at 37°C using HCl and NaOH before use. The size of the ultrasound bath decided upon in the first instance required 1.5 l to 2 l of buffer for each set of experiments.

Heating system

In order to support function of the tissue and replicate physiological conditions, the experiments were performed at body temperature. A heating system was therefore incorporated into the water bath. This consisted of an external temperature controlled water bath held at a temperature several degrees above 37°C. This water bath was fitted with a pump to circulate the water through a tube positioned in the ultrasound water bath. The buffer solution in the bath was heated by the water circulating through the tube and the temperature of the external water bath was adjusted until the correct buffer temperature was achieved. In the first iteration the water was pumped through a plastic tube from the water bath into a coiled copper tube which was immersed in the ultrasound water bath. This provided good heat exchange with the buffer solution but produced several major problems. The coil was quite large and was positioned in the path of the ultrasound beam. The coil was likely to act as a source of reflections, affecting the acoustic intensity at the focal region in a non reproducible manner. The copper of the tube was not stable when immersed in warm salt solution and the pH of the buffer solution was affected. As an alternative to the copper coil, a long piece of plastic tubing was connected to the water bath pump and coiled around the inside edge of the base of the bath several times. Although the plastic tubing was not as good a heat exchanger as the copper, it was inert, could be positioned easily on the periphery of the ultrasonic field and was less likely to cause strong reflections. By using a sufficient length of tubing to form several loops around the tank, the required heating was achieved. The temperature was held consistently at an average of 37.7 ± 0.44 °C [mean ± sd] over all experiments.
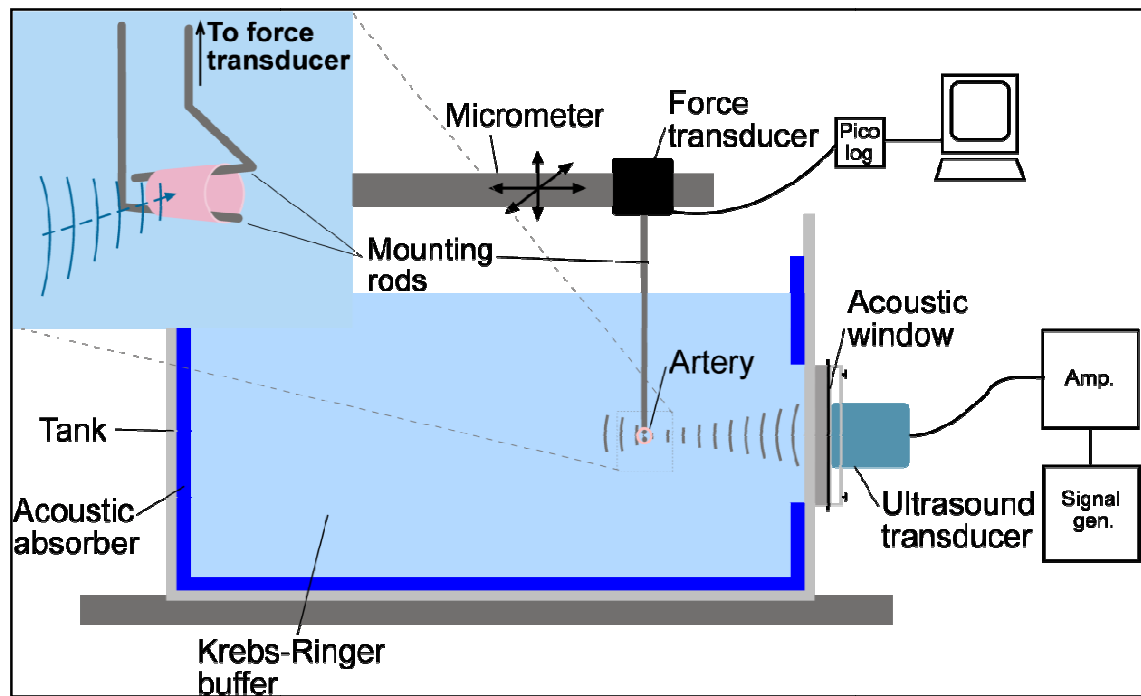
Figure 3.1 Schematic diagram of experimental set up, the tissue is mounted in the focal region of the ultrasound beam on stainless steel hooks attached to the force transducer, the signal is recorded in real time using a PicoLog unit, the tissue is exposed to ultrasound from the transducer mounted at the acoustic window which is driven by a signal amplified by an RF amplifier. The expanded section shows the orientation of the tissue relative to the ultrasound.

Positioning system

A system to enable precise and reproducible positioning of the tissue sample with respect to the focal region was required. A micromanipulator system was used to allow small adjustments independently in 3 orthogonal directions. In order to ensure reproducible positioning of the tissue sample with respect to the focal zone, a holder was built that would geometrically fix the position of the hydrophone tip relative to the tissue. A holder was made for the hydrophone in the form of a Perspex ring which fitted tightly over the hydrophone preamplifier. This was attached by a vertical rod to a connecting block from which another rod extended vertically; this was mounted in the holder attached to the micromanipulator system. Once the acoustic pressure was recorded, the hydrophone was removed and the force transducer was inserted into another hole at a distance of 6 cm away. The hook attached to the force transducer was then positioned in the focal plane, just above the beam, so that the tissue was

stretched through the beam axis when in position. The other stainless steel support was held in another micromanipulator to allow careful adjustment of the vertical position for stretching of the tissue. This was fixed to a base plate that moved along the beam axis with the force transducer. The distance perpendicular to the beam axis was variable.

3.4 Design of apparatus – stage 2

In a later set of experiments it was necessary to add vasoactive chemicals to the buffer for ion channel experiments and endothelial function tests. For safety reasons it was important to reduce the volume of buffer so that a lower chemical concentration could be used. It was also important to ensure that these chemicals were removed from the bath after testing and that this was done with minimal disturbance of the tissue. With this aim, a system was developed to flush the bath with fresh buffer. It was obvious that a smaller container would be required for the tissue bath. The size constraints on the system due to the ultrasound field dimensions and measurement requirements obviously remained unchanged. Therefore an inner chamber was developed that would fit within the original bath with the following constraints. It had to be possible to hold the container in place without interfering with the isometric force measurement and tissue mounting. The walls of the container had to be transparent to the acoustic beam and cause minimal disturbance of the field. The container had to be easy to slot into place after acoustic pressure measurements were made for tissue positioning.

A container was made of a thin polythene tube sealed at one end and clamped through a 6cm diameter circular hole in a sheet of Perspex, against a Perspex ring using 4 plastic thumbscrews. The sheet of Perspex had clips at either side to secure it over the sides of the tank for stable positioning. The stainless steel rods for tissue mounting were passed through the circular opening in the Perspex sheet into the polythene tube. The tube was then filled with buffer and the tissue was mounted in the normal way. The rest of the bath was filled with degassed distilled water. The arrangement is shown in Figure 3.2.

The thickness of polythene used was 62.5 µm; this was strong enough for the purpose and the attenuation was a few percent, which was an acceptable loss. The polythene was bought as a roll of continuous 10 cm wide flat tubing (medium duty layflat tubing, Key Industrial Equipment Ltd., Dorset, UK). Sections were cut from the roll and sealed at one end using a plastic welder. The sections were washed before use to remove any chemicals which may affect the tissue (although the tubing was sold as food grade) and disposed of after use. Bubbles were carefully removed from the surfaces of the polythene membrane during experiments by gentle wiping with a cotton bud.
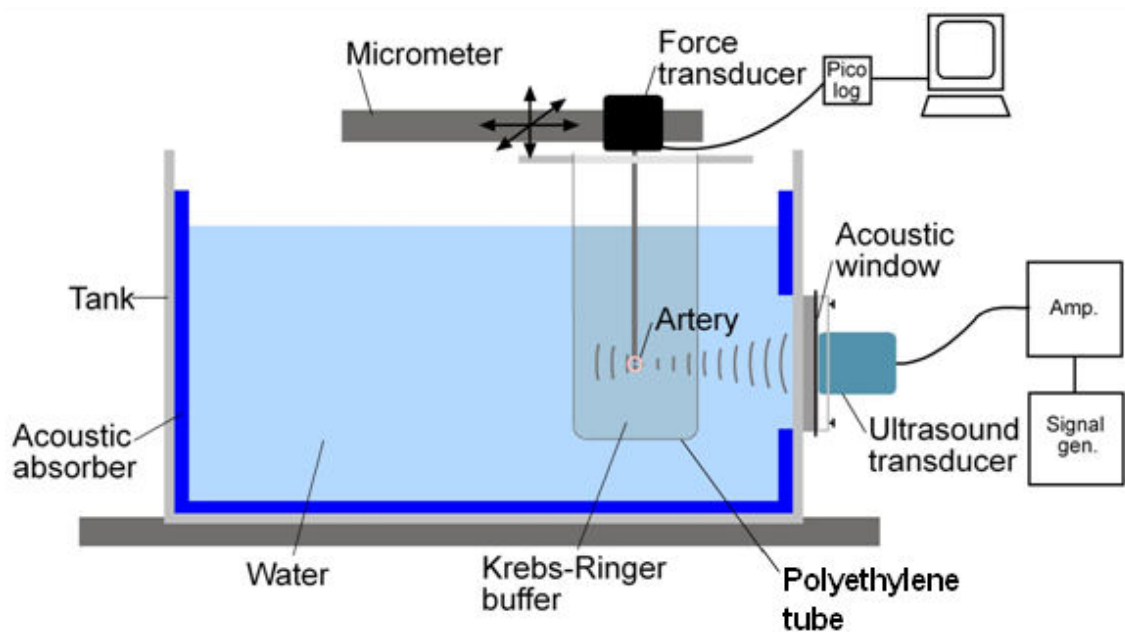
Figure 3.2 Schematic diagram of water filled ultrasound bath lined with acoustic absorber with buffer filled polyethylene tube insert clamped between a Perspex sheet and ring within the bath in order to contain and enable flushing of the buffer. Tissue was positioned within the polythene container, mounted and insonated as previously.

Flushing system

A system of tubes was designed to flush fresh buffer into the bath insert and remove waste buffer to a container for later disposal. Approximately 1.5 times the volume of fluid in the tissue bath was used for flushing. Fluid was preheated to 38°C and pumped from a beaker through a plastic tube by a peristaltic pump. The tube was threaded through a plastic T-piece which was clamped to the Perspex sheet using a hose clip. The tube ran down one side of the polythene container with the tip

positioned at the bottom. The waste tube was held in a similar manner, threaded through a plastic T-piece, this time with the tip positioned at the normal level of the fluid surface. The fluid was pumped through this tube by siphoning the fluid using a syringe inserted into a 3 way tap at a lower height than the fluid level in the bath. A waste bottle was situated on the floor beneath the work bench; fluid continued to drain into it until the surface level dropped below the end of the drainage tube.

This system enabled exchange of fluid without draining the container and exposing the tissue to the air. This was used for processes such as endothelial function tests where the tension was measured as two vasoactive drugs were added. The medium was then refreshed so that the tissue could return to normal and further experiments could be performed. The waste fluid was contained within a bottle which could be safely removed for disposal. The bottle had a lid with two holes, one for the drainage tube to enter, the other for air to escape. This helped to minimise risk of spillage and exposure to chemicals during experiments.

3.5 Design of perfusion myograph system

The next stage of experiments required the design and construction of a new apparatus suitable for mounting much smaller vessels than those used previously. For these small vessels with diameters of the order of 1 mm, a perfusion myograph was constructed, departing from the wire myograph system used previously. The wire myograph system as used for making isometric force measurements on large vessels. The mounting system was too large for mounting of small vessels. The perfusion myograph system was intended for examination of small vessels under more physiological conditions, this system was not large enough to accommodate the large vessels. The requirements for design of the perfusion myograph system were to integrate a vessel mounting rig and pressurisation system, optical imaging system for diameter measurement, buffer flushing system and bath heating with the acoustic field.

The vessels were tied on to small glass pipettes connected to a pressurising system. The pipettes were mounted in a small bath with an optical window in the bottom,

which was placed over the objective of an inverted microscope for imaging of the vessels. The vessel diameter was recorded during exposure to ultrasound. The system is shown in Figure 3.3.
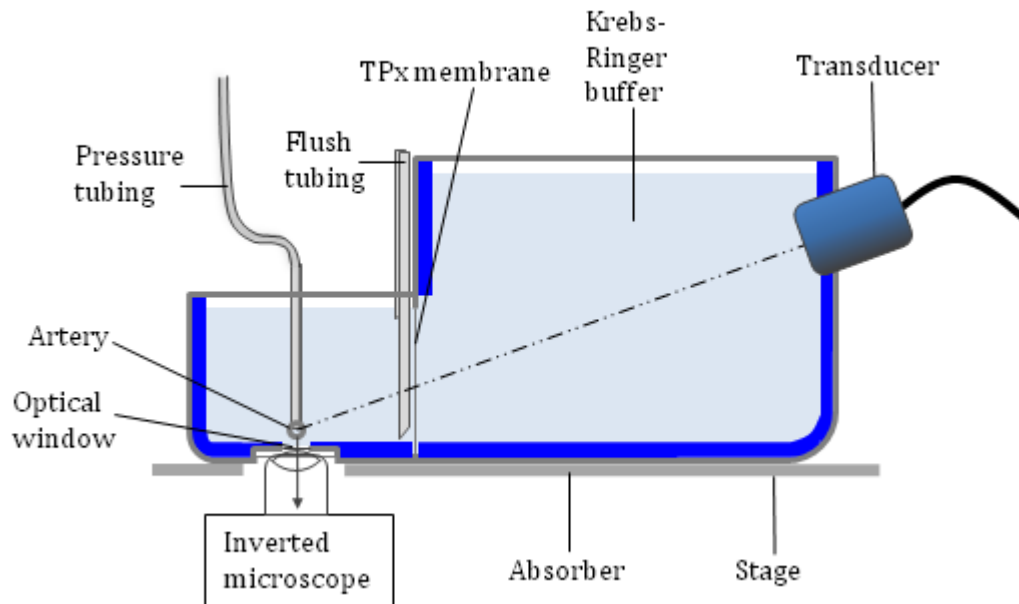
Figure 3.3 Schematic diagram of perfusion myograph system showing the ultrasound transducer coupled into the fluid with the artery in the focal region of the ultrasound and microscope. The two halves of the bath are separated by a membrane; the flushing tubes and pressure system are placed within the small section of the bath.

The same ultrasound transducer was used as described previously. Again the properties of the acoustic field placed constraints on the dimensions of the myograph bath. The mounted vessel had to be located at the focus of the acoustic field so the bath had to be big enough to allow the correct separation between transducer and tissue. Another constraint was placed on the position of the tissue due to the focal length of the optical microscope objective used for imaging of the blood vessel.

For ease of mounting the vessels, the bath had to be fairly shallow and the volume kept relatively small to keep concentrations of drugs low. For these reasons it was not possible to accommodate the hydrophone in the bath for measurement and set up of the system. As the hydrophone could not be used to find the focal zone in this configuration, it was decided that the relative positions of the transducer and tissue

should be carefully calculated and fixed. The transducer was sealed into a Perspex holder in the side of the bath and coupled directly into the fluid.

The transducer was held at an angle of 20° to the horizontal to reduce the length of the bath. This also created space around the beam in the near field and enabled positioning of the beam focus very close to the bottom of the tank, at a suitable position for optical imaging. The shallow depth of the tissue bath was created by splitting the tank into two sections separated by a TPx membrane. A polyethylene food storage box was purchased (Lock & Lock), with dimensions 6 cm by 11 cm by 8 cm deep. A rectangular section was cut out of the top corner of one end to make the shallow tissue bath section with a depth of 3.5 cm. The depth of the section into which the transducer was coupled was greater than that of the tissue bath. Both sections were filled with the same buffer to avoid refraction at the boundary caused by a difference in sound speed between the buffer and water.

After some trials with methods of attaching the membrane to the tank, it was decided that it should be glued directly to the wall to ensure a good watertight fit. This raised an issue in that it is very difficult to strongly bond anything to polyolefins, such as polythene. These are plastics that are inherently non-stick; most glues and epoxies are unsuitable for bonding to this type of plastic. A specialist superglue for bonding plastics was sourced (Loctite All Plastics super glue, Loctite, Henkel Ltd, Hemel Hempstead, UK). The plastic was cleaned with hot soapy water then ethanol. A primer was applied to the surfaces that were to be bonded, then the glue was applied and the surfaces brought together. Another problem was that these glues may not produce a lasting bond when not used in dry conditions. During experiments, the bond would normally be in contact with warm salt solution. In an attempt to protect the bond from water, the join between the TPx film and the plastic of the box was sealed with silicone sealant. Reapplication was necessary at regular intervals as the silicone easily peeled off. It provided a good enough seal however as the silicone was not under strain.

The bath was lined with absorber to stop reflections, which was especially important in this small bath. The Aptflex absorber was again used to line the bath; it was cut roughly to shape with a band saw then sculpted with a scalpel to fit the tank. Some

sections were cut to half thickness with a scalpel to conserve space in the bath. It was important to place absorber on the beam axis, deeper than the focal region as the walls of the bath were close to the focus.

Vessel mounting – pipette tips

The blood vessels were mounted at each end on glass pipette tips held in place by holders anchored in the absorber layer of the tank base. To help hold the vessels on to the pipettes, the tips had to be of a slightly larger diameter than the vessels so they would be stretched slightly when pulled over the tips. The pipettes were sharply tapered to a tip that was narrow enough to fit inside the vessel easily, so that the vessel could be pulled over the tip in a similar manner to putting a sock on. Once the narrow tip opened out, the diameter of the tube had to remain fairly constant for a small distance to provide a flat section to tie the vessel onto. The pipette tips were pulled using a P-87 Flaming/Brown Micropipette Puller (Sutter Instrument, CA, USA). This is designed to make pipette tips for a number of applications which require much smaller tips than required here. Because of this, the normal method of operation of the device was not suitable. Instead the device was used in 'ramp test' mode to create a narrow diameter section at the centre of a 1.5 mm (outer diameter) borosilicate glass capillary tube (Part no. 30-0054, Harvard Apparatus, Kent, UK). This mode is normally used for finding the temperature of the element at which the glass melts enough to allow the two ends of the capillary tube to start moving apart from one another. The temperature of the element is increased until this point is reached, then the element is cooled down and the glass solidifies. This process was repeated twice to produce a section of smaller diameter of a few mm in length. The pipette was then pulled using one of the default programs to create two pipette tips. These were trimmed under a microscope using a glass cutting blade to produce a small clean tapered tip.

The vessels were tied on with 5 gauge (0.1 mm) Ethilon monofilament polyamide suture thread (Ethicon, Livingston, UK); this size and type was chosen after experimenting with other (finer) threads. Two loops were made and threaded over each pipette tip. The vessel was pulled onto the tip then one loop was pulled over the end of the vessel and secured. The second loop was then pulled over and secured also.

It was found that it was easier to tie half a reef knot in the first loop and to tie half a reef knot with an extra half hitch (a surgeon's knot) in the second. The mounting procedure and knots are depicted in Figure 3.4. The loop with the surgeon's knot held more securely but was harder to tighten. It was easier to tighten once the vessel was held in place loosely by the first knot.
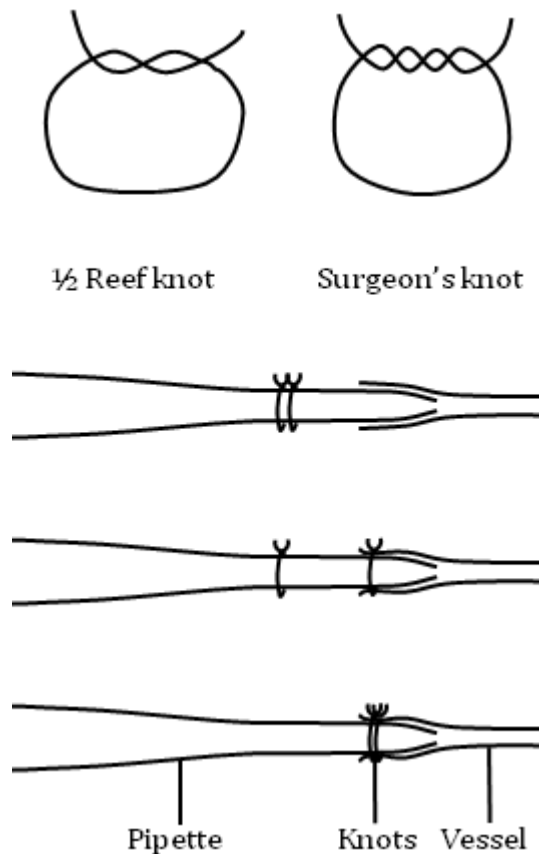
Figure 3.4 Diagram showing knots and procedure for mounting vessels on the pipette tips. One knot of each type is threaded over each pipette tip. The vessel is pulled over the tip then the first knot is pulled over the vessel and tightened; the second knot then secures the vessel.

It was found that it was quite difficult to tie the vessel on to the pipette tips as described in such a way that it would hold when stretched. This was a consistent problem so an alteration to the pipettes was necessary. To solve this problem, a raised band was added to the tip just on the tapered part. The vessel was pulled onto the tip and over this part, and then secured with the ties behind it. When the vessel was stretched, the ties pulled against this raised band but were not able to slip off over it.

The major problem encountered in manufacturing these tips, was in finding a substance to create the raised band that would stay attached to the glass during several hours of immersion in warm salt solution, while under strain. Several methods were attempted. The first and seemingly most simple solution was to try and pull the pipette tips in such a way that a bulge was created in the tube that would act as a stop. This was attempted but it was not possible to change the diameter of the tube rapidly enough in a short enough length of the pipette. The next step was to use soda glass to create a raised band around the pipette tip. This involved melting soda glass crystals onto a wire filament then bringing the glass tube up to the filament to touch the melted soda glass. The tube was then rotated to pick up glass in a ring around the tip. A coarse surface would damage the vessel, but it was very difficult to produce an even ring around the tube and extremely difficult to create a smooth surface. The next possibility that was investigated, was to make a ring around the tip using epoxy resin. A two part epoxy (Stick 2 Rapid Epoxy Tube, Everbuild Building Products Ltd., Leeds, UK) was mixed and applied to the pipette using a needle. This was quite an easy and reproducible method for creating a raised ring around the pipette tips. However, when the pipettes were tested it was found that the epoxy resin came away from the glass after several hours when immersed in water so was not suitable for use in experiments. This method of creating the ring was successful so an alternative glue was tested to see if it would hold for a longer period of time. An optical adhesive (NOA68, Tech Optics Ltd., Kent, UK) cured by exposure to UV light was applied to the pipettes in a similar manner. This stayed attached to the pipette for longer but ultimately still came away from the glass.
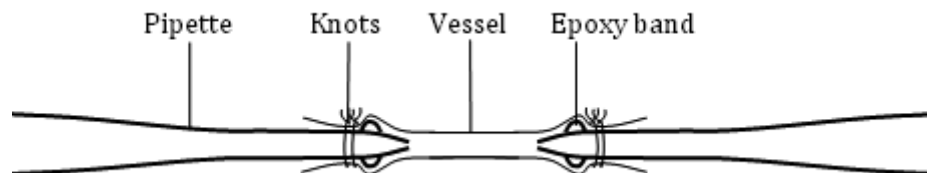
Figure 3.5 Diagram of pipette tips with vessel mounted; the vessel is pulled over the raised band and secured behind it with two knots.

To achieve a better bond with the glass, the pipettes were cleaned thoroughly before application of the glues. The pipettes were first washed in hot soapy water with lens

tissue to avoid linting. They were rinsed in distilled water and then washed in ethanol. They were then soaked in aqua regia (3 parts HCl, 1 part HNO_3) for 10 to 15 minutes. The pipettes were then very carefully removed and soaked in a beaker of distilled water. The aqua regia was neutralised by the addition of aqueous $NaHCO_3$. The pipettes were carefully removed and placed in a large petri dish to dry in an oven over night. Some pipettes were then treated with two part epoxy resin, some with optical adhesive. All pipettes were then placed in an oven at a temperature of 50 °C for at least 24 hours to aid the curing process. The two types of pipette tips were tested and it was found that the baked epoxy resin bands would hold reliably enough to be used for several hours during experiments. The vessels were easily mounted and securely fastened to these tips.

Pressure system

A system of tubes was used to pressurise the vessel to physiological levels during experiments and to vary pressure to establish pressure-diameter relations. The vessel was securely tied onto the pipette tips during mounting to form a watertight seal between the vessel and pipette tip. Small plastic tubes were connected to the ends of the pipettes. A three way tap was connected to the end of each tube. This was used to close the end of one tube and to connect the other to a long tube and an open syringe to form the pressure tower. The syringe was held in a clamp, which could be moved up and down a long pole to change the height of the liquid in the column and thus the pressure. The tubes were filled with Krebs-Ringer buffer in a particular order during mounting of the vessel to eliminate bubbles from the system, which would have damaged the endothelium. The procedure for pressurising the vessels is described later in Section 5.2.3.

Heating

Experiments in this system were again performed at 37 °C so a heating system was required. The simple solution of a plastic tubing heat exchanger fed from a separate temperature controlled water bath as used previously was too cumbersome to work with this bath. The heating system was still formed of a hot water heat exchanger but the radiating part had to be more compact and rigid so it could be positioned securely out of the way of the tissue. Ideally, the radiating part would have been made of

stainless steel or other metal tubing that would be inert in the salt solution. After discussion with the workshop, it was clear that it would be difficult to bend metal tubing into shape to create a radiator that would fit in the bath without the tube collapsing. An alternative solution was to wind thin plastic tubing backwards and forwards between sets of pins anchored to a sheet of metal. It was then decided that the simplest solution was to make a winding groove in the surface of a rectangle of Perspex, then bond it to another thin sheet to create a small solid radiator. Water was pumped through from the external temperature controlled bath as with the previous system. Perspex was chosen because of machining practicalities and because it can be strongly bonded to itself. Two radiators were made, one to fit in each section of the bath. They were 5 mm thick and filled the available area against the side of the bath. The radiator dimensions were 4cm by 5 cm for the large bath section and 3 cm by 2 cm for the small bath section.

Flushing system

A flushing system similar to the one described previously was incorporated into this bath. The inlet and outlet tubes were held in place with blutac at opposite corners of the tank. The tip of the inlet tube was placed at the bottom of the tank, while the tip of the drainage tube was placed at the normal surface level of the fluid. The fluid was flushed as described previously with a volume of fluid approximately twice the capacity of the bath.

3.5.1 Imaging system

The system used to image the blood vessels was a Leica DM IL inverted microscope (Leica Microsystems GmbH, Wetzlar, Germany). Incident light was provided by an external LED light source positioned above the tissue bath. A CCD video camera (KY-F55B, JVC, NJ, USA) was used to capture images from the microscope. A video capture card (194003-USB Live, Hauppauge Computer Works UK Inc., London, UK) was used with Ulead DVD Movie Factory (Ulead Systems, Torrance, CA, USA) video capture software to record and display images in real time. The video was captured at a rate of one frame per second, which was frequent enough to observe changes in vessel diameter and matched the sampling rate used in the previous isometric force

measurements. A low sampling rate was also necessary due to constraints on the size of video files that could be stored and processed.

An objective with 5x magnification (506087, Leica Microsystems GmbH, Wetzlar, Germany) was used as this was found to be sufficient to include the whole diameter of the vessel in the field of view. The distance of the focal plane from the objective was 15 mm. Because of the thickness of the absorbing layer on the base of the tank and the need to place the tissue a small distance away from this surface, it was necessary to add an insert to the tank that raised the optical window away from the base of the tank. The objective could be moved up inside the Perspex insert, closer to the tissue; it gathered light through a small window covered by a circular glass cover slip. To accommodate this set up, a new stage was fabricated for the microscope from a sheet of aluminium.

3.5.2 Image processing

After capturing of video files, pre-processing was performed using VirtualDub software (released under GNU General Public License (GPL)). The files were decompressed, rotated so that the vessel walls were close to the horizontal (necessary for later analysis) and in some cases cropped. The files were then saved and imported to Matlab (The Mathworks Ltd., Cambridge, UK) where they were saved as structural arrays in *.mat files. The rest of the processing and analysis was performed in Octave (GNU Octave, released under GNU GPL), an analogue of Matlab. The aim was to trace the edges of the vessel and measure their separation for each frame of the video using edge based segmentation. Processing was performed frame by frame and the vessel diameter and edge positions were stored in matrices.

The processing algorithm began with the input of a set of points by the user, defining a straight line along each edge of the vessel. Two sets of coordinates were input for each line, these were transformed into a vector with a point at each x value in the image and a corresponding y value. These lines acted as the starting position for the contours that would trace the vessel edges.

The 3 dimensional rgb data was converted into a single grey value for each point on the image. Sobel edge detection filters were created for filtering of the image in both the x and y directions to create an edge image, these are shown below:

$$\begin{bmatrix} -1 & -2 & -1 \\ 0 & 0 & 0 \\ 1 & 2 & 1 \end{bmatrix} \quad \begin{bmatrix} -1 & 0 & 1 \\ -2 & 0 & 2 \\ -1 & 0 & 1 \end{bmatrix}.$$

These filters were convolved with the image, producing a value for each pixel in the image. Where there is no change in grey level in the region covered by the filter, the filter will sum to zero and the edge image at the central pixel will have a zero value. Where there is a change in grey level over the region covered by the filter, the sum will be non zero and the edge image at the central pixel will be non zero, with the magnitude increasing according the gradient of the edge. In the edge image shown in Figure 3.6b, the edges appear white and areas with little or no change in grey level appear dark. There is one filter for horizontal edges and another for vertical edges, the results are combined and normalised to form a complete edge image. The gradient of this image was then calculated as the change in grey value between adjacent points in the x and y directions. This produced two sets of points: the gradient in the x direction and the gradient in the y direction. These gradients were used in the optimisation of the straight lines previously defined to fit the vessel edges on the image. Images showing the steps in the processing procedure are shown in Figure 3.6.

The vessel edges were traced using an active contour method (Kass et al. 1988). The contour was initialised by user input (lines defined along the vessel edges), then optimised using energy minimisation to find a solution which traced the vessel edges properly. Three component forces acted on the contour to evolve its shape: the image gradient force and internal spring and curve forces. In this algorithm, the points were constrained in the x direction; there was one point on the line at each x value in the image, so forces acted only in the y direction. The image gradient force acted to move the contour over the image. The spring force acted to control the distance between the points; it prevented the points from separating too far and helped to create an even contour. The curve force acts on the gradient of the contour, opposing large changes in gradient to smooth the line.
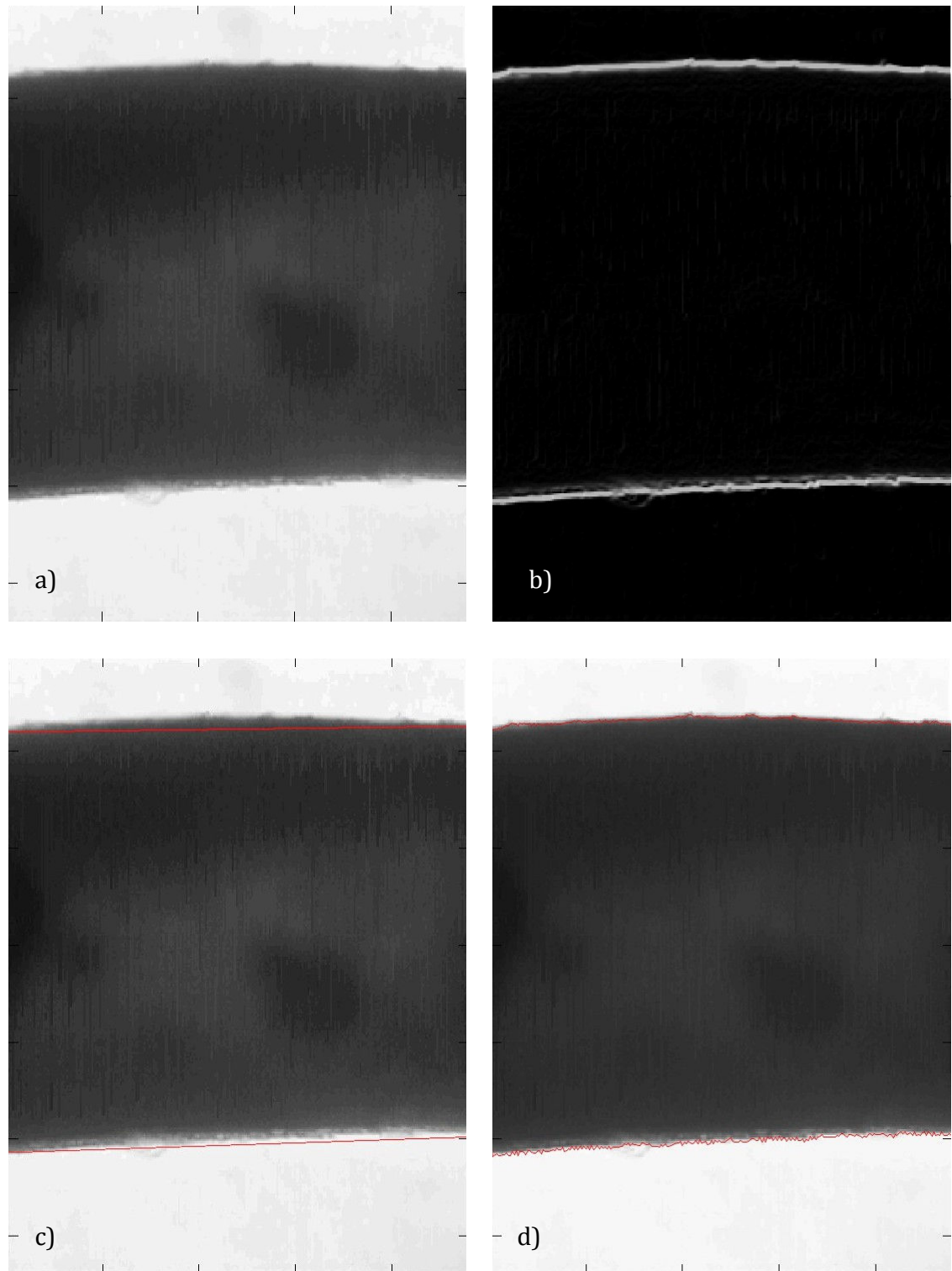
Figure 3.6 Steps in the image processing procedure: (a) original image of the vessel; (b) Sobel filtered edge image, strong edges appear white; (c) original image with contour starting points (red lines); (d) original image with evolved contour tracing the vessel edges.

If the contour is described as $v(s) = \big(x(s), y(s)\big)$ then the energy functional of the contour is

$$E^*_{contour} = \int_0^1 \Big(E_{int}(v(s)) + E_{image}(v(s)) \Big) ds \,. \qquad 3.1$$

E_{int} is the internal energy of the curve originating from the spring and curve forces:

$$E_{int} = \frac{1}{2}\left(\alpha(s)\left|\frac{\partial v}{\partial s}\right|^2 + \beta(s)\left|\frac{\partial^2 v}{\partial s^2}\right|^2 \right), \qquad 3.2$$

where α and β are constants and control the tension and the curvature of the curve respectively. Increasing α will move the points on the contour closer together, pulling out irregularities; increasing β will make the contour more rigid which will have a smoothing effect. E_{image} is the energy associated with the image; it is derived from the image intensity and image gradient as described.

The contour will evolve until the energy functional is minimised, the solution can be found by solving the Euler-Lagrange equation:

$$\frac{d^2}{ds^2}\left(\frac{\partial F}{\partial v''}\right) - \frac{d}{ds}\left(\frac{\partial F}{\partial v'}\right) + \frac{\partial F}{\partial s} = 0 \,. \qquad 3.3$$

By writing the Euler equations separately for x and y and making the equations discrete, they can be solved numerically; this is described by Kass et al. (1988). The expressions for stepping the positions of the points on the contour are derived from this treatment.

Each point on the contour is fixed in the x direction and moved as follows in the y direction:

$$y = y + k_i \, idy + k_s \, sdy - k_c \, cdy \qquad 3.4$$

where k_i, k_s and k_c are constants which control the magnitude of the three forces; idy is the change due to the image gradient force, sdy due to the spring force and cdy due to the curve force.

$$i \, dy = f_y(i) \tag{3.5}$$

$$s \, dy = -(2y_i - y_{i-1} - y_{i+1}) \tag{3.6}$$

$$c \, dy = (y_i - 2y_{i-1} + y_{i-2}) - 2(y_{i-1} - 2y_i + y_{i+1}) + (y - 2y_{i+1} + y_{i+2}) \tag{3.7}$$

The points of the contour were moved by this much then moved again, with a new value of image gradient force due to the change in position. This process was repeated for 500 iterations which were sufficient for the contour to evolve to fit the vessel edge.

Once the contours had evolved, the distance between each point on one edge and the corresponding x location on the other edge was found and averaged. A straight line was fitted to each contour. The angle of the best fit lines to the horizontal was found and the separation of the edges in this direction was calculated. This eliminated errors in vessel diameter introduced by the positioning of the vessels during imaging. This separation was stored and the process was repeated for the next frame using the evolved contour from the last frame as the initial value. This was repeated until all frames had been processed and a complete trace of vessel diameter versus time was produced.

3.6 Beam characterisation

3.6.1 Beam calibrator measurements

An NPL ultrasound beam calibrator (National Physical Laboratory, Teddington, UK) (Preston 1988) at the medical physics department, Royal United Hospital, Bath, was used to perform preliminary measurements for the characterisation of the acoustic field. Beam calibrator measurements were performed to investigate the beam shape and focus position, rather than to obtain quantitative information about the acoustic exposure conditions. The measurements were performed during the early part of the investigation before all equipment was present. A different driving system was therefore used for these measurements, and the pulse regime and acoustic power were significantly different from the conditions used during experiments. The beam was later characterised in terms of peak negative acoustic pressure and acoustic

intensity under experimental exposure conditions using a needle hydrophone, which is described in Section 3.6.2.

The beam calibrator system consisted of a 21 element PVDF membrane hydrophone submerged in a glass water tank filled with degassed, deionised water. The elements of the hydrophone were 0.4 mm in diameter with a centre to centre spacing of 0.6 mm. The transducer was clamped with its face submerged in the water. The bottom of the tank was lined with a sheet of absorbing material. The position of the transducer was adjusted using micrometer screw gauges in two perpendicular directions (perpendicular to the beam axis) and rotated about the beam axis. The hydrophone could be moved along the beam axis to vary the measurement depth. For the measurements described here, the hydrophone was stepped along the beam axis in 2 mm steps. The transducer was driven in pulsed mode, so a pick up coil was placed close to the transducer to collect a trigger signal to start the data acquisition for each pulse.

The beam profile made up of the signal from each hydrophone element was displayed on a computer screen. This was used for alignment of the central element of the hydrophone with the beam axis. The acoustic pulse waveform and peak negative acoustic pressure from the central element were also shown. The software computed the pressure squared integral from the peak negative acoustic pressure, from which other quantities such as the pulse duration, spatial-peak time-averaged intensity (I_{SPTA}), spatial-peak pulse-average intensity (I_{SPPA}), total acoustic power and 6 dB beam width were calculated and displayed under a post processing menu.

In the near field, the beam was wide and relatively flat in the centre with low side lobes at the edges. As the distance from the transducer face increased, these peaks became closer together and a third peak emerged. This increased in amplitude as the beam focus was approached, while the amplitude of the other peaks decreased to zero. In the far field the beam began to diverge and the amplitude of the single peak decreased. These measurements were made in a pulsed wave beam, but the bulk of experimental exposures were continuous wave. The near field of the continuous wave beam will be more complex than the pulsed wave beam, exhibiting more fine structure. More side lobes will be seen and more extreme maxima and zeros in the

field. The near field of a pulsed beam with long pulse duration will also be more complex than that of a short pulse duration beam. The field shape at the focal region and in the main lobe of the far field will not differ significantly however.

The minimum -6 dB beam width of approximately 3.5 mm was observed at the depth of maximum peak negative acoustic pressure and acoustic intensity. This was between 80 and 85 mm deep. There was an error of approximately 2 mm associated with the depth, due to uncertainty in the relative positions of the hydrophone and transducer in the beam calibrator system. The beam width along the beam axis is shown in Figure 3.7.

The observed shape of the pulses showed that propagation was linear in the near field and then became nonlinear as the focus was approached. In this region a shock front was observed in the pulse.
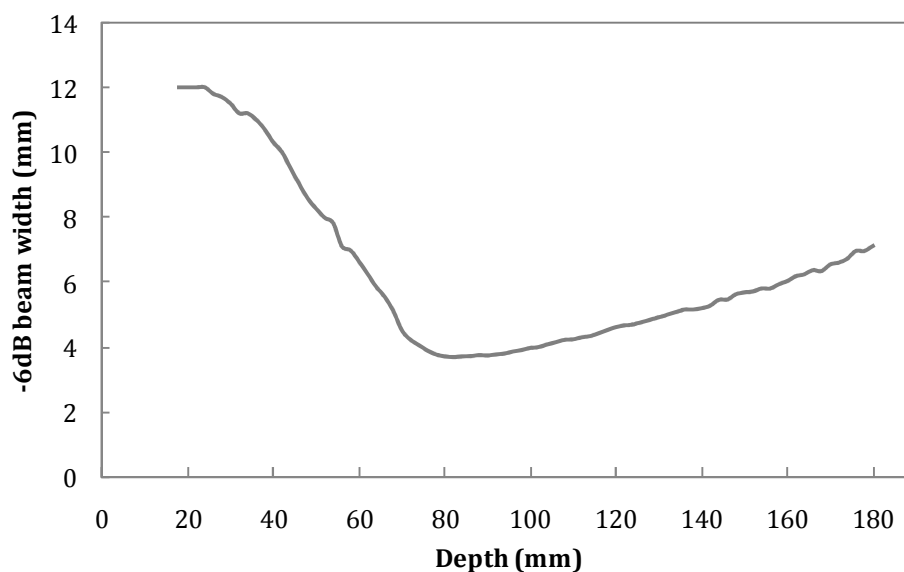
Figure 3.7 -6dB beam width profile, the minimum beam width is between 80 and 85mm deep, this is at the same depth as the maximum peak negative acoustic pressure and I_{SPTA}.

The measurements described above were made at a considerably lower acoustic power than that used during experiments. An acoustic power of 3.8 mW was measured with the power balance, which agreed with values of total acoustic power measured with the beam calibrator close to the transducer face. The transducer was driven in a pulsed regime with very short pulses and a low pulse repetition frequency.

The peak negative acoustic pressure amplitude measured was of a similar magnitude to that measured for the diagnostic type pulse regime used for experiments. It was considerably higher than that measured during continuous wave exposure under the experimental conditions. Because of nonlinear propagation effects, at higher acoustic pressures, the position of the maximum peak negative acoustic pressure may be closer to the transducer by up to 1cm compared to the position during the continuous wave experimental conditions (Duck and Starritt 1986).

3.6.2 Hydrophone measurements

For beam characterisation and experimental set up, peak negative and positive acoustic pressure were measured at the beam focus (assumed to be the point of highest peak negative acoustic pressure) using a 0.2mm diameter PVDF needle hydrophone (Precision Acoustics Ltd., Dorchester, UK), the configuration is shown in Figure 3.8. For measurement, the hydrophone was mounted in a purpose built holder in the tank. The hydrophone position was manipulated in 3 dimensions by micrometer screw gauges.
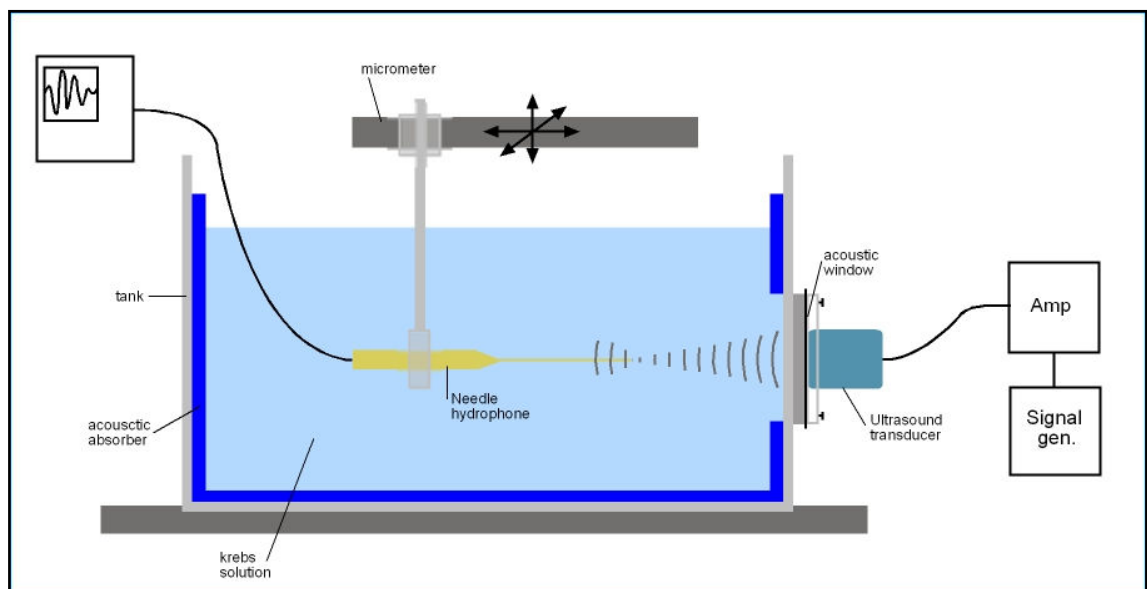
Figure 3.8 Schematic diagram of hydrophone measurement set up; the hydrophone position is manipulated with micromanipulators to find the position of maximum peak negative acoustic pressure, the position is fixed relative to the mounting position of the force transducer to enable positioning of the tissue in the focal region.

The needle hydrophone consisted of a disc shaped 0.2 mm diameter element made of PVDF, a piezoelectric polymer. The small element enabled precise measurement of spatial variations in the field, so the position of highest peak acoustic pressure could be found accurately. Because of the size of the element, the hydrophone does not have a highly directional response as a larger element would. PVDF is thought to have a linear response up to acoustic pressures of about 10 MPa. Needle hydrophones do not have a flat frequency response; a calibration document was supplied. The sensitivity of the hydrophone and amplifier was stated as 68.22 mV/MPa at 3.2 MHz. This value was used throughout for calculation of acoustic pressure from oscilloscope measurements of voltage.

The PVDF element was positioned on the end of a needle (several cm long) which was mounted onto the integrated submersible preamplifier, which had 50 Ω output impedance. This was connected to a DC coupler for power and coupling of the signal from the hydrophone to an oscilloscope or computer for measurement. The transmission line was terminated with a 50 Ω terminator piece.

During this study, three different acoustic fields were used: a continuous wave field and two pulsed ultrasound fields. One of these regimes was similar to a typical diagnostic ultrasound field with 1μs pulse duration and 2 kHz PRF. The other was intended to be more similar to a therapy type pulsing regime with a longer 1 ms pulse duration and 10 Hz PRF. The same time averaged acoustic power was used for both pulsed and continuous wave fields. The acoustic power was lower than would be used for physiotherapy ultrasound for example, and was not intended to replicate these exposure conditions. The peak negative acoustic pressures measured at the focal region of each of the fields are given in Table 3.1. These measurements were used to calculate spatial-peak time-average and spatial-peak pulse-average intensities, which are presented in Table 3.1. In order to make a comparison with the Mechanical Index as defined by the IEC (2007), values of $\frac{p_r}{\sqrt{f}}$ were calculated, where f is the centre frequency of the transducer and p_r is the free-field rarefaction pressure in water at the position of the arterial segment. This quantity was calculated rather than the Mechanical Index, as the acoustic pressure was measured directly at the point of

interest rather than calculated from derated acoustic pressure measurements, as is normal when calculating the Mechanical Index in tissue.
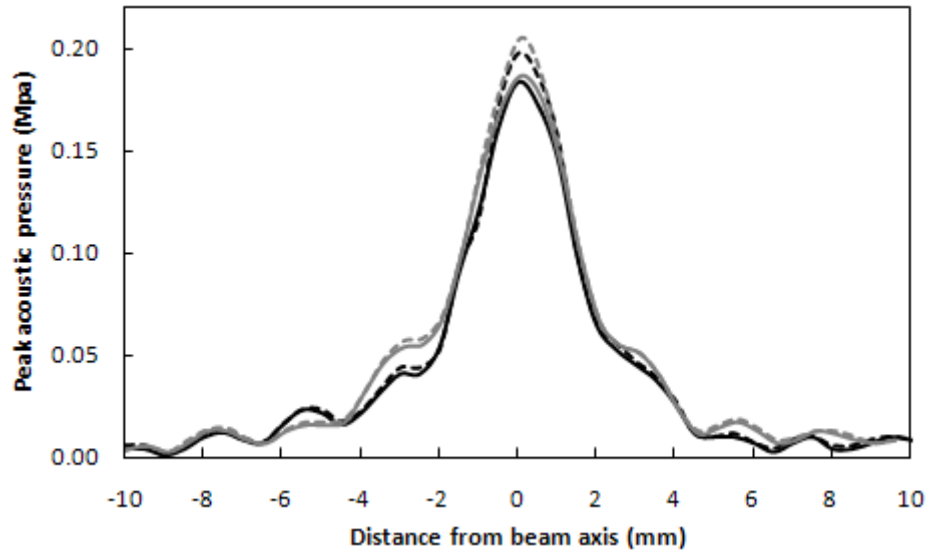
Figure 3.9 Perpendicular peak acoustic pressure profiles measured in the focal plane of the continuous wave ultrasound field; solid lines show peak negative acoustic pressure, dashed lines show peak positive acoustic pressure.

Further measurements of both peak positive and peak negative acoustic pressure were made in the focal plane in order to produce sets of perpendicular transverse beam profiles for each of the fields. The profiles are shown in Figure 3.9 to Figure 3.11. The slight differences between the two perpendicular profiles are likely to originate from slight asymmetries in measurement position on either side of the beam axis. As expected, the continuous wave field (Figure 3.9) had the most complex profile with strong side lobes. The peak negative and peak positive acoustic pressures are similar, indicating a linear field. The diagnostic type pulsed field (Figure 3.10) exhibits a greater difference between peak positive and negative acoustic pressures. The profiles are relatively simple with one small side lobe with no strong zeros, then a relatively smooth decrease as distance from the beam axis increases. The therapy type pulsed field (Figure 3.11) is much more complex, exhibiting several low amplitude side lobes which continue as the acoustic pressure diminishes. There is also a large difference in amplitude between the peak positive and peak negative acoustic pressure close to the beam axis, which may not be expected. The -6 dB beam width is

similar for all fields, varying from approximately 3 mm for the continuous wave field to approximately 5 mm for the diagnostic pulsed field and approximately 3.5 mm for the long pulsed field.
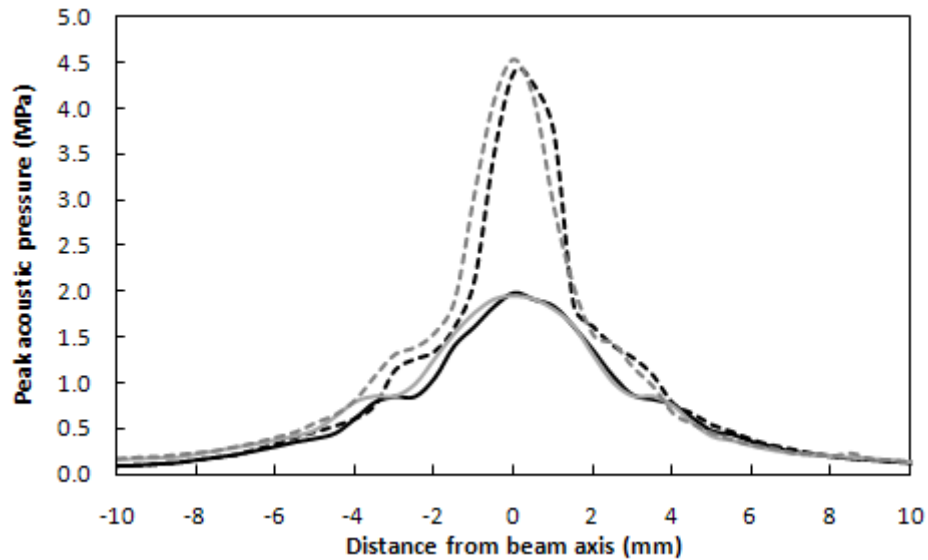
Figure 3.10 Perpendicular peak acoustic pressure profiles measured in the focal plane of the diagnostic type pulsed ultrasound field (pulse duration 1 μs, PRF 2 kHz); solid lines show peak negative acoustic pressure, dashed lines show peak positive acoustic pressure.
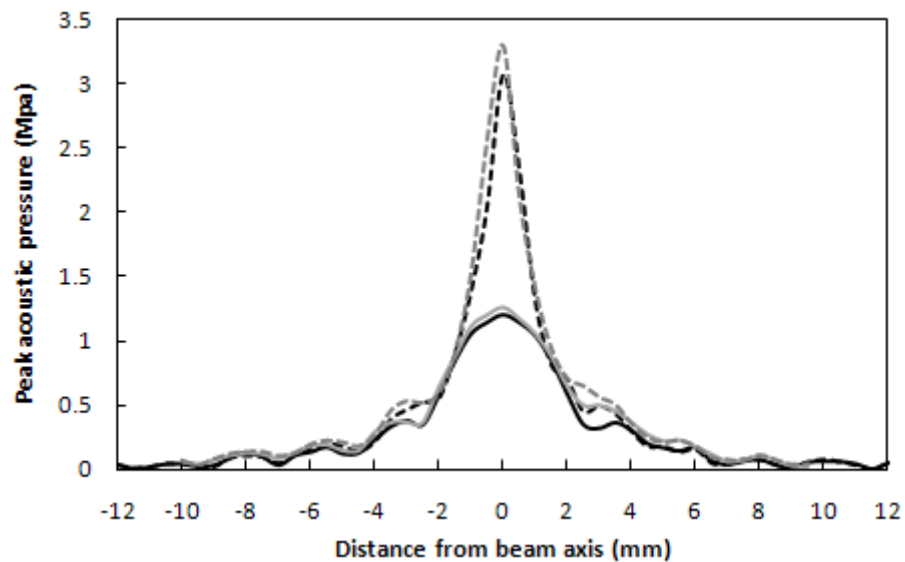
Figure 3.11 Perpendicular peak acoustic pressure profiles measured in the focal plane of the therapy type pulsed ultrasound field (pulse duration 1 ms, PRF 10 Hz); solid lines show peak negative acoustic pressure, dashed lines show peak positive acoustic pressure.

Acoustic intensity calculation

Measurements of the peak negative acoustic pressure were used to calculate the intensity in the acoustic field using the pulse intensity integral, defined in Section 2.1.1. In practical terms, the pulse was imaged with an oscilloscope, acoustic pressure was calculated from the voltage trace, the pulse was squared and the pressure squared integral was calculated by finding the area under the curve. The pressure squared integral was then divided by the acoustic impedance of water, ρc.

Table 3.1 Peak acoustic pressures from needle hydrophone measurements made under experimental exposure conditions and resulting values of calculated intensities and local Mechanical Index. The overall uncertainty at the 95% confidence interval in these calculations was assumed to be about 30% and 36% for the I_{SPTA} and I_{SPPA} respectively and about 15% for the peak negative acoustic pressure; for sources of error see Preston (1988).

Exposure type	Peak positive acoustic pressure	Peak negative acoustic pressure	Acoustic power	I_{SPTA}	I_{SPPA}	$\dfrac{p_r}{\sqrt{f}}$
	(MPa)	(MPa)	(mW)	(W cm^{-2})	(W cm^{-2})	(MPa/MHz^{½})
Continuous Wave	0.14	0.12	72	0.52		0.07
	0.17	0.15	100	0.78		0.08
	0.20	0.18	145	1.07		0.10
Diagnostic pulse	4.68	2.00	145	0.46	190	1.12
Therapy pulse	3.95	1.20	145	1.18	118	0.67

3.6.3 Power balance measurements

The beam power was measured before each experiment using a radiation force balance with a reflecting target (Perkins 1989). The power balance makes use of the radiation force exerted on a target by an ultrasound beam to make measurements of the acoustic power in the ultrasound beam. The force exerted on the target is proportional to the acoustic power in the beam if the whole beam area is incident within the target.

The radiation force,

$$F = \frac{hW}{c},$$

where W is the acoustic power, c is the sound speed in the fluid and h is a quantity depending on the geometry and reflection or absorption properties of the target. This is equal to 1 if the target is perfectly absorbing and theoretically equal to 2 for a perfectly reflecting target perpendicular to the tissue. In practice it would be very difficult to create a perfectly absorbing or reflecting target. This would require perfect impedance matching or mismatching in order to enable either total transmission of the ultrasound into the target or total reflection from the target. Another factor is contained within h to allow for differences in angle of incidence of the beam for focused, phased array or sector scanners. The transducer used in this study was weakly focused. So for a reflecting target, $h = 2\cos^2\theta$, where θ is the angle between the angle of incidence of the beam and the normal to the surface of the target.

The bath balance has a 90° cone reflecting target with an effective diameter of 70 mm suspended with the cone axis positioned horizontally. The target consists of 2 thin metal cones set 2mm apart and sealed together to create an air filled cavity, producing an air backed target which reflects approximately 90-95% of the incident ultrasound. The reflected ultrasound is directed into a cylinder of absorbing material around the target chamber. The chamber is filled with water and the transducer is coupled to a TPx membrane with ultrasound gel.

When the incident beam exerts a force on the target a restoring force is generated by a magnet and coil behind the target. When the target is deflected, a current is induced in the coil which causes a force to oppose the movement of the target. The magnitude of the restoring current indicates the beam power.

Power balance calibration

Before measurements were made with the power balance, it was calibrated against the NPL continuous wave ultrasound check source (NPL, Teddington, UK). The check source operated at 3.5MHz at acoustic powers of 10 mW, 100 mW and 1 W.

The check source was switched on and left to warm up for 30 minutes before use. Before measurements were made using the check source at a particular acoustic power, the source was switched on at this power four times for periods of about 30s as specified in the protocol supplied by the manufacturer. The check source was coupled to the power balance and measurements were made with each sensitivity range appropriate for the radiated power. The power balance has sensitivity ranges of 1, 3, 10, 30, 100 and 300 mW and 1, 3, 10 and 30 W. Sets of 6 measurements were performed for each of the sensitivity ranges, ensuring that the instrument was zeroed before measurement. The indicated acoustic powers during and after exposure were recorded.

A first check of measured acoustic power showed that the balance was reading about 5% low on the 10 and 30 mW, and 1 and 3 W ranges, and about 1% low on the 100 and 300 mW ranges. The balance was adjusted slightly and measurements were repeated. Results are shown in Table 3.2.

Table 3.2 Results of measurements made for calibration of the power balance against the NPL check source.

Nominal radiated power (NPL checksource)		Sensitivity range		Measured power (power balance)		Percentage difference
1	W	3	W	1	W	0
		1	W	1	W	0
100	mW	300	mW	104	mW	4
		100	mW	104	mW	4
10	mW	30	mW	10	mW	0
		10	mW	9.95	mW	0.5

The measured acoustic powers were consistently 4% high for the 100 mW output for both the 100 and 300 mW ranges. A correction factor could be applied when these ranges were in use. The calibration certificate supplied with the check source shows that the radiated acoustic power for the 100 mW nominal power setting is 2% high. Taking this into account, the error for these ranges would be more like 2%. The

measured acoustic power was 0.5% low for the 10 mW output on the 10 mW sensitivity range. This range is very sensitive and picks up a lot of background noise.

The check source is calibrated for radiation into a free field. Here, the difference in measurement conditions introduces an uncertainty of 5%. Some measurements were performed to try and estimate the set up error involved in the measurements. The x, y position of the transducer should not have affected the readings, as long as the beam was incident completely within the target area. However, angular positioning errors will have an effect on the measured acoustic power. The coefficient of variance of these measurements was about 2% for each of the nominal acoustic powers tested. Perkins (1989) quotes axial and small angular positioning errors of up to 5% error in the power balance reading. This produces a total error of between 5.5% and 7%. All differences found between the measured and radiated acoustic powers were within this uncertainty.

There is only one point of adjustment on the power balance. The 100 mW range can be adjusted; the other ranges are mathematically derived from this. For this reason, it is not possible to achieve perfect set up of the balance so that all ranges read the exact radiated acoustic power.

Frequency response measurements

In order to determine the optimum driving frequency of the transducer, the frequency response was tested. The transducer was driven over a range of frequencies, with a constant amplitude input signal, and measurements of the acoustic output power were made using the power balance. As shown in Figure 3.12, there was a clear peak in acoustic output power when the transducer was driven at frequencies between 3 and 3.5 MHz. The maximum was at 3.2MHz; therefore the transducer was therefore driven at this frequency during experiments.
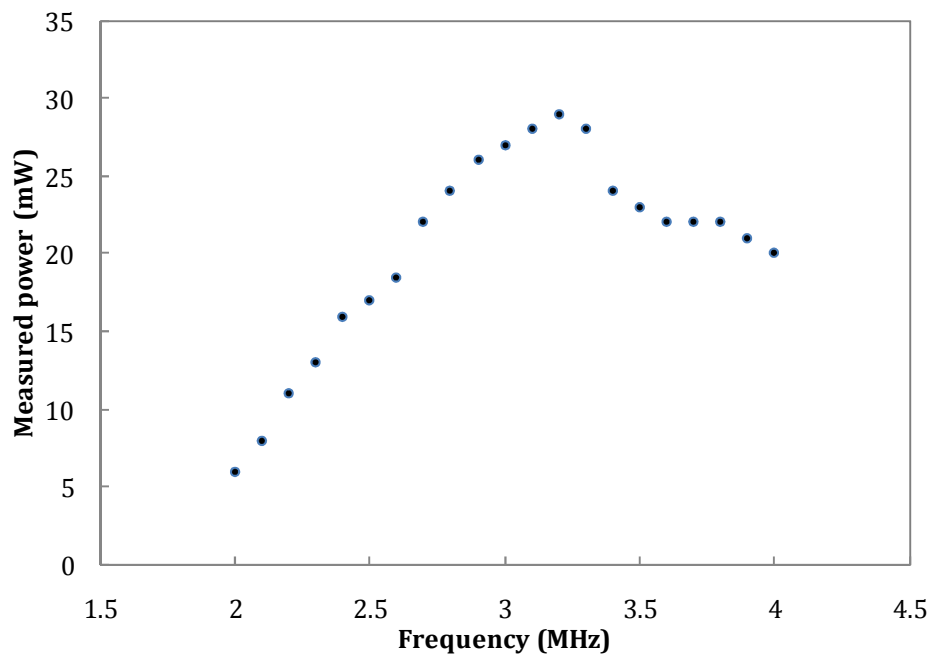
Figure 3.12 Frequency response of the transducer driven with a constant amplitude signal, peak acoustic output power is observed between 3 and 3.5 MHz.

3.6.4 Thermal effects – Thermal Test Object and thermocouple measurements

As previously stated, energy is deposited in a medium when an ultrasound beam passes through it, due to absorption, and this acoustic energy may be converted to heat. The acoustic dose and dose rate, defined in Section 2.1.1, depend on the acoustic intensity profile and properties of the medium. The acoustic dose rate, dose per pulse (for the pulsed exposures) and dose per exposure were calculated from these expressions for each of the exposure conditions employed in these experiments. The density of the medium was taken as 1000 kg m^{-3} and the intensity absorption coefficient $(2\alpha_a)$ was taken as 0.3 nepers cm^{-1}. The values calculated for each of the exposure conditions used in the study are shown in Table 3.3. The acoustic dose per exposure is also calculated for FDA I$_{SPTA}$ limit of 720 mW cm^{-2}. The acoustic dose is lower in this case than all but the lowest acoustic power continuous wave exposure and the diagnostic type pulse exposure.

The initial rate of temperature rise associated with the acoustic energy deposited in the medium, is dependent on the acoustic dose rate and the heat capacity of the medium (see Section 2.1.1). After this, heating depends on the beam width. The final steady temperature reached when the tissue reaches thermal equilibrium will depend on the thermal conductivity of the tissue and other sources of heat loss, such as perfusion. In this study, the tissue was not perfused, so there was no heat loss generated in this way. *In vivo*, there will be increased heating at sites which are more strongly absorbing such as calcified bone surface and foetal bones. Soft tissues close to these sites can be heated by conduction.

Some heating will also be generated at the surface of the transducer due to inefficiency in the conversion of electrical energy to acoustic energy in the piezoelectric element. When coupled to a medium, this heat will be dissipated and may cause some local heating. In this study, the transducer face was about 8 cm from the tissue so this effect was unlikely to be important.

Table 3.3 Table of values of acoustic dose-rate and acoustic dose calculated from values of I_{SPTA} and I_{SPPA} shown in Table 3.2 and assuming a mass density of 1000 kg m^{-3} (1 g cm^{-3}) and absorption coefficient of 0.3 nepers cm^{-1}.

Exposure conditions	I_{SPTA}	I_{SPPA}	Acoustic dose-rate		Acoustic dose	
					per pulse	per exposure
	(W cm^{-2})	(W cm^{-2})	(W g^{-1})		(J g^{-1})	(J g^{-1})
Continuous wave	0.52		0.16			38.4
	0.78		0.23			55.2
	1.07		0.32			76.8
Diagnostic type pulse	0.46	190	0.14	57	6.8×10^{-5}	33.6
Therapy type pulse	1.18	118	0.35	35.4	3.5×10^{-2}	84
FDA limit	0.72		0.22			51.8

The potential for thermal bioeffects was estimated by measuring heating in the beam. It was possible to obtain an estimate of heating at the tissue directly, so Thermal Index

was not used as an estimate of the potential for heating. Measurements were performed to confirm the order of magnitude of the temperature rise only. There were problems associated with both methods of temperature measurement used here. When using a wire thermocouple, there may be increased heating due to viscous heating (Morris et al. 2008) and possibly thermal conduction along the thermocouple wires. The use of a thin film thermocouple would eliminate these problems; this solution was not available during this study.

The temperature profile around the focus of the continuous wave acoustic field was also measured using a soft-tissue thermal test object (NPL, Teddington, UK), (Shaw et al. 1999) which was scanned across the beam and stepped along the beam axis. Again these measurements were intended to confirm the order of magnitude of the temperature rise and to provide some idea of the pattern of heating the tissue. The test object did not perfectly represent the experimental conditions. Another way to obtain information about the expected temperature rise in the tissue during exposure to ultrasound would be to construct a mathematical model of the heating. There are difficulties in doing this in this situation. Methods of modelling temperature rise including finite element modelling and the bioheat transfer equation are evaluated by Doody et al. (2000) and the required assumptions are discussed. The bioheat transfer equation can only include one set of parameters such as thermal conductivity, heat capacity, absorption coefficient and the acoustic impedance. This would require simplification of the thermal properties of the tissue in this case which is made up of layers which have different structural properties and therefore, possibly differing thermal properties. The tissue is situated within the buffer fluid which would also have different thermal properties. Finite element modelling could include different thermal properties for different layers of the tissue and can model convection at the boundaries of the tissue, but estimation of the thermal parameters is still required. A model can be simplified if the subject has axial symmetry. In this case, the tissue does not possess such symmetry, so the model would have to be 3 dimensional, making it more computationally demanding. A comprehensive model of this type is beyond the scope of this project and it was not deemed necessary to quantify the temperature rise precisely for the remaining part of the study.

In preliminary experiments, a small thermocouple was sewn onto the inside wall of a section of artery for measurement of changes in tissue temperature during insonation. The tissue was then mounted on the stainless steel supports at the beam focus in the usual manner. The tissue and thermocouple were insonated for 4 minute periods at an acoustic power of 145 mW, with an off time of at least 15 minutes between exposures, to mimic the exposure protocol during experiments. The measurements showed that the temperature did not increase by more than 0.3 °C during any 4 minute exposure to ultrasound. The attenuation through the artery wall (thickness 1.75 mm) was calculated as 0.28 dB (α = 0.5 dB cm^{-1} MHz^{-1}) at 3.2 MHz, so 94% of the beam is transmitted through the vessel wall. The temperature rise will therefore be similar on the front and back walls of the vessel (within ± 0.02 °C).
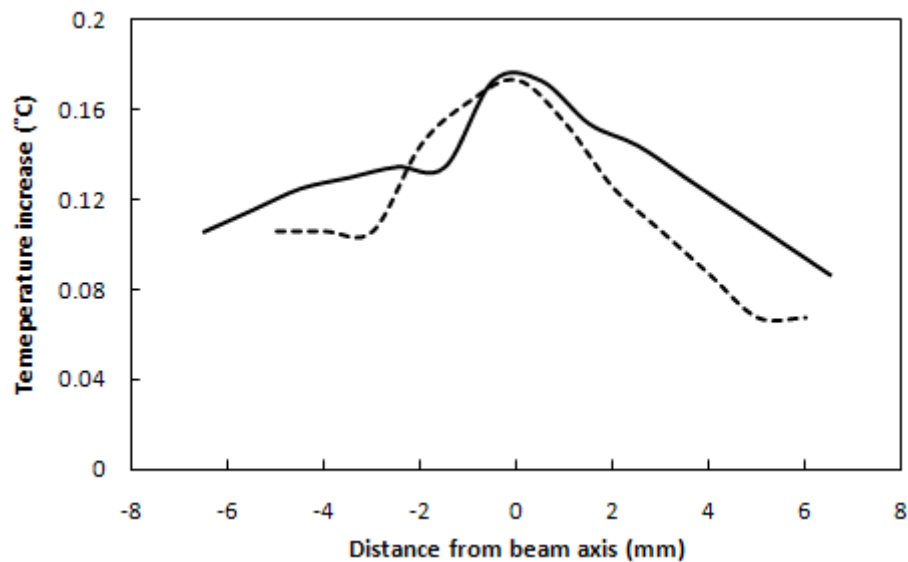
Figure 3.13 Orthogonal profiles centred on the beam axis showing ultrasound induced temperature elevation in the NPL thermal test object in the focal plane of the field; the temperature elevation is the peak value induced by a 4 minute exposure.

An NPL thermal test object was used to build up a profile of heating in the plane perpendicular to the beam axis at the focus depth. The test object contained a thin film thermocouple embedded 6 mm deep in tissue mimicking material, with another 6 mm of tissue mimicking material below it, on top of a layer of absorber. The test object was set up horizontally in a large water bath (the beam calibrator tank) and the

transducer was mounted with the radiating face immersed in the water. Short exposures were made and adjustments to the position of the transducer in the x and y directions and the test object in the z direction were made until the focus depth and beam axis were found (the position of maximum heating). Once this position had been established the transducer position was changed in 1 mm steps in either the x or y direction to build up profiles of heating in the focal plane.

Thermal test object measurements showed that the maximum temperature rise over a 4 minute exposure was approximately 0.2°C. Two perpendicular temperature profiles are shown in Figure 3.13. The maximum temperature rise occurred over a width of 2 to 3 mm centred on the beam axis. The temperature rise reduced to less than 0.1 °C at a distance of approximately 5 mm from the beam axis. The highest temperature rise was found at the point of highest acoustic intensity, i.e. on the beam axis. It then decreased slowly over a distance of several millimetres. Some heating was therefore generated by the ultrasound energy deposited over this area. During the course of the exposure, heat was also conducted through the tissue from the regions of maximum heating out to more peripheral regions. This is illustrated by the time course of heating observed; an example is displayed in Figure 3.14. The temperature increased rapidly for the first 40 seconds to reach about 60 % of the maximum until heat began to dissipate. Temperature then continued to rise at a slower rate until the beam was turned off. The temperature increase was slower at later times because the 'tissue' was closer to thermal equilibrium. The increase in temperature caused by deposited ultrasound energy was more closely balanced by heat loss due to conduction of heat through the tissue. It would be expected that differences in the time course of heating would be seen as the distance from the beam axis increases. On the beam axis a rapid temperature increase will be seen when the beam is switched on. Further from the beam axis the initial rise will be much slower as the heating is produced mainly by dissipation of heat.
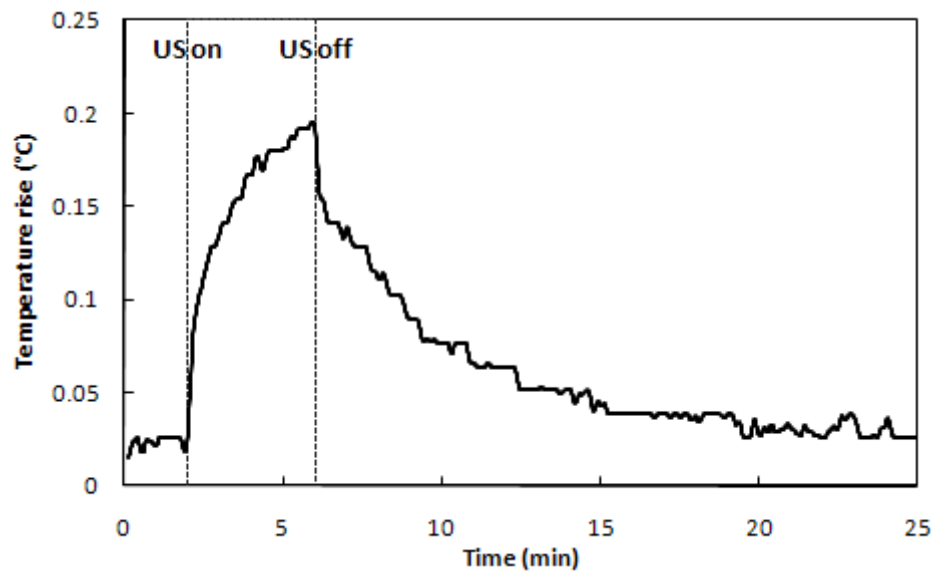
Figure 3.14 Time course of temperature rise during ultrasound exposure (period between dashed lines) and subsequent cooling.

These temperature profiles provide us with some idea of the expected heating patterns in the tissue during experiments. Although the cross sectional area of the beam only covers a few square mm, the measurements show that there was still some degree of heating in the tissue outside this area. The asymmetries observed in the profiles may be accounted for by a slight misalignment of the beam axis, which would mean that the measurement plane would not be exactly perpendicular to the beam axis, and by a small degree of asymmetry in the beam. Obtaining these measurements was time consuming and they were difficult to reproduce, which added an extra source of uncertainty. The variation of the profile in planes both deeper and more superficial than the focus depth was not investigated due to time constraints and the limited stability of the measurement system.

3.6.5 Non thermal effects

The previous section presented measurements and calculations related to thermal effects in this study. In this section investigations into the possibility of mechanical and non-thermal non-mechanical effects are presented.

Streaming

The transducer used throughout this study was used in an earlier study on measurement of streaming using MRI by Starritt et al. (2000). Streaming in a water filled Perspex tube was measured during exposure to a diagnostic type pulsed ultrasound field. At an acoustic power of 39 mW and peak negative acoustic pressure of 0.96 MPa, a streaming velocity of 3.2 mm s^{-1} was measured. At higher acoustic powers and acoustic pressures the velocity could not be measured due to flow instability. This acoustic pressure is much higher than the acoustic pressure during continuous wave exposure in this study and lower than that during diagnostic type pulsed exposure in this study. For continuous wave exposure, although the conditions are different, it may be expected that streaming velocities would be very small, less than 1 mm s^{-1}. Flow instability may be present during diagnostic pulsed ultrasound exposure in this study. The measured streaming velocities are insignificant relative to the velocity of blood flow which is of the order of 100 cm s^{-1}.

A brief investigation of streaming around the artery under the experimental conditions was conducted here. The artery preparation was mounted in the normal configuration and a small drop (1 μl) of Evans blue solution (1% w/v in buffer) was placed close to the artery on the side at which the beam was incident; the beam was switched on for 4 minutes. The position of the dye was observed using a digital camera, while the beam was switched on and for several minutes after it was switched off.

When the beam was switched on, the dye droplet migrated around the artery ring and moved along the tank in the direction of the beam axis. The mean velocity of the dye was 3-4 cm per minute. The dye continued to migrate for a short time after the beam was switched off. In the absence of ultrasound the dye dispersed diffusively with a slight density-driven convection towards the bottom of the tank. Because of the difficulty of introducing the droplet reproducibly, no attempt was made to quantify its behaviour.

Cavitation

At the acoustic pressures used during continuous wave insonation of the tissue, cavitation is unlikely. It may be possible at higher acoustic pressures such as those present during pulsed wave exposure. The influence of the pulsing regime on the response of artery rings to ultrasound was tested and the results are presented in Chapter 4. The pulsing regimes employed provided different levels of acoustic pressure. If cavitation was involved in the response, it may be evident in the response of the artery to the different pulse regimes. No attempt was made to detect cavitation directly in this study as it did not seem to be a major factor in the response.

4 Response of large arteries

4.1 Introduction

This section details the methods and results of experiments performed on large conducting arteries to investigate the effects of ultrasound on vascular tone.

The first series of experiments was performed on sections of equine carotid arteries. This type of artery was chosen as an example of a large, muscular artery. The arteries were obtained from horses as they provide a suitable large mammal model and were readily available. The carotid arteries were easy to remove from the animal after death due to their superficial position. A further set of experiments was performed on a large artery taken from the equine mesentery, acting as another example of a relatively muscular artery. The aim of repeating the experiments in this second type of artery was to confirm earlier findings and to explore whether or not the response is limited to the carotid artery and to explore the dependence on vessel structure and mechanics.

The series of experiments performed on each type of artery were designed to first confirm and quantify the effect of ultrasound on the vessel tension, then to investigate the effects on this response of changing the exposure protocols, ultimately to identify the mechanism of interaction of the ultrasound with the cells.

4.2 Experimental methods

4.2.1 Tissue acquisition and dissection

Carotid arteries

Equine carotid arteries were collected at a local abattoir (Potters, Taunton, UK) immediately after death. They were excised from the animal by an abattoir worker a

few minutes after exsanguination and placed in cold (4 °C) Krebs-Ringer buffer for transport to the laboratory. Tissue was available from animals of all ages slaughtered for various reasons not limited to old age. In this study, very old horses were excluded and tissue was obtained from horses mainly under approximately 15 years old.

The dissection was performed under buffer at 4 °C to minimise shock and endothelial damage. The surrounding muscle, fat and loose adventitia was gently dissected free and the vessel was cut with a scalpel into segments of length 12.7 mm (mean), avoiding side branches. The cut sections were transferred to fresh buffer and stored at 4 °C until needed.

Mesenteric arteries

Sections of the lateral cecal mesenteric artery were collected from the fatty envelope which runs along the large intestine of the horse; this was accessible approximately 10 minutes after death and the tissue remained warm and blood filled. Sections of the artery within the fatty envelope were removed and placed in warm Krebs-Ringer buffer for transport back to the laboratory. Warm buffer was used for transport as it kept the fatty tissue around the artery soft, aiding dissection. The fatty tissue around the carotid artery did not solidify in the same way when cooled.

The tissue was pinned out in a container with a rubber base, submerged in buffer. The large artery was carefully dissected away from the surrounding tissue and cut into sections of approximately 13 mm in length with a scalpel. The artery sections were stored in buffer at 4 °C until needed.

4.2.2 Mounting procedure

The large water bath was lined with the acoustic absorber tiles and filled with warm (~37 °C) Krebs-Ringer buffer and the heat exchange coil was placed in the bath. Hydrophone measurements were made to determine the position of the focal region as described in Section 3.6.2. The force transducer and mounting rods were then positioned accordingly. A section of artery was taken from the fridge and placed into the water bath. The wire supports were aligned closely parallel to one another and the artery ring was carefully placed over them. The vessels were left to equilibrate for approximately 5 minutes before a wall stress of 3.9 ± 0.5 mN/mm^2 (mean $\pm$ sd) was

applied by extending the fixed wire support. This level of wall stress was chosen after preliminary experiments, as reproducible results with relatively low noise levels were consistently achieved. The artery was held at constant strain and was left to equilibrate for approximately one hour before exposures to ultrasound were made. Before exposure, a small syringe was used to gently flush fluid across the outer surface of the vessel to remove small bubbles, both visible and microscopic, which may have collected and acted to screen the tissue from the beam. The TPx membrane was carefully wiped with a cotton bud before exposures, also for this reason.

4.2.3 Tissue characterisation

To enable useful comparison of results obtained from the two types of large arteries, their physical and mechanical properties were investigated. Force extension curves were produced for sections of both types of artery. Vessel sections of 11 to 12 mm in length were mounted over two stainless steel supports, one of which was attached to the force transducer and the other to a micromanipulator and displacement transducer. The vessels were immersed in a beaker of Krebs-ringer buffer at 37 °C. Three stretch-relaxation cycles were performed on each vessel section. Stress and strain were calculated from these curves; stress, σ is given by

$$\sigma = \frac{F}{A} = \frac{F}{2tl}, \qquad\qquad 4.1$$

where F = force applied on the transducer, t = wall thickness measured in the relaxed state and l = length of vessel section. Wall stress was calculated in this manner for all experiments. Strain, ε is given by

$$\varepsilon = \frac{L - L_0}{L_0}, \qquad\qquad 4.2$$

where L = length of tissue, in this case distance between mounting rods and L_0 = length of tissue at which the force first deviates from zero. The incremental elastic modulus, E_{inc} at the level of wall stress exerted during experiments was calculated also:

$$E_{inc} = \frac{\Delta\sigma}{\Delta\varepsilon}. \qquad\qquad 4.3$$

The density and orientation of smooth muscle cells was determined for both vessels. Cross sectional and longitudinal histological sections of 20 μm thickness were prepared from fixed frozen tissue blocks. The sections were stained with haematoxylin and eosin (Drury and Wallington 1967) and examined under a microscope. The number of smooth muscle cells per square millimetre was counted on the cross sectional sections. The orientation of the smooth muscle cell nuclei was observed from both the cross sectional and longitudinal sections.

4.3 Experiments on carotid artery

4.3.1 Exposure of carotid arteries to ultrasound

The following experiments were performed using sections of carotid artery mounted as described in Section 4.2.2, in the large water bath in the configuration shown in Figure 3.1. Endothelial function tests were not performed due to the large volumes of buffer required. Instead the presence of endothelium was examined histologically at a later time. Measurements of the effect of noradrenaline (Sigma Aldrich) on vessel tension were performed on vessels mounted in a smaller bath. Concentrations ranging from 10^{-7} – 10^{-3} M were used. The results were used to assess the physiological significance of the effects of ultrasound and for comparison of the response of different types of vessels.

Establishing presence of a response

A series of experiments were performed to determine the response to ultrasound in general. After mounting and equilibration as described in the previous section, the vessels were exposed to continuous wave ultrasound at an acoustic power of 145 mW for 4 minute periods. After each exposure there was a gap of at least 10 minutes before the next. Some vessels were also exposed to pulsed ultrasound to determine whether a response was also provoked in this way. Artery sections that had been previously frozen and metabolically inhibited with sodium azide, were mounted and exposed to ultrasound to eliminate the possibility of radiation pressure artefacts or a passive response.

Endothelial dependence of the response

In order to test the dependence of the response on the endothelium, some vessels were de-endothelialised before mounting by brushing the endothelial surface with a soft brush. The vessels were then exposed to 4 minute periods of continuous wave ultrasound at an acoustic power of 145 mW. The response of these vessels was compared to the response of paired segments from the same vessel that had intact endothelium.

Power dependence

To investigate the mechanisms of interaction of ultrasound involved in the response, the dependence of the response on acoustic power was tested. A dependence on acoustic power would suggest the involvement of a thermal mechanism. Vessels were exposed to continuous wave ultrasound for 4 minute periods with a gap of at least 15 minutes between exposures. The acoustic power was alternated from one exposure to the next between 145 mW and 100 mW in half of the experiments, and 145 mW and 72 mW in the other half of experiments. The responses to ultrasound at these three levels were then compared; these levels represented 50%, 69% and 100% of the maximum acoustic power used.

Dependence on pulse regime

To investigate the dependence of the response on the acoustic pressure and pulse duration, the responses to two different pulsing regimes were used and compared to the response to continuous wave ultrasound exposure. The total acoustic power was kept constant at 145 mW throughout. One of the pulsing regimes was analogous to a diagnostic pulsed Doppler ultrasound beam, and the other was more similar to a therapeutic pulsed ultrasound beam with a longer pulse duration and lower pulse repetition frequency. The diagnostic type pulsing regime employed a pulse duration of 1 μs and a pulse repetition frequency of 2 kHz. The therapy type pulsing regime employed a pulse duration of 1 ms and a pulse repetition frequency of 10 Hz. The peak negative acoustic pressure was greater in the diagnostic pulsed field (2.00 MPa) than in the therapy pulsed field (1.20 MPa) and much greater than in the continuous wave field (0.18 MPa). The spatial peak time averaged intensity was 0.46 W cm^{-2} in

the diagnostic pulsed field, 1.18 W cm^{-2} in the therapy pulsed field and 1.07 W cm^{-2} in the continuous wave field.

Sustainability of response and recovery

The sustainability of the response was examined by exposing vessel segments to continuous wave ultrasound for periods of time up to 15 minutes. The aim was to determine if there was a point after which the vessel would be 'saturated' and would not contract further or whether contraction would decrease despite continued exposure. There is a limit to the contraction that can be induced by vasoactive drugs, such as noradrenaline; a similar limit may be observed here.

In the experiments described above, a recovery period of 15 minutes was allowed during which time the vessel tension returned to baseline. A series of exposures were performed to investigate the effects of shorter recovery periods on the vessel. Vessels were exposed to continuous wave ultrasound at an acoustic power of 145 mW for periods of between 60 minutes with recovery periods ranging from 2 seconds to 15 minutes.

Power threshold of response

A set of low acoustic power continuous wave ultrasound exposures was performed to investigate the possibility an acoustic power threshold for the response. Vessels were exposed for 4 minute periods to acoustic powers of 30 mW and below.

Histological examination

At the end of the exposure cycle the artery sections were fixed in 10% formol saline. They were later stained with haematoxylin and examined *en face* under a low power microscope to establish the integrity of the endothelium. Frozen 20 μm thick cross sections were also prepared, stained with haematoxylin and eosin and examined under the microscope.

4.3.2 Response of carotid arteries to temperature changes

The results obtained from experiments on the exposure of artery sections to ultrasound suggested that the response was thermally mediated. In order to test

whether a similar response could be provoked purely by thermal means, the effect of temperature changes on the arterial wall tension was investigated.

Segments of artery were mounted as described in Section 4.2.2. The vessel was left to equilibrate for 60 minutes before being exposed to a series of changes in temperature of 1 to 2 °C above the normal bath temperature (37.5 °C). Tension was recorded as the temperature was slowly increased then lowered back to normal.

4.4 Results: Carotid artery

In total, 40 artery rings taken from 17 carotid arteries were used in the following experiments. From these 40 experiments, a total of 32 usable data sets were obtained. The remaining data sets were discarded for reasons including a lack of response to ultrasound, failure of the vessel to relax and reach the required state, or large amplitude noise in the data. On average the vessels had an internal diameter of 4.5 mm, an external diameter of 8.0 mm and a length of approximately 12 mm.

4.4.1 Vessel characterisation

Force extension curves

Force extension curves were plotted for 4 sections of carotid artery. A typical set of curves is shown in Figure 4.1. Three stretch relaxation cycles are shown with arrows indicating the time sequence of data acquisition. Hysteresis is observed in all three cycles, to a lesser extent in each subsequent cycle. On the initial cycle, increase in force begins at a low extension. In later cycles, greater extension is needed to apply the same level of force. This behaviour is commonly observed during mechanical testing of blood vessels as described by Dobrin (1978) who links the hysteresis to changes in active stress levels during stretching.

Stress and strain were calculated for the artery rings, a typical curve is shown in Figure 4.2. The mean wall stress during the period when arteries were exposed to ultrasound was 2.3 ± 0.7 mN/mm^2. The incremental elastic modulus at this level of stress was 14.1 ± 3.9 mN/mm^2.
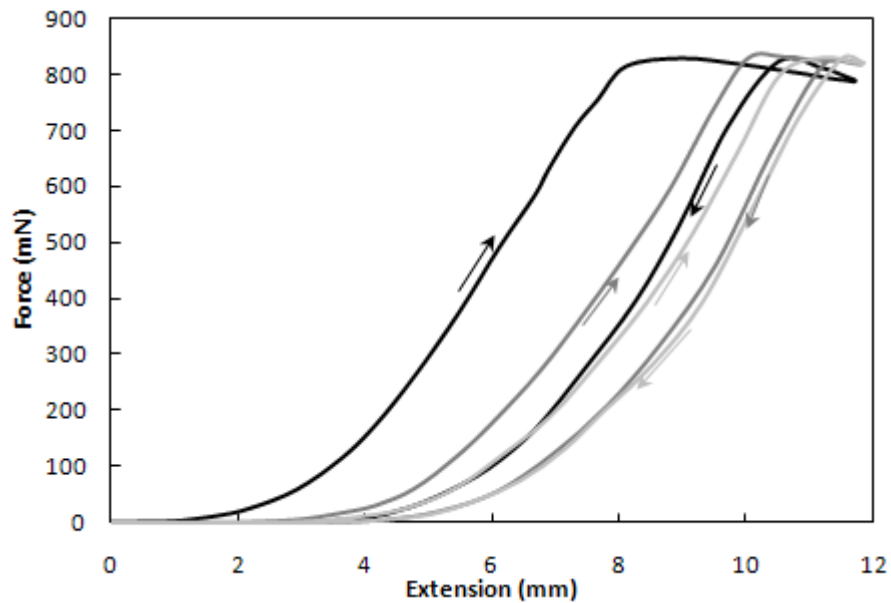
Figure 4.1 Force extension curves obtained from a section of carotid artery; 3 stretch-relaxation cycles are shown: ▬ 1st cycle, ▬ 2nd cycle, ▬ 3rd cycle. The arrows indicate the time sequence of data acquisition and show which legs were acquired during stretch and which were acquired during relaxation.
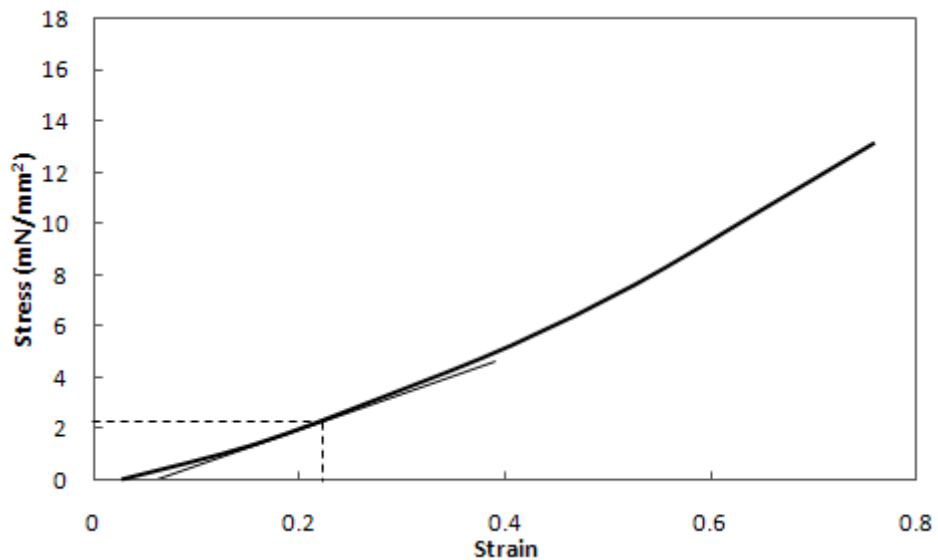
Figure 4.2 Typical stress-strain curve for carotid artery ring; the mean level of wall stress during exposures to ultrasound is marked by the dotted line. The incremental elastic modulus was calculated at this value.

Histological characterisation

Figure 4.3 shows the results of histological examination of carotid artery sections. The cell nuclei stained with haematoxylin are dark purple, the cytoplasm and other material is stained light purple or pink. The basement membrane can be seen, it appears as a brownish layer in the tissue. Figure 4.3 a) shows a tissue section under low magnification. The endothelium can be seen at the top of the picture, the basement membrane below this and then a regular structure of smooth muscle making up the bulk of the wall area. In b), which shows a similar section under higher magnification, the endothelial cell nuclei can be seen clearly along the top of the photo. The basement membrane is again visible as a layer beneath the endothelium. This section appears to be in a state of contraction as can be seen by the folding of the endothelium and basement membrane. The smooth muscle nuclei in this section also look contracted; they look slightly folded or crumpled. Photo c) shows a similar section, this time from the mid media. The smooth muscle nuclei are all aligned with similar orientations, stretching around the vessel wall circumferentially. This section appears to be more relaxed than the previous sections, as can be seen from the straighter smooth muscle nuclei and elastic lamellae. Photo d) shows a longitudinal section through the wall of a carotid artery section. The smooth muscle nuclei again appear dark pink purple but this time appear as dots. This indicates that the smooth muscle nuclei are aligned perpendicularly to the plane of the section, i.e. circumferentially.

The number of smooth muscle cells per unit area in the mid media was counted from similar images of histological sections, the carotid artery sections were found to contain 2830 ± 40 nuclei per mm^2.

Histological examination of sections of artery fixed after mounting and exposure to ultrasound, revealed that in most preparations, the endothelium was intact except in regions in direct contact with the supporting rods. The structure of the vessels was otherwise unaffected.
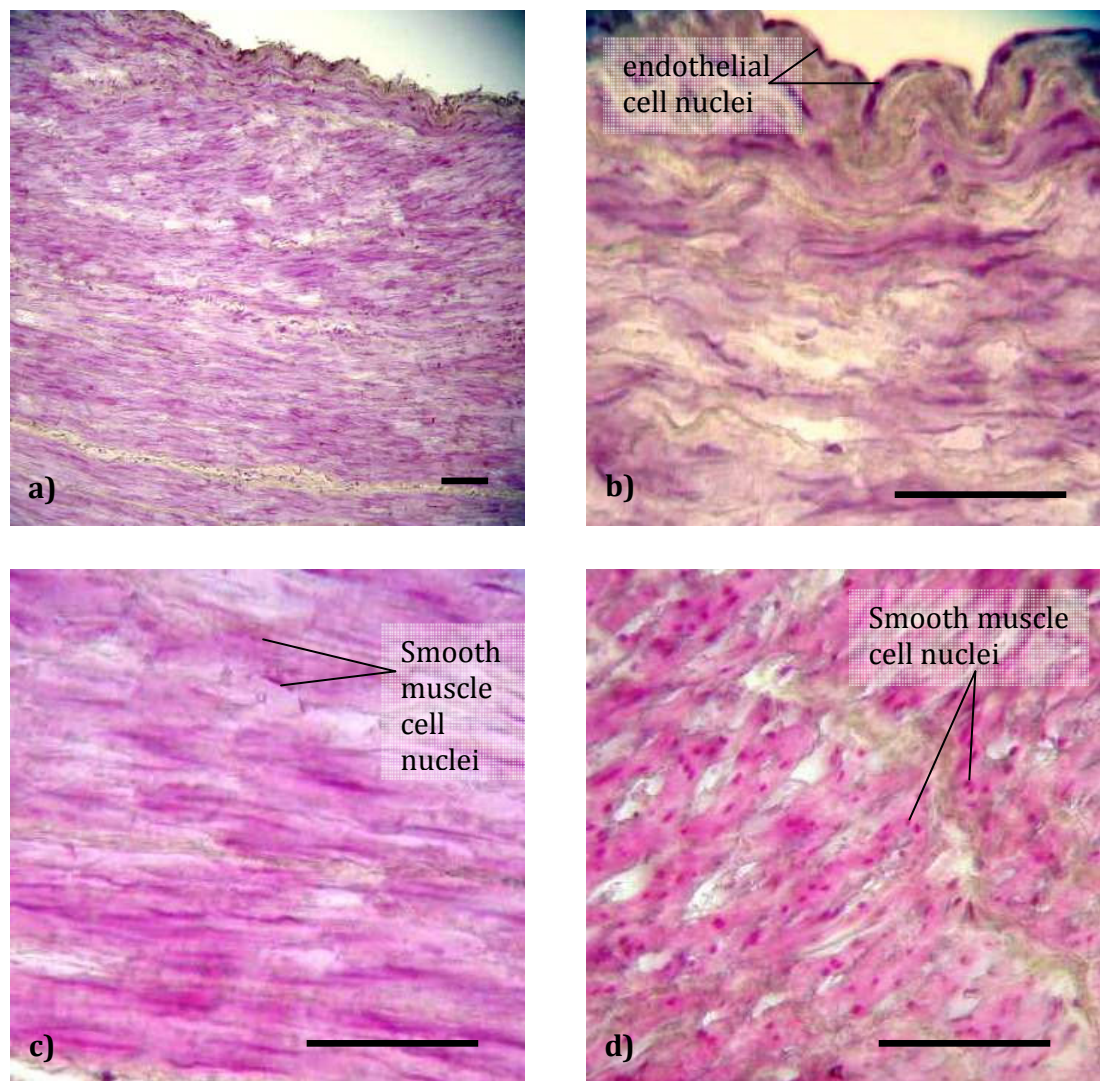
Figure 4.3 Histological sections of carotid artery stained with haematoxylin and eosin, cell nuclei are stained dark purple; a) endothelium, basement membrane and smooth muscle in the vessel wall under lower magnification; b) transverse cross section showing endothelial cells on the luminal edge and basement membrane over smooth muscle cells; c) smooth muscle cells stretching around the vessel wall in the mid media; d) longitudinal section: smooth muscle cell nuclei appear as dots confirming circumferential ring like orientation of cells around the vessel. Bar = 100 µm.

Response to vasoactive drugs

In order to relate the magnitude of the response to ultrasound to maximal muscular contraction, tension was induced by doses of noradrenaline (0.1 µM - 0.1 mM) added to the tissue bath in 6 artery rings. On average, the wall stress increased by 0.7 mN/mm^2, with a maximum increase of 1.4 mN/mm^2 in one vessel. Two typical dose response curves are shown in Figure 4.4; both are shown as they exhibit slightly

117

different behaviour. One curve shows a slow increase in tension at low doses, followed by a steeper rise at higher doses. In the other curve, there is a more rapid increase in wall stress at low doses followed by a slight levelling off of the surve at higher doses. Other rings tested exhibited similar behaviour either of these curves. The variation in magnitude between the responses of the sections tested was very large, but the behaviour was similar in each. The variation may be due to the initial state of the vessels and differences in tension during administration of the noradrenaline. These values are not intended to be absolutely quantitative, but instead provide some insight into the level of increase in wall stress induced by vasoactive drug, so that comparisons can be made with the change in wall stress induced by ultrasound. When the vessel was exposed to ultrasound immediately following maximal contraction by noradrenaline, no response was observed.
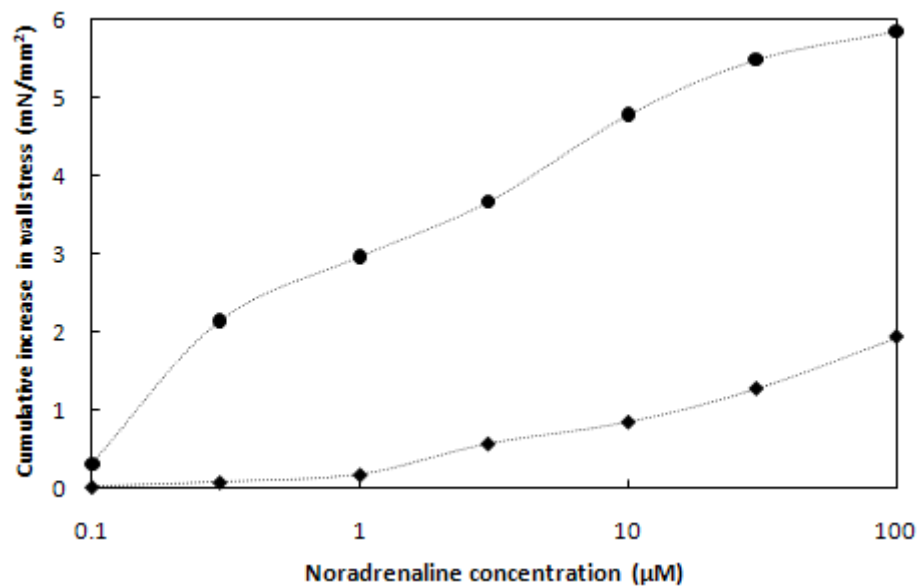
Figure 4.4 Typical noradrenaline dose response curves: cumulative increases in wall stress induced by doses of noradrenaline (0.1-100 μM) in carotid artery rings held under constant strain. The two curves exhibit slightly different behaviour, the behaviour of other rings tested was similar to one of these curves.

4.4.2 Response to ultrasound

Vascular Response

The artery sections were held at constant strain throughout each experiment. An initial wall stress of approximately 3.9 mN/mm² was applied; after this the basal wall stress generally decreased by approximately 60% over a period of 45 min. It then began to rise at a slow, almost linear rate. In some samples, during the initial decrease in wall stress, spasming of the vessel was observed. During this period, the wall stress oscillated as it decreased; the magnitude of the oscillations ranged from approximately 0.15 to 1.3 mN/mm² in different samples. The oscillations generally decreased in magnitude as the baseline wall stress decreased, and ceased by the time it reached a minimum. The artery wall stress was allowed to decay and enter the later phase of steady increase before all exposures to ultrasound or temperature changes. For analysis of results, this steady increase in wall stress was fitted with polynomial functions and subtracted from the data, to bring the baseline to zero. Therefore, the reported changes in wall stress are above baseline values.

The effect of the initial tension in the vessel on the magnitude of the response was investigated by making measurements at different levels of the initial tension by changing the separation of the support rods. It was found that the initial tension had no consistent effect on the response. The initial tension used throughout the experiments was chosen after some experimentation, to be one at which it was shown that reliable and consistent results could be obtained, with relatively low levels of background noise. However, variation in the magnitude of the response between artery sections may in part be due to a dependence of the response on the basal tension, which varied during the experiment.

Exposure of artery sections to ultrasound induced an increase in wall stress above the baseline, which began when the beam was turned on and continued until it was turned off. Figure 4.5 shows a typical response of a carotid artery segment to a 4 minute exposure to 145 mW ultrasound at a frequency of 3.2 MHz. Contraction began within a few seconds of the start of insonation and tension rose rapidly and almost linearly over approximately 2 minutes. The increase in tension then continued at a slower rate until the acoustic field was turned off. When the field was switched off, tension

decayed fairly rapidly at first and then gradually slowed as it returned to baseline over a period of approximately 10 minutes. When the ultrasound exposure was repeated after a recovery period of at least 10 minutes, the second response was indistinguishable from the first. With a recovery period of this length, the response could be continually reproduced over a 2 hour period. Also shown in this figure is the response of a section of artery, which had been metabolically inhibited; a small change in wall stress was observed during exposure to ultrasound. The change was a small fraction of the change observed in a fresh artery ring, and so significant passive effects on the tissue during exposure were ruled out.
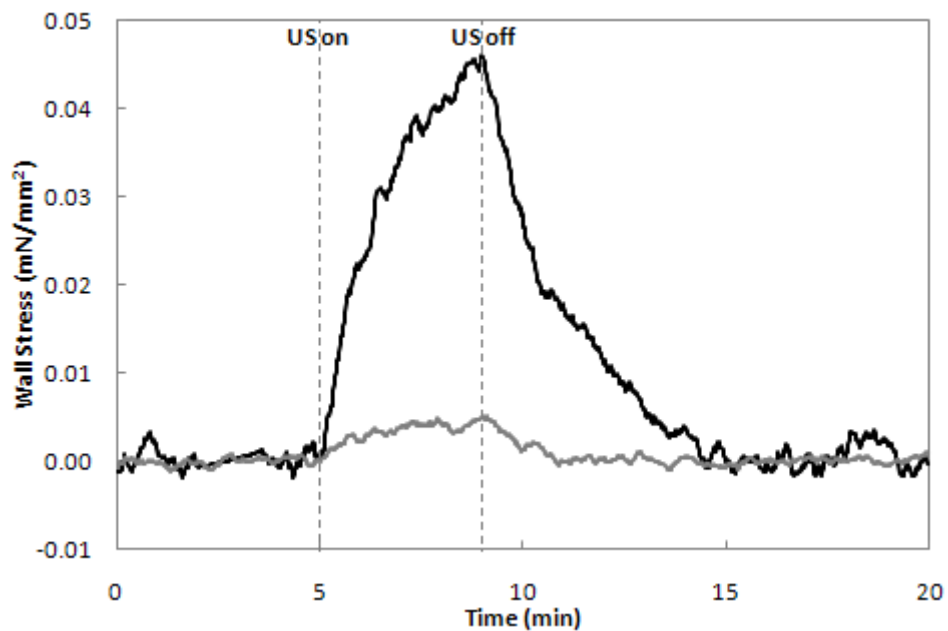
Figure 4.5 Typical response curves for carotid artery rings exposed to ultrasound for a 4 minute period at an acoustic power of 145 mW. ▬ shows the response of a ring of fresh tissue; ▬ shows the response of an artery ring after metabolic inhibition with sodium azide. Increase in wall stress above baseline which has been set to zero is shown; the dotted lines indicate the beginning and end of the exposure. In the live section, wall stress increases during the period of exposure, slowly returning to baseline afterwards. There is a very slight increase in the wall stress measured for the dead ring.

The mean response of artery rings to ultrasound at an acoustic power of 145 mW was 0.020 ± 0.018 mN/mm^2 (mean ± s.d, n = 77). This was about 4% of the mean maximal response to noradrenaline and approximately 8% of the increase in wall stress

induced by a 1 μM dose of noradrenaline. The response was qualitatively similar in all specimens, but quantitatively the response varied by approximately 35% between exposures for a single segment, approximately 45% between segments of the same vessel and by approximately 75% between vessels.

Endothelial dependence of the response
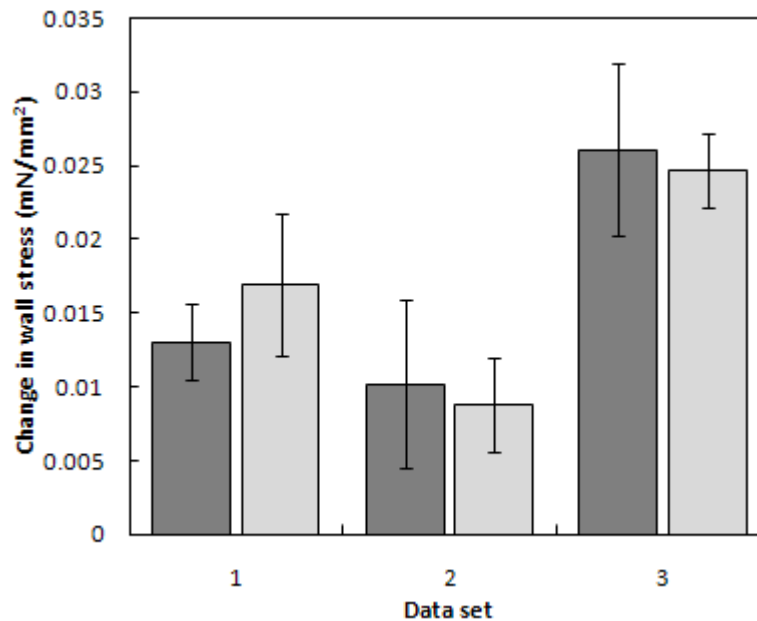
Figure 4.6 The graph shows mean change in wall stress due to ultrasound exposure from 3 sets of paired segments with intact ■ and denuded □ endothelium; error bars show the standard deviation of the means.

The dependence of the effect on the endothelium was investigated by comparing the responses of arterial segments that were de-endothelialised prior to mounting, to the response of paired segments with intact endothelium (n = 26 measurements on 3 pairs of artery rings taken from two equine vessels; the data from a further pair of rings was discarded due to high levels of noise). The mean change in wall stress for each of the artery rings grouped in their pairs is shown in Figure 4.6; the standard deviations of these means are shown as error bars on the graph. As can be seen from this figure, for two out of the three pairs, the mean response was slightly smaller in the denuded sections than in the intact sections and was slightly larger in the remaining case. There was no significant difference between the response of intact and denuded samples in any case as verified by a Student's T test. No differences were observed in

the time-course of the response, or recovery after exposure, between groups. The ultrasound induced contraction is therefore considered to be endothelium independent.

Power dependence
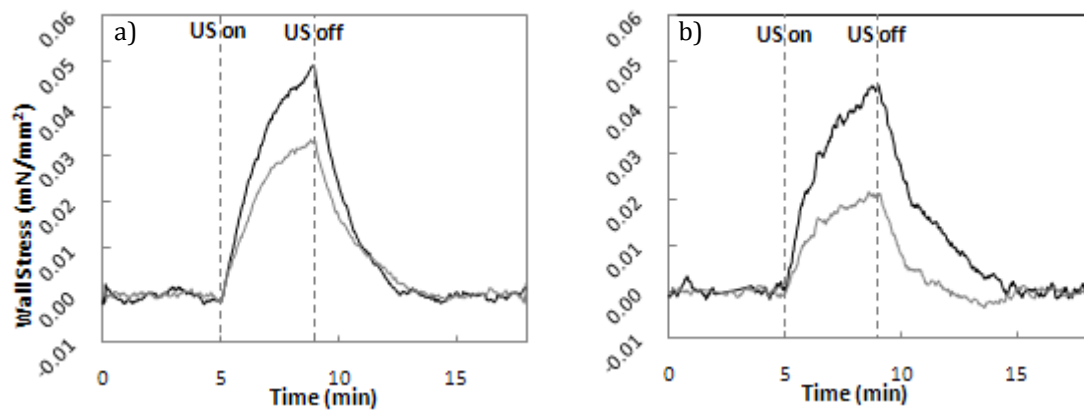
Figure 4.7 Typical responses to 4 minute ultrasound exposures at different acoustic power levels of two different samples of carotid artery ring; a) ▬ exposure to ultrasound at 145 mW, ▬ exposure to ultrasound at 100 mW; b) ▬ exposure to ultrasound at 145 mW, ▬ exposure to ultrasound at 72 mW; the dotted lines show the times at which the exposure began and ended. The wall stress is shown as an increase above baseline, which is set to zero.

The effects of beam power were investigated by exposing artery rings to continuous wave ultrasound at different acoustic powers. A difference in magnitude of the increase in tension due to ultrasound was clearly observed between exposures to different acoustic powers in each artery ring. The mean amplitude of the ultrasound-induced tension increase for each sample decreased with decreasing beam power. As shown in Figure 4.7, the time course of the response was unaffected by the acoustic power of the beam.

Experiments were performed on 14 artery rings in total, from which ten useful data sets were obtained. The remaining data was discarded for reasons stated at the beginning of Section 4.4. Figure 4.8 shows the results obtained for artery rings exposed to ultrasound at 145 mW and 100 mW (69% of the maximum acoustic power). The mean increase in wall stress during exposure at both acoustic power
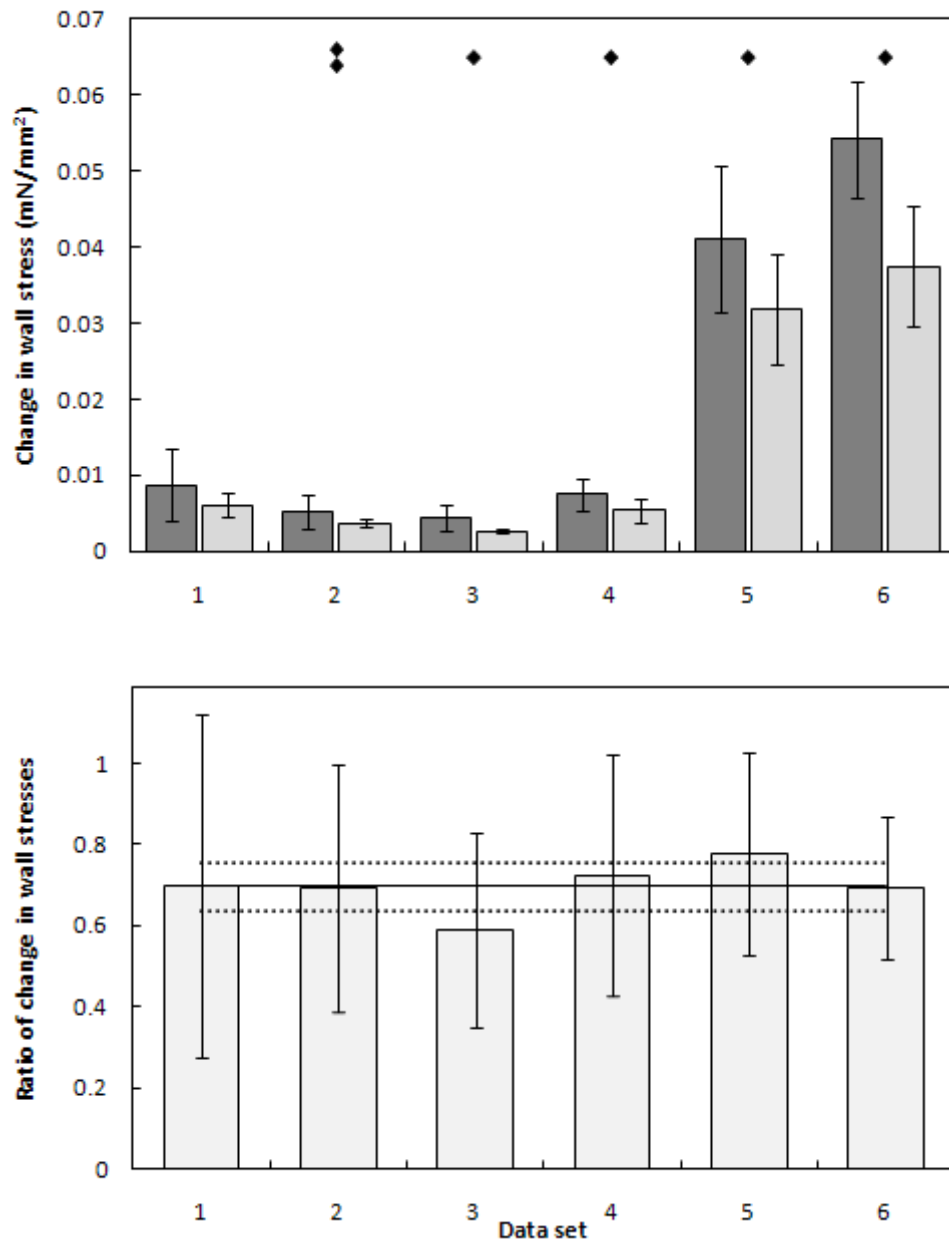
Figure 4.8 Results from experiments performed on 6 artery rings (numbered 1 – 6 on horizontal axis) exposed to ultrasound at 100% and 69% acoustic power levels. The top graph shows the mean change in wall stress due to exposure at the 100% acoustic power level ■ ; and the 69% acoustic power level □ ; the error bars show ± 1 standard deviation of the mean. ✦ shows a P-value of ≤0.1, ◆ shows a P-value of ≤0.05. The bottom graph shows the ratio of the means for each data set. Error bars show error computed from the standard deviation of the means shown in the top graph. ▬ shows the mean of the ratios over all data sets; …. shows ± 1 standard deviation of the mean.

Figure 4.9 Results from experiments performed on 4 artery rings (numbered 1 – 4 on horizontal axis) exposed to ultrasound at 100% and 50% acoustic power levels. The top graph shows the mean change in wall stress due to exposure at the 100% acoustic power level ■ ; and the 50% acoustic power level □ ; the error bars show ± 1 standard deviation of the mean.✦ shows a P-value of ≤0.1, ◆ shows a P-value of ≤0.05. The bottom graph shows the ratio of the means for each data set. Error bars show error computed from the standard deviation of the means shown in the top graph. ▬ shows the mean of the ratios over all data sets; …. shows ± 1 standard deviation of the mean.

levels is shown for each artery ring. Figure 4.9 shows the results for the case when the ultrasound exposures were at 145 mW and 72 mW (50% of the maximum acoustic power level). As can be seen, the increase in wall stress due to exposure to the lower acoustic power level is smaller in each case. The standard deviations of these means are shown as error bars on the graphs. In some cases, these are large as there was a high degree of variability between responses to ultrasound, as observed in the previous results presented in this chapter. A Student's T test showed that the differences were in fact significant in 9 out of 10 cases (p-value ≤0.05 in 7 cases and ≤0.1 in the other 2 cases). There was also a high degree of variability in the magnitude of the responses from one artery ring to another, up to a factor of 10 in some cases. However, the ratio of the responses was relatively consistent, regardless of their magnitudes. The lower graph in each of these figures shows the ratio of the response induced by exposure to the two acoustic power levels for each artery ring. The solid line shows the mean ratio of the responses across all rings. The uncertainty on these values was computed from the standard deviation of the means; they are large and encompass the mean ratio in all cases.

Normalising the response at 145 mW to unity, the response at 100 mW was 68 ± 7% and at 72 mW was 53 ± 5% of the maximum. These acoustic power levels represent 69% and 50% of maximum acoustic power respectively; it appears that the increase in tension induced by exposure to ultrasound is related to the acoustic power in an approximately linear fashion.

Dependence on pulse regime

In a series of six experiments, a comparison was made of the effects of continuous wave and diagnostic and therapeutic pulsed ultrasound at the same time averaged acoustic power. Five useful data sets were obtained from these experiments; the remaining data set was discarded for reasons given at the beginning of Section 4.4.

The mean responses to each of the pulse regimes for each experiment are shown in Figure 4.10. The response to therapy type pulsed ultrasound is slightly larger than for continuous wave ultrasound in 3 out of 4 cases. The response to diagnostic ultrasound is smaller than for continuous wave ultrasound in 2 out of 3 cases. These slight differences may show some consistent behaviour, but a Student's T test used to test

the significance of these differences gave p-values ranging from 0.25 to 0.7 suggesting that the differences were not significant.
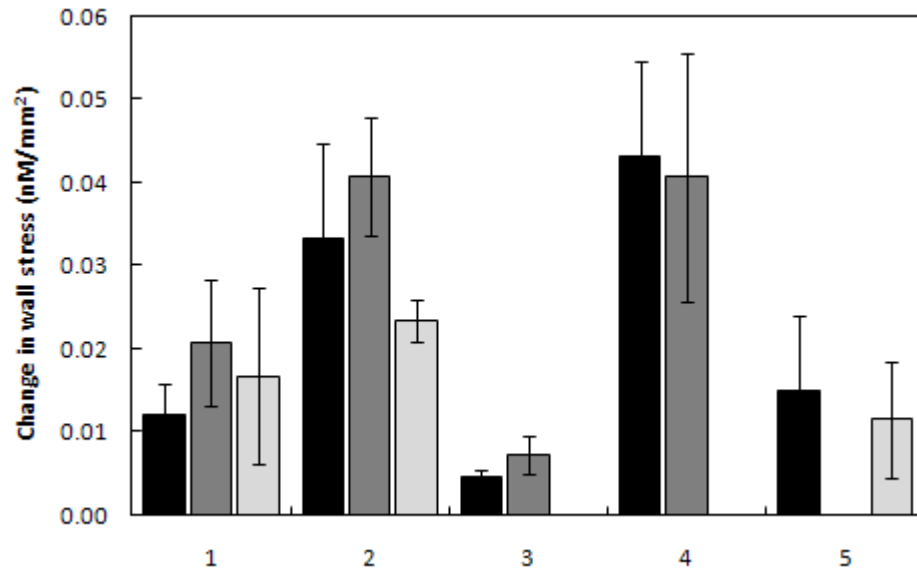
Figure 4.10 The graph shows results from experiments on 5 artery rings (numbered 1 – 5 on the horizontal axis) exposed to at least 2 out of 3 different pulse regimes. The columns show the mean response to ■ continuous wave ultrasound, ▨ therapy pulsed ultrasound, ☐ diagnostic pulsed ultrasound. Error bars show the standard deviation of the means.

If there was any real difference between the response to the continuous wave ultrasound and the diagnostic pulsing regime, it may be explained at least partially by acoustic power loss at the focal region due to nonlinear propagation associated with the high peak negative acoustic pressure during the pulses. This would be difficult to quantify. However, it is clear that any dependence on pulse regime is not as strong as that on beam power. No evidence was found that the ultrasound induced increase in wall stress was dependent on the pulsing regime in these cases. A more thorough investigation of the dependence of the response on different pulsing regimes would be required to fully eliminate dependences on acoustic pressure, pulse duration and pulse repetition frequency.

Sustainability of the response and acoustic power threshold

The sustainability of the ultrasound induced increase in wall stress was investigated by exposing artery rings to ultrasound for extended periods of time. When exposure

was prolonged for up to 15 minutes, the increase in wall stress continued throughout, though at a decreasing rate. A typical example is shown in Figure 4.11. After a recovery period of at least 10 minutes, one response was similar in magnitude to the next and the following response was not affected. After shorter recovery periods the response was attenuated. For recovery periods of less than a minute, the response was on average 50% of that initially. For very short 'off' periods of only a few seconds, the increase in tension continued as if the tissue had been exposed continuously.
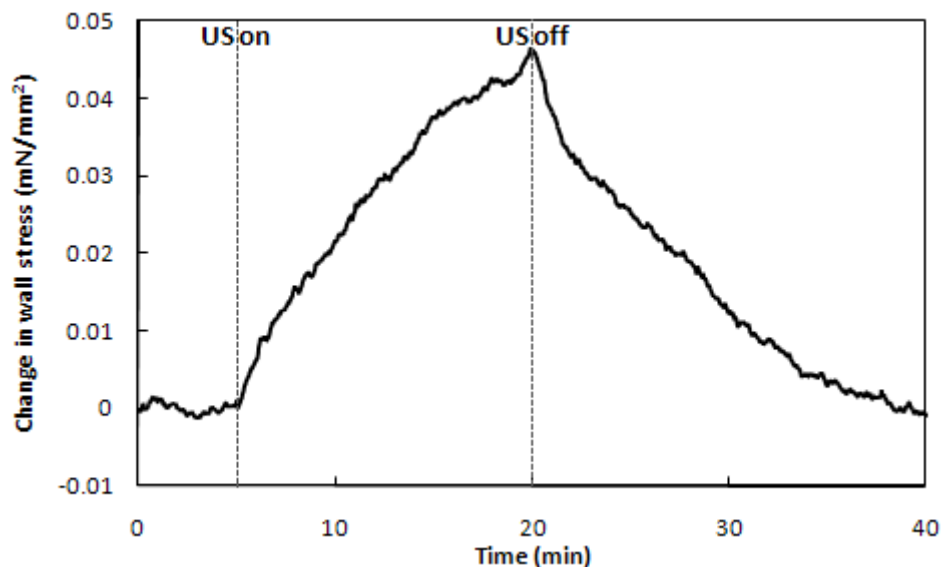
Figure 4.11 Typical response of wall stress in a ring of carotid artery to an extended period of exposure to ultrasound, the dotted lines show the beginning and end of the period of ultrasound exposure. Wall stress continues to increase during the period of exposure although at a decreasing rate; wall stress slowly returned to baseline after exposure.

Acoustic power threshold

Three sections of artery were exposed to ultrasound at decreasing acoustic powers. The magnitude of wall stress increase appeared to follow the linear dependence discovered previously. At acoustic powers below 30 mW, the response could no longer be resolved against the background noise. It was concluded that there was no observable threshold for the response in this system; the measurement of the response to small acoustic powers was limited by system noise.

4.4.3 Response of carotid arteries to temperature changes

To investigate the possible involvement of a thermal mechanism in the response to ultrasound, as may be suggested by the dependence on acoustic power, artery rings were exposed to increases in temperature of 2 to 4 degrees above 37 ℃.

As the bath temperature was increased, wall stress increased in an approximately linear fashion at a rate of 0.18 ± 0.07 mN/mm °C (n = 6). An associated decrease in wall stress was seen during decreases in temperature back to baseline levels. These data suggest that only a very small change in temperature is required to cause an increase in wall stress of a similar magnitude to that induced by exposure to ultrasound. It has been shown in Section 3.6.4 that the temperature rise in the focal region of the ultrasound beam was no more than 0.3 ℃ after a four minute exposure to ultrasound at 145 mW. It is estimated that a temperature rise of 0.3°C would produce an increase in wall stress of approximately 0.05 mN/mm². This is more than twice the mean increase in wall stress measured in response to ultrasound exposure. There is some difficulty in comparing these two results, as the conditions differ significantly. The results described here were obtained by changing the ambient bath temperature, so the whole tissue volume would be heated to the same temperature. The heating caused by the ultrasound beam would be localised in the tissue, as the beam area at the focal region is smaller than the tissue. Therefore, there would be a temperature gradient across the tissue and heating would take place at different rates depending on the location relative to the beam axis. It is difficult to estimate the spatial patterns of temperature increase in the tissues during the exposure. At the end of the exposure there was a temperature increase over an area larger than the focal region, although it was lower than on the beam axis (see Section 3.6.4). This profile was measured using a thermal test object with homogeneous thermal properties; the temperature profile in the tissue may vary from this.

It is not known exactly how these differences in heating would affect the cellular response, and as such, we can not draw direct comparison between these results. However, we can conclude that heating from a source other than the ultrasound beam influences wall stress in a similar manner to ultrasonic heating. The cellular mechanisms of this response are pursued further in Chapter 6.

4.5 Experiments on mesenteric arteries

4.5.1 Exposure of mesenteric arteries to ultrasound

A series of experiments was performed to compare the response of vascular tone to ultrasound exposure in mesenteric arteries which differ in physiological function, extracellular matrix and cellular structure from carotid arteries.

The artery sections were mounted in the same manner as the carotid arteries. All experiments were performed in the configuration shown in Figure 3.2 with the polythene container in place. The container was filled with 150 ml of Krebs-Ringer buffer as a standard amount. This configuration was used so that vessel function tests could be performed on each section before ultrasound exposure.

Vessel function tests

The artery sections were mounted, stretched and left to equilibrate for 45 minutes. Vasoconstriction was induced with a 1 µM dose of noradrenaline (Sigma Aldrich). When the tension had reached a maximum level, which happened approximately 1 minute later, a 1 µM dose of acetylcholine was added to the bath. In artery sections with intact endothelium this induced vasodilatation; in artery sections where the endothelium was not intact, an increase in tension was induced (Furchgott and Zawadzki 1980). Once the function test had been performed, the buffer contained within the polythene container was refreshed with 300 ml of fresh buffer; the final fluid volume in the container was 150 ml. After the medium was refreshed, the vessel was again allowed to equilibrate until the tension had returned to a stable level and the temperature of the bath had stabilised.

Vascular response, endothelium and acoustic power dependences

The response of mesenteric artery rings to ultrasound was investigated using the same methods as for the carotid artery rings. Experiments were performed to establish the presence and magnitude of the response to ultrasound at 145 mW. The endothelium dependence and acoustic power dependence was also tested.

4.6 Mesenteric artery results

The following results were obtained from experiments on a total of 26 artery rings taken from 13 mesenteric arteries. Twelve of these arteries either failed to respond to either noradrenaline or ultrasound, did not relax to the correct state after stretching or exhibited highly fluctuating tension. It was presumed that these vessels were either dead, or were severely affected by damage sustained during initial handling. The rings used in these experiments had a length of 13.2 ± 1.1 mm (mean ± sd), an internal diameter of 3.4 ± 0.8 mm (mean ± sd), an external diameter of 6.7 ± 1.1 mm (mean ± sd) and a wall thickness of 1.5 ± 0.1 mm (mean ± sd).

4.6.1 Vessel characterisation

Force extension curves
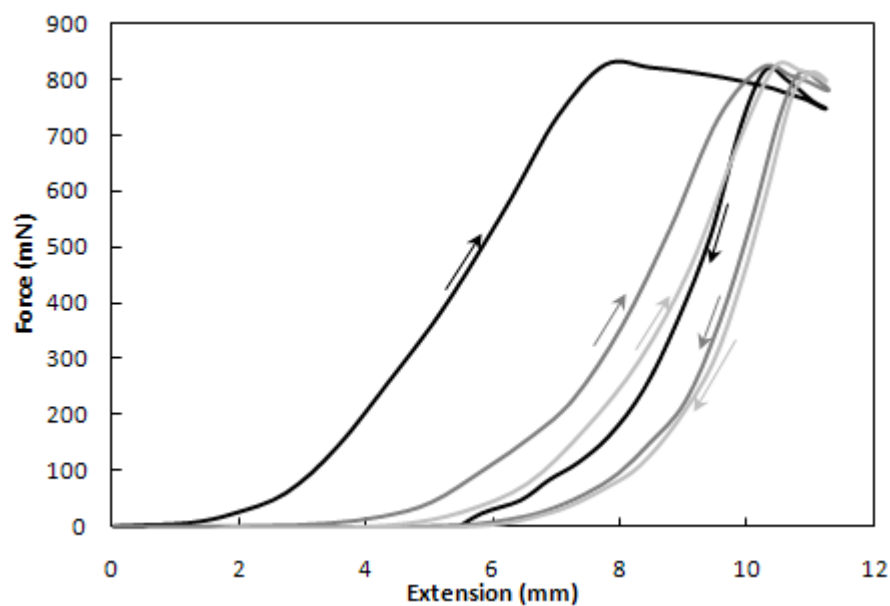
Figure 4.12 Force extension curves obtained from a section of carotid artery; 3 stretch-relaxation cycles are shown, ▬ 1st cycle, ▬ 2nd cycle, ▬ 3rd cycle. There is a large degree of hysteresis in the first cycle, it then decreases with each subsequent cycle.

Force extension curves were plotted for a group of mesenteric artery sections. A typical set of curves is shown in Figure 4.12. Three stretch relaxation cycles are shown with arrows indicating the time course of data acquisition, showing which legs were acquired during stretching and which during relaxation. The curves take the

form of hysteresis loops, the degree of which decreases between each cycle and the next. A much larger force is generated for a given extension in the first stretch cycle than in later ones. Stress and strain were calculated from these curves, a typical stress strain curve is shown in Figure 4.13. The mean wall stress during exposure of the arteries to ultrasound was 1.4 ± 1.2 mN/mm^2. The incremental elastic modulus at this stress was 18.1 ± 2.9 mN/mm^2, 25% higher than for the carotid arteries.
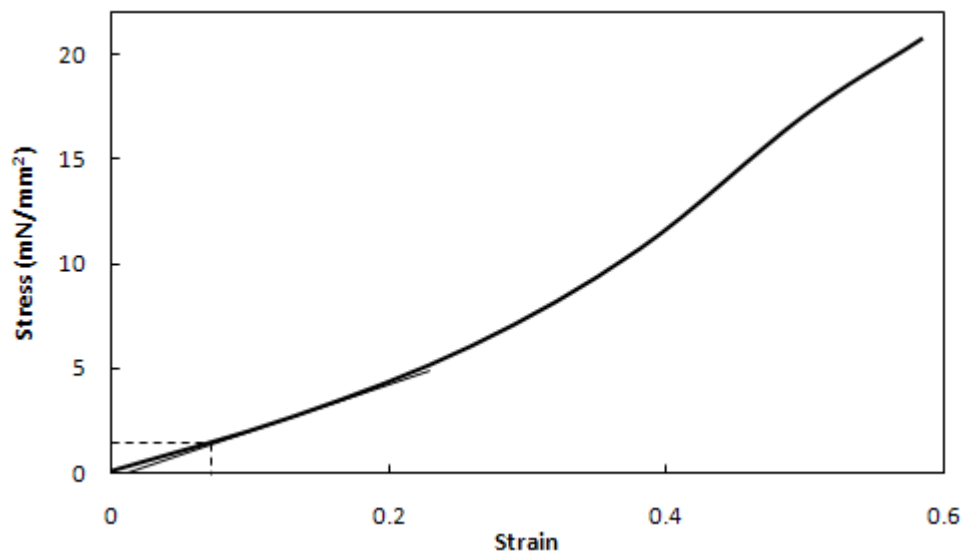
Figure 4.13 Typical stress-strain curve for mesenteric artery ring; the mean level of wall stress during exposures to ultrasound is marked by the dotted line. The incremental elastic modulus was calculated at this value.

Histological characterisation

Figure 4.14 shows images of 20 μm thick histological sections of mesenteric artery, stained with haematoxylin and eosin. Smooth muscle nuclei are stained dark purple or pink, the remaining tissue is stained lighter pink or purple and the elastic layers appear brownish. Photo a) shows a section of the vessel wall under low magnification. The luminal surface of the vessel is at the top of the photo. The endothelium and basement membrane can be seen running along this edge, and below them is the vessel wall made up mainly of smooth muscle nuclei. At the lower edge of the tissue, the adventitia can be seen; this tissue is tearing away from the outside of the vessel. Photo b) shows a similar section under higher magnification. The luminal surface is at
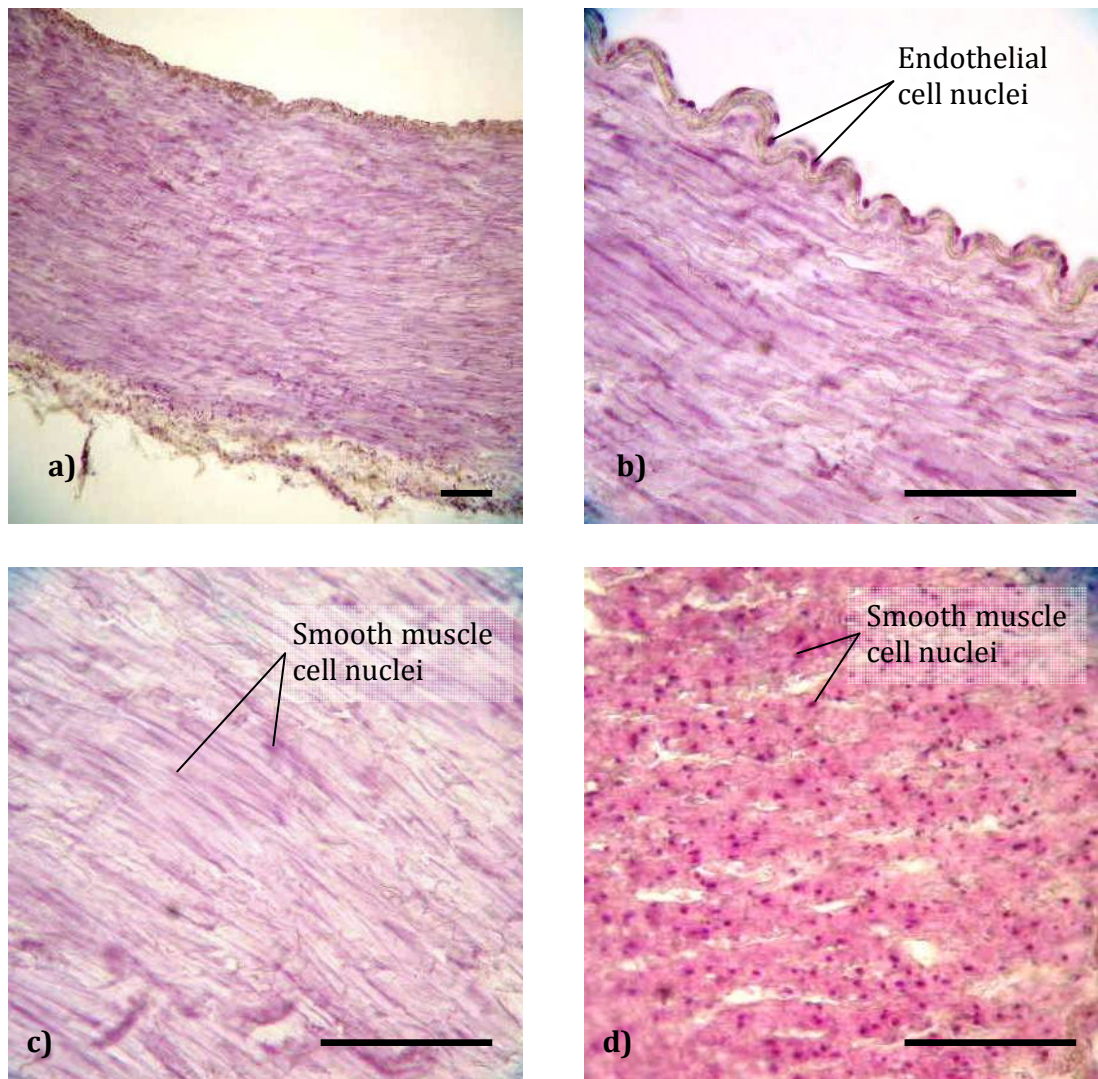
Figure 4.14 20 μm thick histological sections of mesenteric artery stained with haematoxylin and eosin, cell nuclei are stained dark purple; a) endothelium, basement membrane and smooth muscle in the vessel wall under lower magnification; b) transverse cross section showing endothelial cells on the luminal edge and basement membrane over smooth muscle cells; c) smooth muscle cells stretching around the vessel wall; d) longitudinal section, smooth muscle cell nuclei appear as dots confirming circumferential ring like orientation of cells around the vessel. Bar = 100 μm.

the upper edge of the tissue and endothelial cells can be seen lining it. A thin layer of basement membrane is also visible. Below this lies the medial region where smooth muscle nuclei can be seen running circumferentially around the vessel wall. The section appears to be contracted, as can be seen by the folding of the endothelium. c) shows an area from the mid media of the vessel wall from a similar segment. Smooth muscle cell nuclei can be seen as lines running through the wall aligned with one

another. Photo d) shows a longitudinal section through the vessel wall of another segment of mesenteric artery. The smooth muscle nuclei appear as dots confirming the perpendicular orientation to the cross section and their circumferential arrangement around the vessel wall. This also confirms that there is no significant spiral arrangement of the cells along the vessel wall.

The smooth muscle cell density in this tissue was estimated by counting the number of cell nuclei per unit area on similar images of histological sections. The mesenteric artery sections were found to have a cell density of 4080 ± 340 nuclei per square millimetre, which is 44% more than the carotid artery.

Vessel function tests
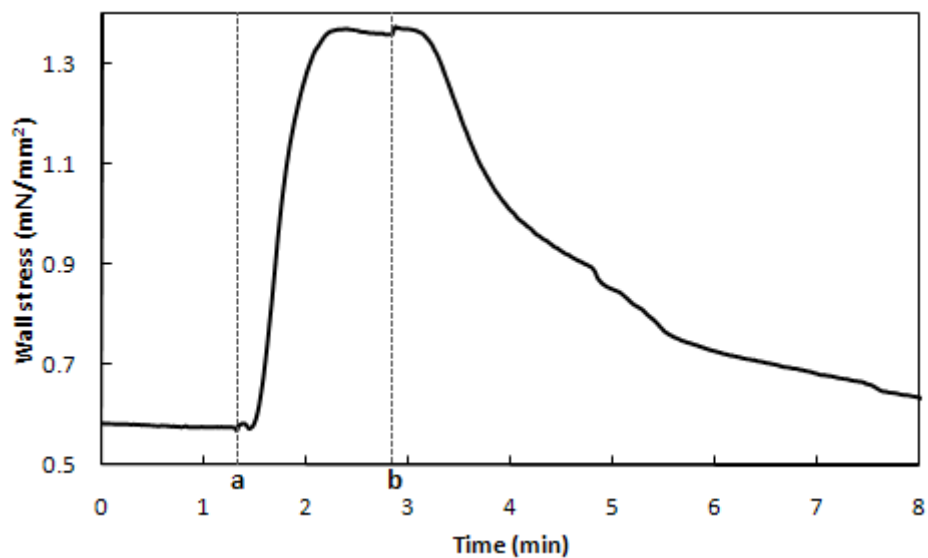
Figure 4.15 Typical curve showing time course of changes in wall stress induced by noradrenaline (1 μM) added at time **a,** and acetylcholine (1 μM) added at time **b**, in a mesenteric artery section with intact endothelium.

The presence of endothelium was confirmed in all samples used, except for those where the endothelium was purposely removed. Noradrenaline (1 μM) induced vasoconstriction increased the tension by approximately 0.4 mN/mm^2 on average. This was 60% higher than the average increase in tension induced in carotid artery rings by the same concentration of noradrenaline. Vasodilatation induced by acetylcholine (1 μM) in intact segments had the effect of relaxing the vessel. In

denuded segments, acetylcholine had the effect of increasing the tension. Figure 4.15 shows a typical tension curve during function testing.

4.6.2 Response to ultrasound

Vascular response

As was observed in the carotid artery experiments, after the artery rings were stretched to an initial wall stress of 4.1 ± 0.7 mN/mm^2, wall stress decreased by approximately 80 % over approximately 60 minutes while strain was kept constant. Once the wall stress had reached a minimum, it began a steady increase. It was during this period that all exposures to ultrasound were performed. Again, the steady tension increase was fitted with polynomial functions and subtracted from the data set to provide a zero baseline. Results are quoted as the change in wall stress above the baseline.
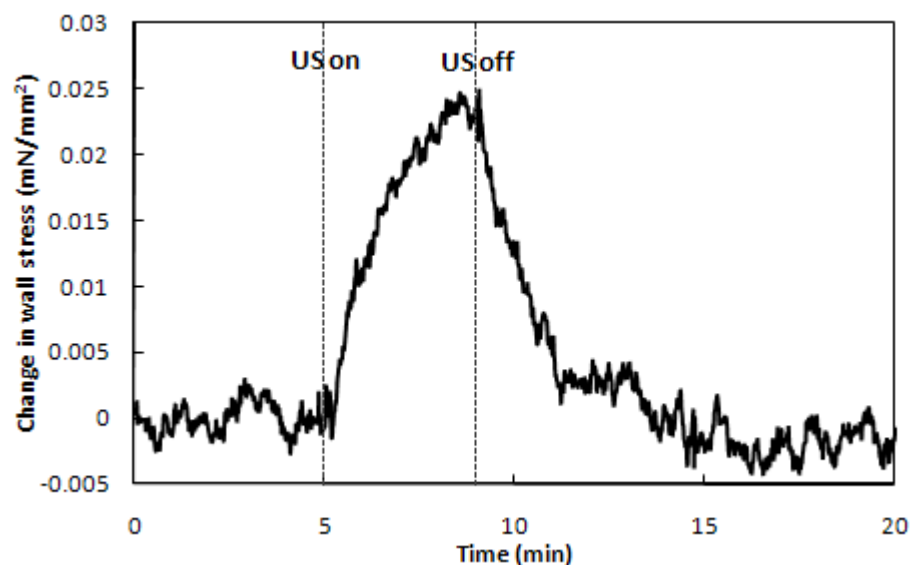
Figure 4.16 A typical response of a mesenteric artery section during a 4 minute exposure to ultrasound at 145 mW; the dotted lines indicate the beginning and end of the exposure. Wall stress increases during the period of insonation, rapidly at first, then at a decreasing rate, before slowly returning to baseline after the exposure.

Exposure of mesenteric artery sections to ultrasound induced reversible vasoconstriction. The wall stress of the artery rings increased during the period of exposure with a similar time course to that seen during exposure of carotid artery

sections to ultrasound. The initial tension increase on exposure to ultrasound was rapid. After approximately 45 s, the rate of vasoconstriction decreased but continued until the end of the exposure period. After this point, the tension began to decay, rapidly at first then more slowly until it reached baseline level after approximately 10 minutes. A typical response is shown in Figure 4.16. The response was consistently repeated during a period of several hours, as long as a recovery period of at least 15 minutes was allowed between exposures.

The mean increase in wall stress was 0.020 ± 0.017 mN/mm^2 (mean ± sd, n = 34). This was approximately 5% of the mean increase in wall stress induced by a 1 μM dose of noradrenaline. This is lower than for the carotid artery, where the mean increase in wall stress was approximately 8% of the increase induced by the same concentration of noradrenaline. The magnitude of the response varied by approximately 30 % between exposures of the same artery ring, by approximately 56% between exposures of rings taken from the same vessel and by approximately 80% between exposures of rings different vessels.

Dependence on acoustic power
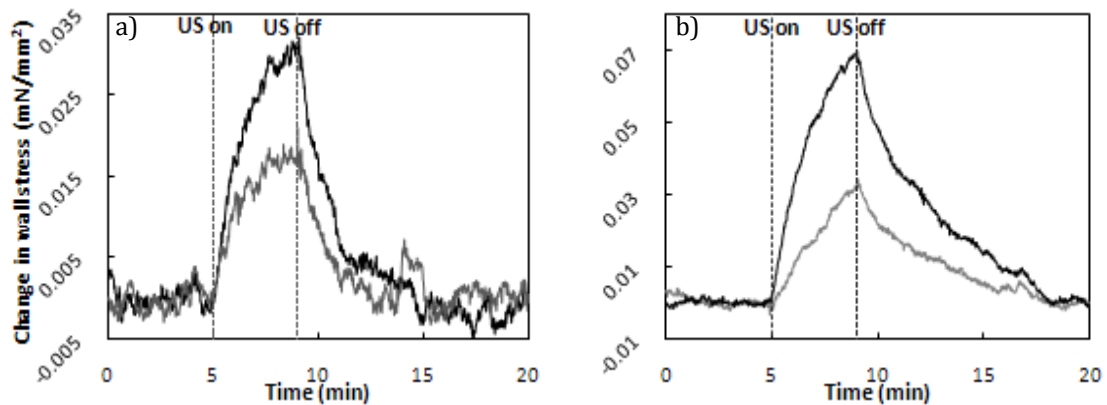
Figure 4.17 Typical responses to 4 minute ultrasound exposures at different acoustic power levels; a)— exposure to ultrasound at 145 mW, — exposure to ultrasound at 100 mW; b) —exposure to ultrasound at 145 mW, — exposure to ultrasound at 72 mW; the dotted lines show the times at which the exposure began and ended.

Exposure of mesenteric artery rings to ultrasound at different acoustic power levels demonstrated that as in the carotid artery, ultrasound induced contraction was
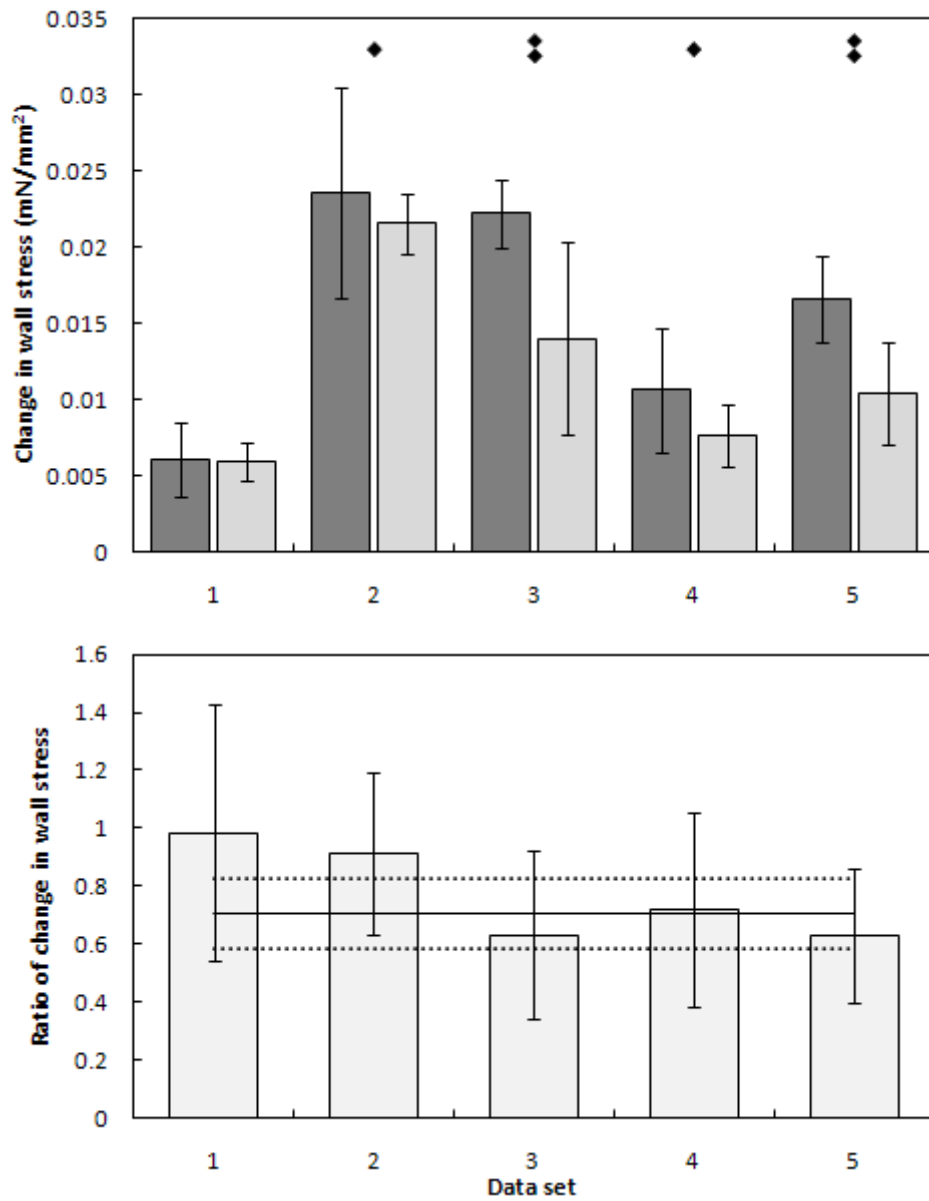
Figure 4.18 Results from experiments performed on 5 vessel sections (numbered 1 – 5 on horizontal axis) exposed to ultrasound at 100% and 69% acoustic power levels. The top graph shows the mean change in wall stress due to exposure at the 100% acoustic power level ■ ; and the 69% acoustic power level □ ; the error bars show ± 1 standard deviation of the mean. ♦ shows a P-value of ≤0.1, ♦ shows a P-value of ≤0.05. The bottom graph shows the ratio of the means for each data set. Error bars show error computed from the standard deviation of the means shown in the top graph. — shows the mean of the ratios over all data sets; …. shows ± 1 standard deviation of the mean.
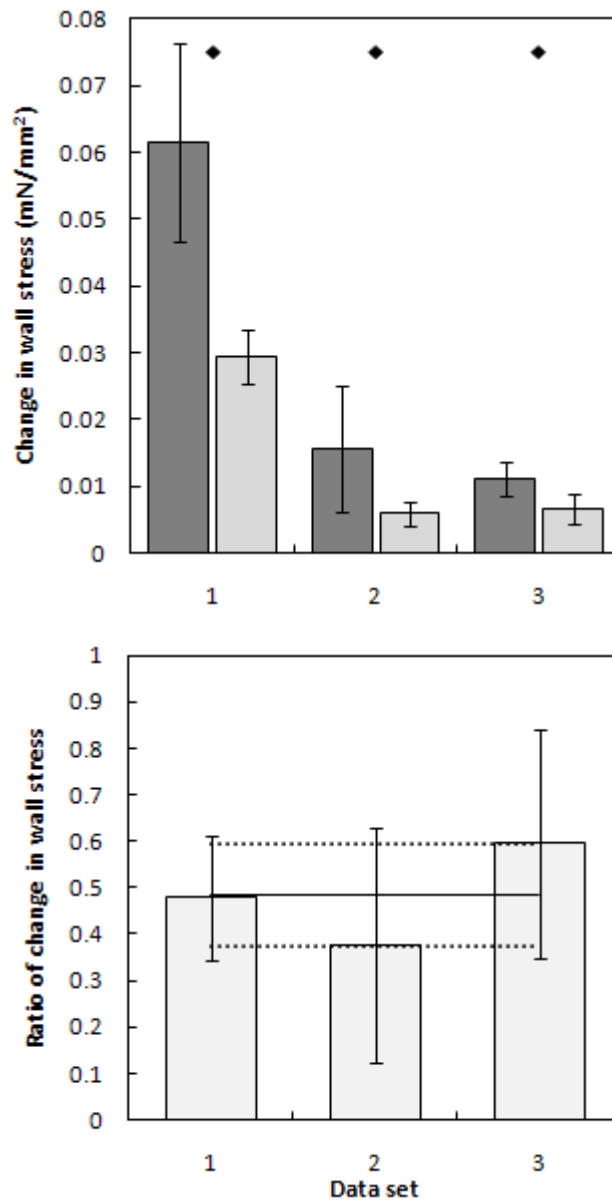
Figure 4.19 Results from experiments performed on 3 vessel sections (numbered 1 – 3 on horizontal axis) exposed to ultrasound at 100% and 50% acoustic power levels. The top graph shows the mean change in wall stress due to exposure at the 100% acoustic power level ■ ; and the 50% acoustic power level □ ; the error bars show ± 1 standard deviation of the mean.❖ shows a P-value of ≤0.1, ◆ shows a P-value of ≤0.05. The bottom graph shows the ratio of the means for each data set. Error bars show error computed from the standard deviation of the means shown in the top graph. ▬ shows the mean of the ratios over all data sets; .... shows ± 1 standard deviation of the mean.

dependent on acoustic power. The mean change in tension induced by exposure to each acoustic power level was compared for each artery ring used. The ratios of the tension increase induced by either the 50% or 69% acoustic power level to the tension increase induced by the reference acoustic power level (100%) were calculated for each artery ring used. 14 experiments were performed in total, and from these 8 useful data sets were obtained. Data was discarded for the reasons given in Section 4.6. For each data set, a difference was seen in the magnitude of the response between exposures at the higher and lower acoustic power levels. The magnitude of the response decreased with decreasing acoustic power, but the time course did not appear to differ otherwise. For all exposures, a high initial rate of tension increase was observed, followed by further increase at decreasing rates for the duration of the exposure. A set of typical responses is shown in Figure 4.17, illustrating the differences in wall stress increase between exposures to different acoustic powers.

Results are shown in Figure 4.18 for each ring exposed to ultrasound at acoustic powers of 145 mW and 100 mW. Results are shown in Figure 4.19 for artery rings exposed to ultrasound at acoustic powers of at 145 mW and 72 mW. The mean increase in wall tension for each acoustic power is shown for each ring; the standard deviations of these means are plotted as error bars. In each case, the mean response to the lower acoustic power was smallest. The standard deviations are large in some cases reflecting the high degree of variability between responses. A Student's T test showed that the differences between the means were significant in 7 out of 8 cases, with a p-value of 0.1 (≤0.05 in 5 of these cases).

The mean ratios of the responses for each artery ring and across all experiments in this series were then found; the results are shown in the lower graphs of these figures. Again, the ratios were fairly consistent across all experiments, although there were large variations in the magnitude of responses from ring to ring. The mean ratio of the responses to those at the maximum acoustic power level was 0.71 ± 0.14 for the 69% acoustic power level and 0.48 ± 0.11 for the 50% acoustic power level. The changes in tension are proportional to acoustic power in an approximately linear fashion.

Dependence on endothelium

Experiments were performed on 6 pairs of artery rings. Each pair included one ring with intact endothelium and another with denuded endothelium. Of these 6 pairs, usable results were obtained from only two pairs, again for reasons given in Section 4.6; these results are displayed in Figure 4.20. In one pair, the denuded sample exhibited a larger increase in wall tension on exposure to ultrasound, while in the other pair the denuded ring exhibited a slightly smaller response. A Student's T test showed that the first result showed a significant difference between the mean responses, while the second result showed no significant difference. These results are inconclusive; a much larger number of data sets would be required in order to confirm the behaviour. This particular investigation is relatively difficult to perform consistently as the variation between different sections of the same artery can be so large (56 % on average).
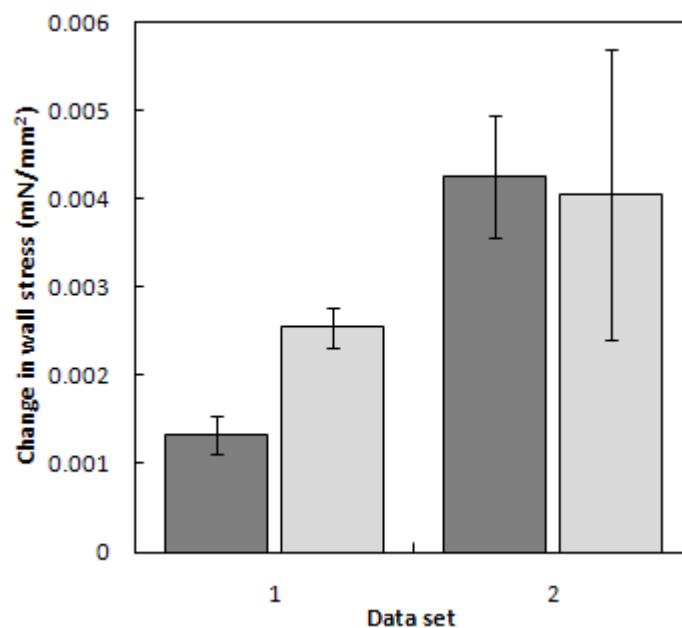
Figure 4.20 Mean changes in wall stress due to ultrasound exposure recorded in two sets (of 6 sets in total) of paired segments with intact ■ and denuded □ endothelium; error bars show standard deviation of the means.

4.7 Discussion and Summary

General comparison of response

It has been demonstrated that exposure to ultrasound at 3.2 MHz caused contraction in the carotid artery and also in the large lateral cecal mesenteric artery *in vitro*. The response was reversible and reproducible from sample to sample and over a period of several hours for each sample. The observed responses were qualitatively consistent and reproducible between vessels, but there were quite large quantitative variations between exposures, from sample to sample and between the two different vessel types. A similar response was established in both vessel types. The time course was indistinguishable between the two vessels and the response was of the same magnitude on average. On average, responses were larger in carotid artery rings in proportion to the vasoconstriction induced by a 1μM dose of noradrenaline. In the carotid artery, the mean change in wall stress was approximately 8% of the change in wall stress induced by 1 μM noradrenaline. In mesenteric arteries, it was 5% of this change. Histological analysis showed that the two types of vessels were structurally similar. The orientation of smooth muscle nuclei was the same in both types of vessel, but they differed in terms of smooth muscle cell density. The number of nuclei per mm^2 was 44% higher in the mesenteric arteries than the carotid arteries. The two vessel types also appeared to differ in their mechanical properties. The mesenteric arteries were stiffer. The incremental elastic modulus at the mean level of wall stress during the ultrasound exposure period was 25% higher in the mesenteric arteries than the carotid arteries. The overall average response of the vessels was of the same magnitude for both types. These structural and mechanical differences appear to compensate for each other to create a similar response. However, it must be noted that the average responses were calculated from a far larger data set than the elastic modulus and smooth muscle density.

Although their response to ultrasound was similar to the carotid artery, data obtained from mesenteric arteries generally had a greater level of noise and a greater proportion of the data sets were discarded. Vessel function tests were successful in most vessels, confirming that the endothelium was intact. This was not the case in the carotid artery rings where it was difficult to establish this response. Some of the

differences may arise from the different histories of the vessels at the abattoir. The mesenteric arteries were possibly better preserved when they were acquired from the animal. The tissue was still warm, intact and the vessels were still filled with blood. The carotid arteries were obtained after exsanguination of the animal from the neck. They were therefore almost completely drained of blood when they were acquired. The differences in position and function of the two types of vessels may also be involved in the differences seen in the data. The mesenteric artery is positioned along the large intestine and is placed under varying strain during peristalsis. This tissue is deep within the animal and so is held at a fairly constant core temperature. The carotid arteries are relatively superficial. Temperature may vary more, and although the arteries will experience movement along with movements of the animal's neck, these are likely to be more uniform than the movements associated with peristalsis.

These physiological differences may account for some variation between results from the two vessel types, but there may also be many other factors. It was established that the effect was independent of endothelial integrity in the carotid artery. Although the data obtained from mesenteric arteries was inconclusive, it seems likely that the effect would also be endothelium independent in this tissue, as the response was similar otherwise. The response is therefore assumed to be a direct effect on the smooth muscle. Whether other factors affecting the response were associated with biological variations between arteries, cellular viability, muscle tone or physical variation in, for example, positioning the vessel at the focus of the ultrasound beam could not be established. Errors in positioning of the vessel of 1-2 mm from the beam axis may be likely. The profiles of heating in the focal plane (Figure 3.13) show that heating decreased to about 75% of the peak value at this distance from the beam axis. If the increase in wall stress was proportional to the temperature elevation then this may account for variations in wall stress of up to 25%. However, the artery rings were large compared to this, so if the tissue was positioned a few millimetres off axis, the focal region would still fall within the tissue.

Exposure to prolonged periods of ultrasound showed that the vessel continued to contract over longer periods of time, although the rate at which it did so decreased. It is possible that after some length of time, the wall stress may cease to increase and

instead remain at a steady elevated level. This may correspond with stabilisation of the temperature. If the heat added by ultrasound exposure was balanced by the heat loss from the tissue and then the tank, then the tissue would reach a stable temperature and vessel tone may remain constant. The recovery period obviously also had some influence on the amplitude of the response. Very short recovery periods, where the wall stress barely had time to change before increasing again, seemed to have little effect. Where the recovery periods were slightly longer and the wall stress began to decay, there seemed to be more influence. The response was only reproducible over several exposures if a long recovery period was allowed.

The carotid artery was selected for study as a relatively muscular, large artery in which resistance is tightly controlled to maintain brain perfusion. The mesenteric artery was also chosen as a reasonably large muscular artery, in which the resistance is known to vary. This artery was studied to verify that the response is not specific to the carotid artery and is present in other locations in the circulation. However, it can not be concluded from these results whether or not the response could be induced in all large arteries. Further investigation would be required to establish whether or not this would be the case.

The ultrasound exposures employed generated up to 1.5% increase in wall stress in the carotid artery and up to 2% in the mesenteric artery. A commensurate change in diameter in a vessel at constant pressure would cause a substantial change in haemodynamic resistance, which varies as the 4th power of the radius. Assuming all larger arteries respond in a similar manner, the physiological effects would depend on the position of the vessel in the vasculature. The responsiveness of different vessels requires further study. One might speculate that arterioles and small muscular arteries might be more responsive, because their primary function is to control local blood flow by adjusting wall tension and they have a higher proportion of smooth muscle in their walls. This could have implications for the therapeutic application of ultrasound. One of the next stages in this study will be an investigation of this response in smaller arteries so that these questions can begin to be answered.

In exploring the mechanisms of transduction of the ultrasonic wave to a change in vascular tone, three factors require consideration: fluid streaming, radiation forces

and local heating. Blood vessels are exquisitely sensitive to fluid mechanical shear stress, sensed by the endothelial cells (Davies 1995). The fact that the response was unaffected by endothelial coverage renders this mechanism unlikely. Furthermore, the streaming velocity observed here and the values quoted by Starritt et al. (2000), whilst consistent with measurements in diagnostic pulsed Doppler fields (Starritt et al. 1989) were an order of magnitude lower than blood velocity. The possibility that smooth muscle cells respond to ultrasound-generated flow through the extracellular matrix cannot be totally excluded.

Radiation force on the intact tissue was negligibly small. The similarity of the responses of carotid artery to continuous wave and pulsed ultrasound also suggests that acoustic pressure effects are not involved in the response. The time-averaged acoustic power in the two pulsing regimes employed and the continuous wave field was the same, but there was a large difference in pulse duration and a 10 fold difference in peak negative acoustic pressure. There was also the possibility of nonlinearity in the diagnostic type pulsed field, which would alter absorption in tissue. This may be responsible for small differences in response between different pulsing regimes which did not reach statistical significance in this study. The $\frac{p_r}{\sqrt{f}}$ at the focus was 0.10 MPa/MHz$^{1/2}$ for the continuous wave field; the likelihood of cavitation is therefore very low. However, the values of $\frac{p_r}{\sqrt{f}}$ were 1.12 MPa/MHz$^{1/2}$ and 0.67 MPa/MHz$^{1/2}$ for the diagnostic and therapeutic pulse regimes respectively, but no differences were observed in the response under these conditions. It seems therefore that the effects of cavitation on the cells, or the associated generation of free radicals or other reactive species, were not factors in the vascular response. If significant differences had been observed in the responses to these pulse regimes, then a more thorough systematic investigation of the dependence on these factors would have been performed.

The most probable mechanisms of transduction were therefore thermal. A consistent linear dependence on acoustic power was established for responses in both types of artery. This, along with the similarity of the time course of heating to that of contraction, is consistent with this hypothesis. The time course of the response was

similar for each acoustic power; the initial increase in tension was faster and gradually slowed until the end of exposure. As mentioned previously, it seems that after some time the heat loss from the tank will balance the heat deposited by the ultrasound. As the time course of wall stress was similar for each acoustic power, it seems that the temperature rise does not have to reach a certain level before dissipation.

Increases in bath temperature affected vascular tone. The resulting increases in wall stress were of an order of magnitude consistent with the changes in wall stress measured in response to ultrasound exposure and the temperature rise of 0.3 °C measured in the focal region of the beam. As previously mentioned, the effect of local changes in temperature in the tissue could be different to the bulk changes caused by raised bath temperature. A thermal mechanism would also be consistent with the differences in effect of MHz frequencies observed here and kHz frequencies reported in the literature, since absorption characteristics would be different in the two frequency ranges. The responses to kHz ultrasound presented in the literature suggest that blood vessels are also capable of responding to non thermal stimuli. The responses to kHz ultrasound were much larger than the responses measured here. It would be interesting to investigate where the boundary falls between the two opposite effects measured in response to kHz and MHz ultrasound. As the ultrasound frequency decreases, the absorption coefficient will decrease, therefore absorption and heating in the tissue will also decrease. At low frequencies, the temperature rise would be too low to induce contraction. As the frequency continues to decrease, it may be that some other mechanism instead becomes dominant and will induce relaxation.

Also consistent with our hypothesis are recent studies on the effects of temperature on tension in the carotid artery (Mustafa and Thulesius 2005). In this case, the effect is mediated by a potassium channel in the membrane of the smooth muscle cell. Studies on isolated cells have shown that the activity of such channels is affected by ultrasound (Mortimer and Dyson 1988; Liu et al. 2006). A further step in this study will therefore be to investigate this possibility in these tissues.

5 Response of small arteries

5.1 Introduction

The experiments described in this section were conducted on small mesenteric arteries obtained from the same general location as those used in the previous section. These arteries were branches from the large artery and were selected to have a diameter of approximately 0.5 to 1 mm. The aim of these experiments was to investigate whether the response established in large arteries was also present in smaller arteries. These small arteries are the resistance arteries and should have a larger influence over local blood flow than the large arteries previously tested. It may be postulated that for this reason a response may be of greater physiological importance and could be larger in magnitude.

The experiments in this section follow a similar pattern to those described in the previous section, but the myograph system is of a different design.

5.2 Experimental methods

5.2.1 Tissue acquisition

The blood vessels used in these experiments were first or second order branches from the lateral cecal mesenteric artery. The tissue was collected from horses, post mortem at a local abattoir. Large sections of tissue were cut from the fatty envelope which runs along the large intestine; this contains the large mesenteric artery used in the previous experiments as well as the large vein, many smaller blood vessels, lymphatics and connective tissue. These sections were transferred to a flask of warm Krebs-Ringer buffer (temperature around 37°C) and transported back to the lab for dissection.

5.2.2 Dissection

Sections of tissue were pinned out on a cork mat submerged in buffer. The large artery and some of the fatty tissue were carefully removed, leaving the ends of the first order branches from this vessel exposed, but under buffer. Smaller sections were cut containing up to three branches and transferred to a Petri dish with a rubber base. The sections were pinned out and placed under a dissecting microscope. Arteries have stiffer walls than veins and so maintain their tubular shape, while veins collapse when not under pressure. Arteries were identified by this shape and their wall thickness and were pinned out for dissection. The fatty tissue was carefully removed from around the vessel using fine vannas type dissection scissors and watchmakers forceps.

Once cleaned, small sections of approximately 4 to 5 mm in length were cut from the vessel; the vessels were carefully inspected to avoid side branches. The sections were transferred to a beaker of fresh Krebs-Ringer buffer and stored at 4 °C until needed. The dissection process was repeated until 5 to 10 vessel sections were obtained. Several vessel sections were used for experiments; a surplus was required in case of difficulty in mounting or leakage through undetected side branches.

5.2.3 Mounting procedure

The small tissue bath was lined with the absorber sections, pipette tips were mounted in the holder in the base of the bath and the small plastic tubes were attached. The bath was half filled with cold Krebs-Ringer buffer (from the fridge). Before mounting the vessel, the pressure system was filled. The configuration of the pressure tubing and taps is shown in Figure 5.1. The three way tap on the pressure tower side of the bath was opened from input [2] to [3] and the tap was filled from a syringe. The pressure tower tube was attached to input [3] and buffer was pushed through until it leaked from input [2] of the syringe tap. This input was screwed shut and fluid was pushed through into the syringe ensuring there were no bubbles. The syringe was removed from input [2] of the pressure side 3 way tap, fluid was allowed to leak and then the input was screwed shut. The tap was opened from the tower [3] to the bath [1] and the tube was filled, pushing the air out into the bath. The tube was carefully checked for bubbles as they would cause damage to the endothelium if allowed to pass

into the vessel. The bath was then closed off from the tower at this tap and the tube was closed off at the syringe tap. The tower tube was removed from input [3]. Next the other side of the system was filled. The syringe was connected to input [3] of the stop tap, fluid was pushed through to input [2] and this was screwed shut. The tap was opened to the bath [1] and fluid was pushed through the tube, again pushing the air into the bath. The tube was carefully inspected for bubbles. The syringe was removed and the tap closed off.
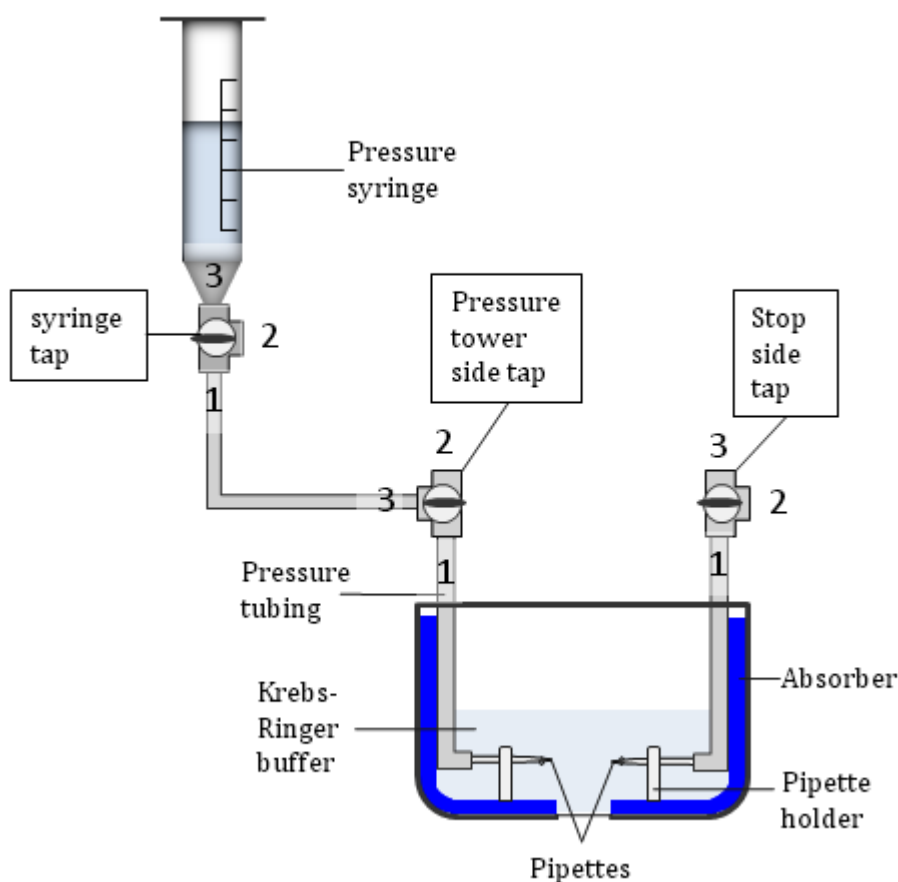
Figure 5.1 Schematic diagram showing the configuration of the pressure tubing and taps. The vessel is mounted on the pipettes and pressurised using the system of tubing and taps filled with buffer. When under pressure, the 'stop side tap' is closed off and the pressure syringe is raised and open to the vessel.

The bath was carefully transferred to another bench for mounting of the vessel under a magnifying lens. A vessel was selected and placed in the bath. Loops of suture thread (described in Section 3.5) were placed over the pipette tips. The vessel was

manipulated using two pairs of watchmaker's forceps, one straight and one with curved tips. The vessel was carefully placed over the tip of the stop side pipette and pulled up over the raised band. The first knot was brought over and loosely secured around the vessel. The second knot was then used to secure the vessel more tightly. The stop tap was opened to allow fluid to pass through the vessel, removing blood from the endothelium. This tap was left open until the pressure system was reconnected. The other end of the vessel was mounted by moving the tip of the other pipette until the tip was level with the end of the vessel. The forceps were used to move the end of the vessel over the very end of the pipette tip. The pipette was moved further inside the vessel until the vessel could be pulled over the raised band on the pipette. This end of the vessel was secured with two knots in the same manner as the other end. The pipette was then moved to stretch the vessel slightly.

Once the vessel was mounted, the tissue bath was transferred to the microscope stage. The pressure system was reconnected to the bath. Input [3] of the tower tap was filled with buffer with a needle and syringe to avoid the introduction of bubbles to the system. The syringe tap was opened and fluid allowed to leak from the end of the tube, it was then connected to input [3] of the tower side tap. The tap was opened from the tower [3] to the bath [1] and the stop tap was closed. The tower was raised and the pipette tips were moved apart to take up the slack in the vessel. The vessel was pressurised to approximately 45 mm Hg during experiments.

The heating system was placed in the bath and both sections of the bath were filled with warm Krebs-Ringer buffer and slowly brought up to temperature. The inflow and outflow tubes of the flushing system were put in place. The microscope was focused on the vessel and an image was displayed in the video capture window.

5.2.4 Vessel characterisation

Pressure-radius curves

Pressure-radius curves were determined for several vessels for investigation of their mechanical properties and to help compare the results of experiments on the different types of vessel. The vessels were mounted as normal, but the pressure tower was not raised. The vessel was stretched between the pipettes and left to warm up to 37.5 °C

and equilibrate. Video capture was started several minutes before the pressure was altered. The tower was raised in 5cm increments, starting with the column height equal to the height of the vessel, up to a height difference of 80cm. The tower was left in each position for 20 seconds before being raised again. The exact height of each position and the time (video capture time) was recorded. The pressure tower was raised and lowered 3 times for each vessel. The video file was analysed as described in Section 3.5.2 to yield the time course of the vessel diameter. The diameter at each pressure was then determined.

Histological characterisation

Arteries were examined histologically to determine the orientation and density of smooth muscle cells. Cross sectional histological sections of 20 μm thickness were prepared from frozen blocks of embedding medium containing fixed arteries. The sections were stained with haematoxylin and eosin and examined under a microscope and the number of smooth muscle cell nuclei was found.

Vessel function test

Once the vessel had reached the correct temperature and was correctly pressurised and stretched, it was left to equilibrate for 30 minutes. The function of the vessels was tested with vasoactive drugs before further experiments were performed. Doses of noradrenaline (1 μM) and acetylcholine (1 μM) were used to check endothelial function and to provide a measure of the responsiveness of the vessel. Video capture was initiated about 10 minutes before the introduction of the drugs.

The drugs were made up into stock solutions prior to the experiment and stored on ice in the fridge, shielded from light. A 1μM dose of noradrenaline was administered to the bath using a micropipette, to induce contraction. The vessel was observed in the video capture window; when the vessel diameter appeared to have reached a minimum (usually after approximately one minute) a 1μM dose of acetylcholine was administered in the same way. If the endothelium of the vessel was intact then the acetylcholine would induce relaxation. After a few minutes, the medium in the bath was refreshed with fresh Krebs-Ringer buffer adjusted to pH 7.4 at 37 °C. Video

capture was continued throughout this process. The vessel was left to equilibrate for 30 to 60 minutes before experiments were begun.

5.2.5 Exposure of vessels to ultrasound

A series of experiments was performed to investigate the response of small arteries to ultrasound.

In open field

Video capture was started and was left to run for approximately 15 minutes before exposure to ultrasound. The vessels were exposed for 4 minute periods with a gap of at least 15 minutes between exposures to mimic the regime used in large vessel experiments. Video capture was run throughout and the films were analysed to extract vessel diameter afterwards.

With absorber in place

A further set of ultrasound exposure experiments were performed on 3 vessels, this time with a square of Aptflex absorber (Precision Acoustic Ltd., Dorchester, UK) (dimensions 25 mm x 22 mm x 5 mm) positioned vertically a few mm from the vessel. This was intended to provide some heating by convection during exposure, to mimic blood vessels close to bone and replicate the temperature rise measured in the large vessel experiments.

Several more exposures were made, during which the temperature rise at the vessel was measured both with and without the absorber section in place using a thermocouple positioned to touch the vessel.

5.2.6 Response of small arteries to temperature changes

A series of experiments was performed in order to investigate the response of small mesenteric arteries to changes in temperature.

Experiments were performed on vessels mounted on the myograph and pressurised to 45 mmHg. An endothelial function test was performed on each vessel before the temperature was varied. One vessel was de-endothelialised by passing a bubble through the lumen during mounting. Each vessel was exposed to four temperature

increases of approximately 1 °C above the baseline temperature of 37.5 °C. The bath temperature was increased by the introduction of a stainless steel mass previously heated in hot water. The water bath was allowed to return to baseline temperature and stabilise before another temperature rise was induced. Temperature was measured and recorded using a thermocouple placed in the bath linked to a PicoLog recorder as previously. Video capture was run throughout, the films were analysed to extract vessel diameter at a later time as described previously.

5.3 Results

5.3.1 Vessel characterisation

Pressure-radius curves
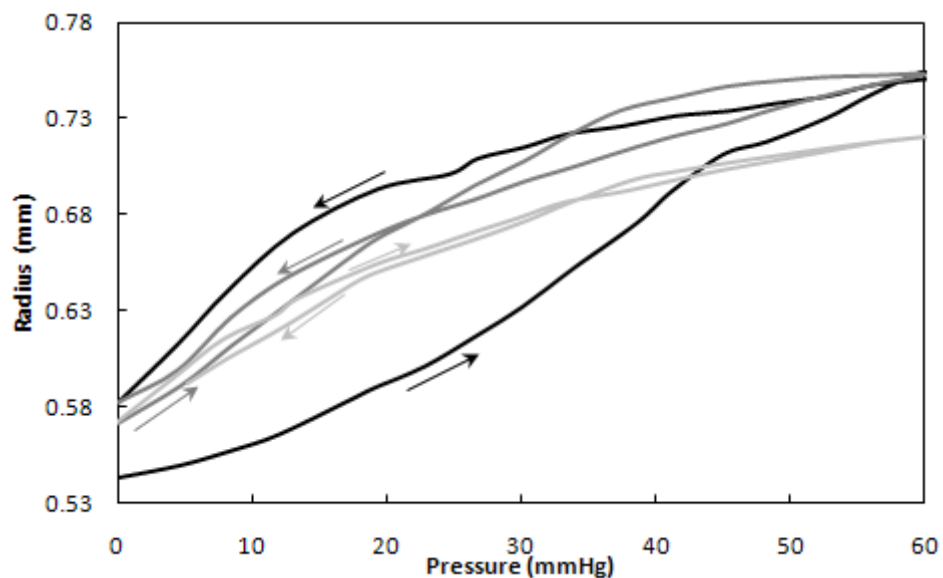
Figure 5.2 Pressure radius curves for 2nd order mesenteric artery; 3 pressure cycles are shown, ▬ 1st cycle, ▬ 2nd cycle, ▬ 3rd cycle. Hysteresis is observed in the first cycle, which diminishes in further cycles. The vessel dose not return to the starting diameter after the initial pressure increase suggest that it is stretched.

A typical set of pressure-radius curves for a 1st order branch from the lateral cecal mesenteric artery is shown in Figure 5.2. The vessels showed some hysteresis and in the second and third cycles did not return to the starting radius, although the

maximum radius remained the same throughout. Stress and strain were calculated from these curves; a typical example of the stress-strain curve is shown in Figure 5.3. During experiments, the arteries were pressurised to approximately 45 mmHg; the incremental elastic modulus at this pressure was 260 ± 46 mN/mm². This is much higher than for the large vessels, which had incremental elastic moduli a factor of 10 smaller than this.
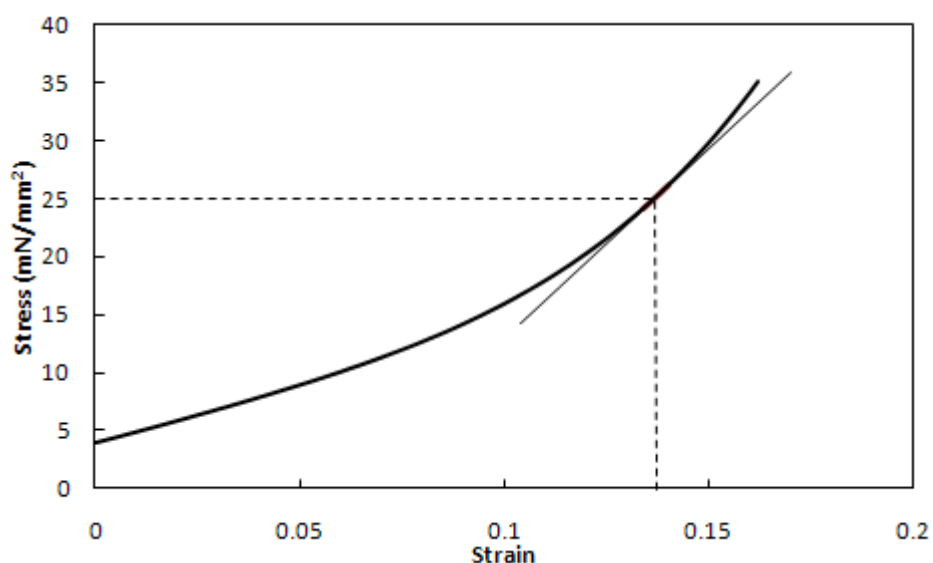
Figure 5.3 Typical stress-strain curve for a 1st order branch mesenteric artery section; the mean level of wall stress during exposures to ultrasound is marked by the dotted line. The incremental elastic modulus was calculated at this value.

Histological characterisation

Figure 5.4 shows images of 20 μm thick histological sections of small mesenteric arteries of the type used in these experiments. The sections are stained with haematoxylin and eosin, cell nuclei appear dark pink or purple. Photo a) shows a complete section under low magnification, the vessel wall is approximately 0.2 mm thick and the vessel appears to be in state of contraction as shown by the corrugations in the luminal surface. Photo b) shows part of this section under higher magnification. The luminal surface is at the top of the image; folding of the endothelium can be seen, indicating contraction. A thin layer of basement membrane can be seen below this,

then a regular arrangement of smooth muscle cell nuclei running circumferentially around the vessel wall.

The number of smooth muscle cell nuclei per unit area was counted from images of histological sections to quantify the cell density in this tissue. These arteries were found to have a cell density of 4810 ± 130 nuclei per mm^2.
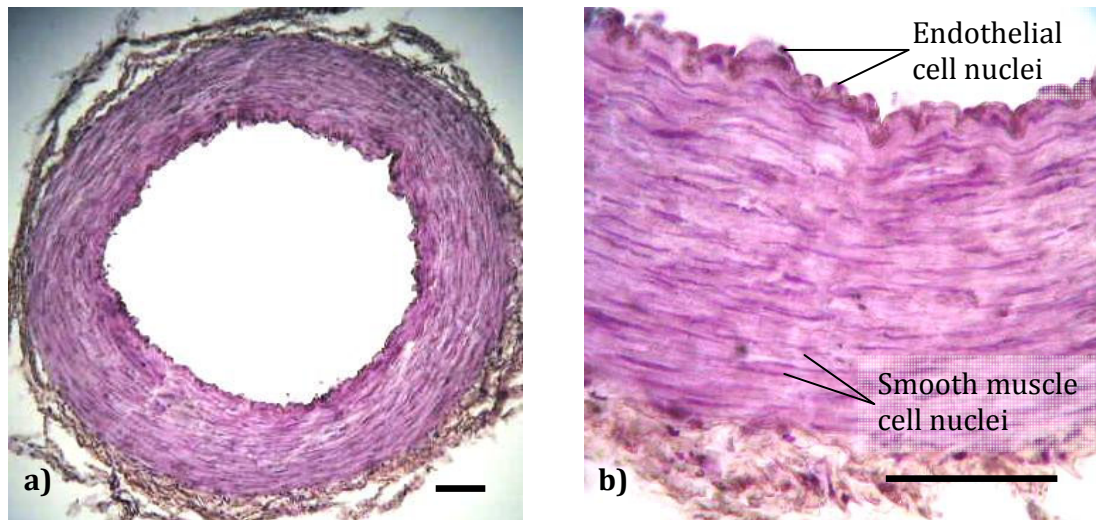
Figure 5.4 20 μm histological sections of small mesenteric artery stained with haematoxylin and eosin, cell nuclei are stained dark purple; a) cross section through the vessel; b) section of vessel wall under higher magnification, cell nuclei can be seen stretching around the vessel wall. Bar = 100 μm

Vessel function tests

Figure 5.5 shows a typical time course of vessel diameter induced by noradrenaline and acetylcholine. The noradrenaline (1 μM) was added at time **a** marked on the axis; this induced vasoconstriction, causing a reduction in diameter of approximately 10% in this case. Acetylcholine (1 μM) was added at time **b** marked on the axis; this induced vasodilatation which increased the vessel diameter quickly at first and then brought it slowly back towards the original diameter. The time course of these responses was similar to the equivalent response in the carotid and large mesenteric arteries. The change in wall stress was approximately 2.8 mN/mm^2; this is an order of magnitude larger than the change in tension induced by the same test in the large arteries.

In this case, some spasming of the vessel was observed during relaxation, similar in time course and magnitude to that observed during relaxation of carotid and large mesenteric arteries.
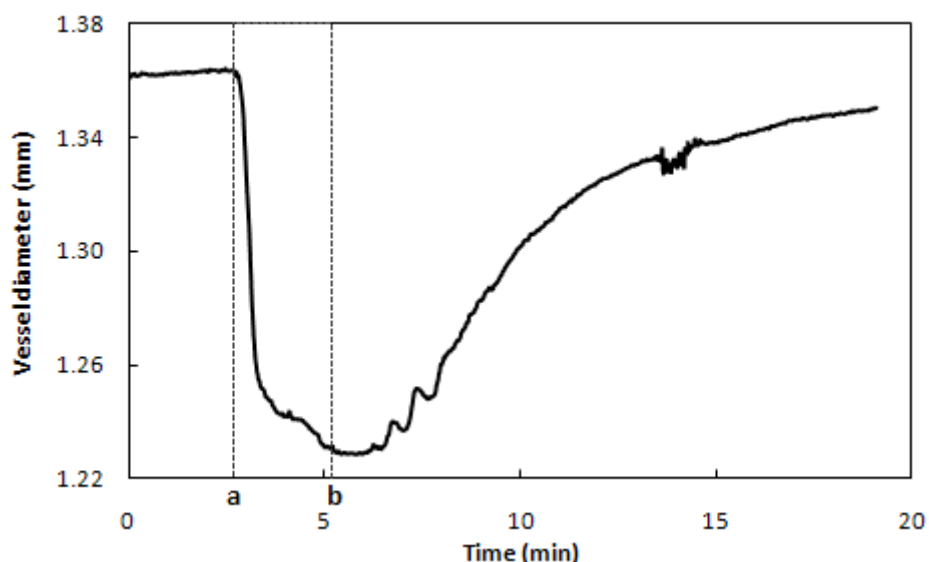
Figure 5.5 Typical time course of vessel diameter during vessel function test; noradrenaline was added to induce vasoconstriction at time a, acetylcholine was added to induce relaxation at time b.

5.3.2 Response of small arteries to ultrasound

Eight vessels were exposed to ultrasound for four minute periods at an acoustic power of 145 mW (exposure parameters as previously) in the open field configuration. The vessel diameter showed no consistent changes during ultrasound exposure in either de-endothelialised or intact samples. Some fluctuations were observed in the time course of the vessel diameter, but did not correlate with periods of ultrasound exposure and were mainly of a magnitude of less than the size of a pixel in the image. Changes in diameter of a few percent would be larger than the size of one pixel. The results suggest that vessels from this location in this particular preparation either do not respond to ultrasound, or if they do the response was too small to be measured by this system. Any response too small to measure here would be less than a 1% change in diameter.

It was hypothesised that the lack of response in the vessels exposed to ultrasound without an absorbing layer in place may have been due to a lack of heating in the

vessel. The vessels were approximately 1 mm in diameter with a wall thickness of a fraction of this. Energy deposited in the tissue from the ultrasound beam would be able to escape easily and would be lost quickly from the thin wall, so heating to the same degree as that within the large arteries was unlikely. It was hypothesised that introducing an absorbing mass close to the vessel could help replicate the heating conditions present in the large arteries.
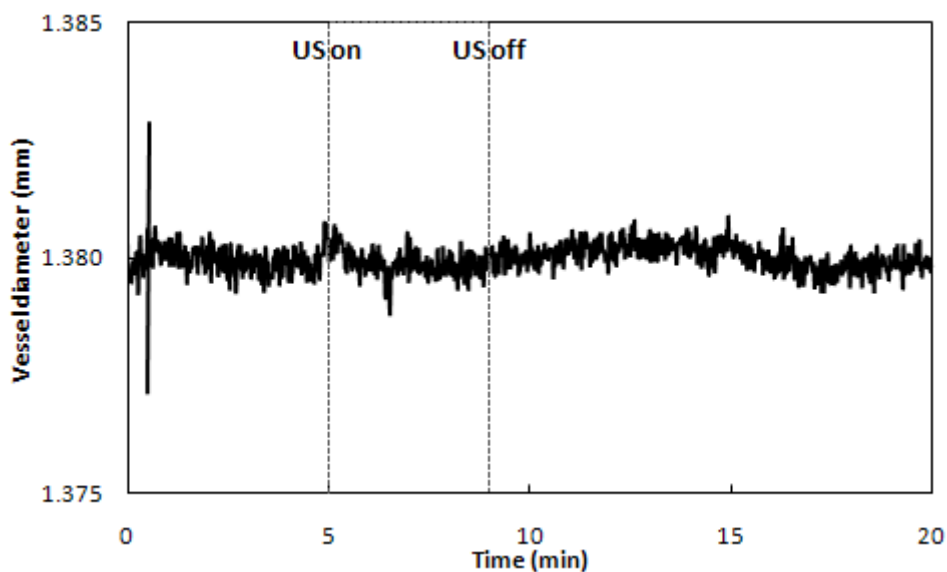
Figure 5.6 Typical response of vessel diameter during exposure to ultrasound for a period of 4 minutes denoted by the dotted lines where a section of absorbing material was placed close to the vessel to increase heating; the vertical black line illustrates the size which corresponds to 1 pixel on the images of the vessel.

Three vessels were exposed to ultrasound for four minute periods at an acoustic power of 145 mW with a section of absorbing material placed next to them. A section of the Aptflex absorber (Precision Acoustic Ltd., Dorchester, UK) used to line the water bath was used as it is designed to be an effective absorber of ultrasound. Again the vessel diameter showed no consistent changes during ultrasound exposure; increasing the temperature in this way had no measureable effect on the vessel diameter. A typical trace of vessel diameter with time is shown in Figure 5.6. Again some fluctuations were observed in vessel diameter, but they did not coincide with periods of ultrasound exposure. The temperature rise measured with a thermocouple placed

at the vessel during ultrasound exposure was less than 0.1 °C in the open field and approximately 0.2 °C with the absorbing mass in place.

5.3.3 Response of small arteries to temperature changes
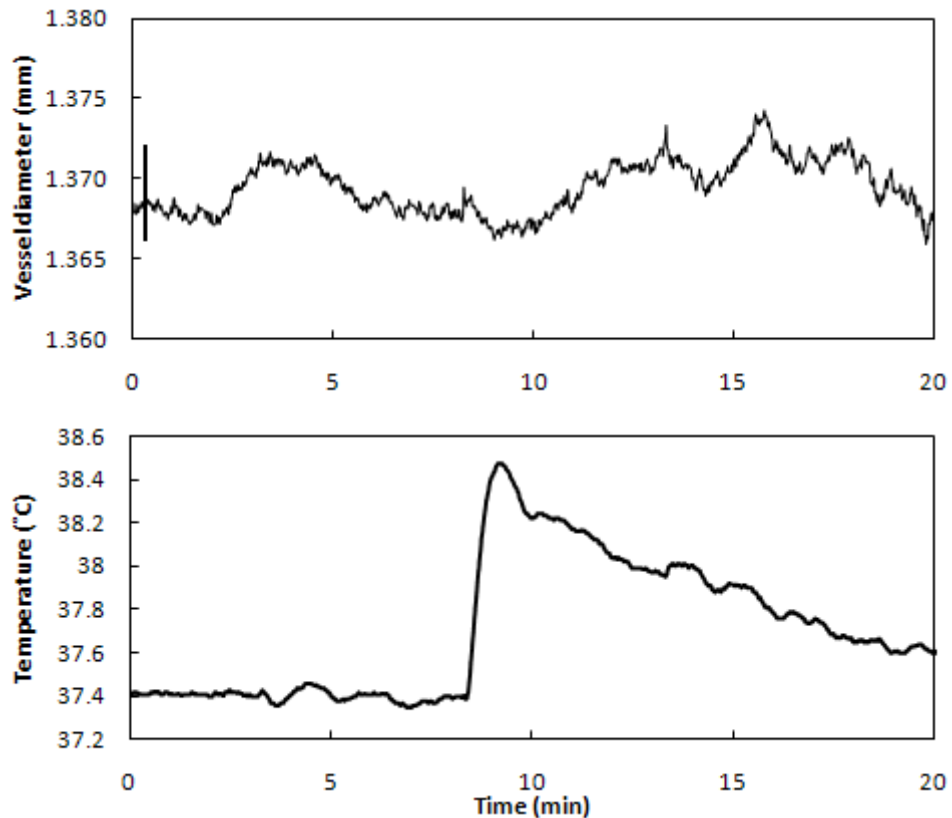
Figure 5.7 Typical response of vessel diameter during a period of rapid temperature increase of approximately 1 °C followed by cooling back to baseline temperature. On the top graph the vertical black line illustrates the size which corresponds to 1 pixel on the images of the vessel.

Three vessels were mounted in the myograph and exposed to temperature changes of approximately 1 °C. The vessel diameter extracted from the video capture files showed no consistent changes correlating with periods of increased temperature in either intact or de-endothelialised vessels. Again fluctuations did not correlate with periods of increased temperature and were in most cases not of a magnitude large

enough to be anything other than noise and artefact, i.e. they were not larger than the size of one pixel. This can be observed on the trace of vessel diameter during a period

of temperature elevation and cooling shown in Figure 5.7; the accompanying temperature trace is also shown.

The temperature changes induced here were larger than those measured during ultrasound exposure. If a similar response to temperature was found in these vessels as in the large arteries then the corresponding diameter change would be easily measureable with this system. No response was observed in these experiments suggesting that any response to temperature would be very small indeed.

5.4 Discussion

Experiments on small mesenteric arteries (diameter $0.5 - 1$mm) have shown no evidence that exposure to either MHz ultrasound or temperature changes of approximately $1°C$ above baseline caused changes in vessel diameter. These results are contrary to the findings in the large mesenteric arteries that these small arteries branch from and carotid arteries, in which exposure to ultrasound and temperature changes induced contraction. The activity of all vessels used in these experiments was tested with noradrenaline and acetylcholine and were found to function in the expected manner. The lack of response was therefore not caused by inactive tissue.

Exposures of vessels to ultrasound in the myograph with an open field first showed no response. The wall thickness of these vessels is small, approximately 0.2 mm, compared to the 1.5 to 2 mm wall thickness of the large vessels. For this reason there would be little absorption of ultrasound in the wall so therefore little heating. If a thermal response was to be generated then this would be unlikely under these conditions. To increase heating around the vessel and help provoke a thermal response, a mass of absorbing material was placed in the beam, close to the vessel. This would absorb energy from the ultrasound beam and heat the vessel by convection during ultrasound exposure. The temperature elevation at the vessel during ultrasound exposure in this configuration was comparable to the temperature rise measured at the tissue surface for a carotid artery ring in the focal region of the acoustic field. A response was still not induced in this configuration.

In the carotid artery, relatively large changes in wall stress were induced by temperature changes of 1 to 2 °C. Small vessels were exposed to temperature increases of this magnitude above baseline temperature to try to induce a more pronounced response. No response was observed in this case either.

Initially it was hypothesised that if a response was measured in these arteries that it may well be of greater magnitude than the response measured in large arteries. Indeed the density of smooth muscle cells was observed to be greater in these arteries than in the large mesenteric and carotid arteries. The incremental elastic modulus of these vessels at the pressure they were under during these experiments was a factor of ten greater than for the large vessels tested in the previous chapter. The vessels therefore have a greater stiffness, which may play a part in preventing diameter changes in the vessel, preventing a response to ultrasound or temperature changes appearing in this way.

The myograph system designed for this study was capable of measuring diameter changes of equivalent magnitude. The resolution of the system was approximately 7 μm; if the change in artery diameter induced by ultrasound exposure or temperature changes was smaller than this then it would not be measured by this system. This would represent a change in diameter of less than 1%, which is smaller than the equivalent change in wall stress measured in the carotid and large mesenteric arteries. It was expected that if these vessels did respond to ultrasound that their response would be of a greater magnitude and physiological significance.

One possible reason for a lack of response in these vessels is the experimental preparation. The vessels are dissected away from the surrounding fatty tissue. The smooth muscle in this type of vessel is innervated and signals are transmitted between the cells to control vessel diameter. Signals may be transmitted from the brain to increase blood flow in a particular vascular bed or organ for example. When the tissue is dissected, clearly these nerves are severed. The nerves will not be present in this preparation and the vessel may be unable to respond directly to ultrasound or temperature changes if there are no local sensors. This seems an unlikely explanation as this preparation is widely employed successfully for a variety of applications.

Small arteries branching from the lateral cecal mesenteric artery were found not to respond to MHz ultrasound or temperature changes above the baseline. As discussed previously, a lack of response in the vessels tested here does not rule out the possibility that vessels of a similar size from different vascular beds could respond to ultrasound and temperature changes. Again a detailed investigation would be required to answer this question and it would be possible to extend this investigation to smaller vessels, the true resistance arteries and arterioles where the response may be different.

6 Ion channel experiments

6.1 Introduction

The response of the carotid and mesenteric arteries to ultrasound was associated with thermal effects, but the cellular sensing mechanisms involved in the response required clarification. The cells must respond in some way to the small temperature elevation produced during ultrasound exposure and a signalling pathway is initiated which results in a contraction of the artery.

The literature suggests that a temperature induced vasoactive effect is mediated by the action of potassium ion channels (inward rectifier, Ca^{2+}-activated, ATP-sensitive) in the cell membrane (Mustafa and Thulesius 2005). A series of experiments was therefore performed to ascertain the involvement of potassium ion channels in the response of these arteries to ultrasound in this study, as a first step towards understanding the cellular processes involved in the response.

The signalling pathways within cells that lead to vasoconstriction involve calcium ions, as was discussed in Chapter 2 (Section 2.3.3). When depolarisation of the cell membrane occurs, either during stimulation of an action potential or a graded depolarisation, voltage-gated sodium channels open to allow sodium ions to flow into the cell, causing further depolarisation. Voltage-gated calcium channels also open and allow calcium ions to flow into the cell. Potassium ion channels open in response to depolarisation and allow flow of potassium ions out of the cell, causing repolarisation. The increase in intracellular calcium concentration during depolarisation leads to vasoconstriction. Intracellular calcium levels can also be raised by release of calcium ions from intracellular stores in the endoplasmic reticulum (calcium-induced calcium release). During repolarisation, the voltage-gated channels will close again and calcium flow into the cell will cease. The calcium ions will either be pumped back into

the sarcoplasmic reticulum for storage, or be pumped out of the cell causing reversal of the vasoconstriction. It can be seen that inhibiting the function of the potassium channels would prevent repolarisation of the membrane and allow calcium ions to continue to flow into the cell, increasing the degree of vasoconstriction induced by a given stimulus. Potassium ion channels also help to maintain resting tone; blocking them can also cause depolarisation from the resting state.

To obtain more insight into the ion channel activity during the response of blood vessels to ultrasound and temperature changes, two groups of experiments were performed. Mustafa and Thulesius showed that the vasoconstriction induced by a small degree of temperature elevation above body temperature was enhanced by a range of potassium channel blockers. They concluded that the inhibition of potassium channel activity was therefore the mechanism. In the first group of experiments presented in this chapter, this possibility was explored by investigation of the effect of potassium ion channel blocking on the response to ultrasound. In the second group of experiments presented here, changes in intracellular calcium concentration associated with temperature changes were investigated using calcium sensitive fluorescent dyes. As stated above, vasoconstriction is induced by increases in intracellular calcium, so increases would be expected during periods of elevated temperature which induce vasoconstriction. This observation would provide further confirmation of ion channel inhibition and membrane depolarisation.

6.2 Effects of potassium ion channel blocking on response to ultrasound

Experiments were performed on rings of equine carotid artery to explore the possibility that the vasoconstriction induced in them by ultrasound, is mediated by the inhibition of potassium ion channels. Barium chloride, a potassium channel blocker that is specific to potassium inward rectifier channels at low concentrations, was used in these experiments.

The function of the inward rectifier channels is to help maintain resting vessel tone and to help return the cell to resting potential following membrane depolarisation.

Inhibition of the inward rectifier channels prevents this function, promoting depolarisation of the membrane, which allows more calcium to flow into the cell. If the response to ultrasound was mediated by inhibition of inward rectifier potassium channels, then inhibition of these channels by a chemical blocker will serve to enhance the response. If the response to ultrasound was not mediated by these ion channels then blocking them would provide no change in the response. At the concentration used, barium chloride should have no effect on the basal tone of the vessels.

6.2.1 Experimental methods

Tissue acquisition

Two groups of experiments were performed in this part of the study; one using 12 sections taken from 5 equine carotid arteries. A second group of 4 experiments was performed using sections from 2 equine mesenteric arteries. The arteries were acquired from a local abattoir and dissected as described in Section 4.2.1.

Vessel mounting and set up

Artery rings were mounted on two stainless steel rods within a thin polythene container inside the main water bath, which was filled with Krebs-Ringer buffer as described previously (see Figure 3.2). The polythene container was necessary to contain the potassium channel blocker and to enable flushing of the medium. The artery rings were mounted and left to equilibrate for 5 minutes before an initial wall stress was applied by moving the steel supports apart. The rings were left for approximately one hour to equilibrate under constant strain.

Ultrasound exposure protocol

After equilibration, each artery section was subject to a minimum of 3 periods of ultrasound exposure lasting 4 minutes each, with a recovery period of at least 15 minutes between exposures. Continuous wave ultrasound at an acoustic power of 145 mW was used. Following this set of exposures, a 4 μM dose of $BaCl_2$ (Sigma Aldrich) was added to the bath. A further set of at least three exposures to ultrasound was made. Increases in tension during ultrasound exposure before and after the addition of $BaCl_2$ were compared.

6.2.2 Results

Carotid arteries

Experiments were performed on 12 artery rings from 5 carotid arteries; of the 12 data sets obtained one was discarded as the tissue failed to respond to ultrasound. An initial wall stress of 4.0 ± 1.8 mN/mm^2 was applied to the vessels, wall stress then decreased by 79 ± 13 % over a period of approximately 45 minutes, before steadily increasing while under constant strain, as described for artery rings in Chapter 4. Again all exposures were performed during the steady increase in wall stress.
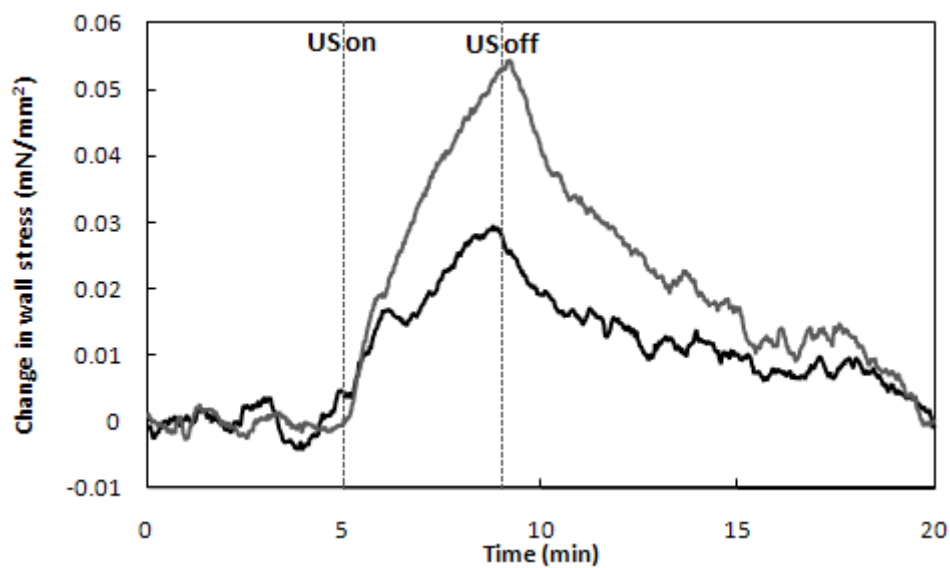
Figure 6.1 Typical response to 4 minute ultrasound exposure before (━) and after (━) the addition of BaCl$_2$ to a concentration of 4 μM in the bath, the dotted lines show the beginning and end of the period of ultrasound exposure. Wall stress increased during ultrasound exposure both before and after the addition of BaCl$_2$; the magnitude of the change was increased in the presence of BaCl$_2$.

Exposure to ultrasound induced reversible contraction of carotid artery, both before and after the addition of barium chloride to the medium. The addition of barium chloride had no effect on basal vessel tone in the absence of ultrasound exposure. The time course of the response to ultrasound and recovery after exposure were not affected by the addition of barium chloride, but the magnitude of the response was increased as can be seen from the set of typical response shown in Figure 6.1. The

increase in tension induced by ultrasound after the addition of 4 μM barium chloride was larger than the tension increase before; the data are shown in Figure 6.2.
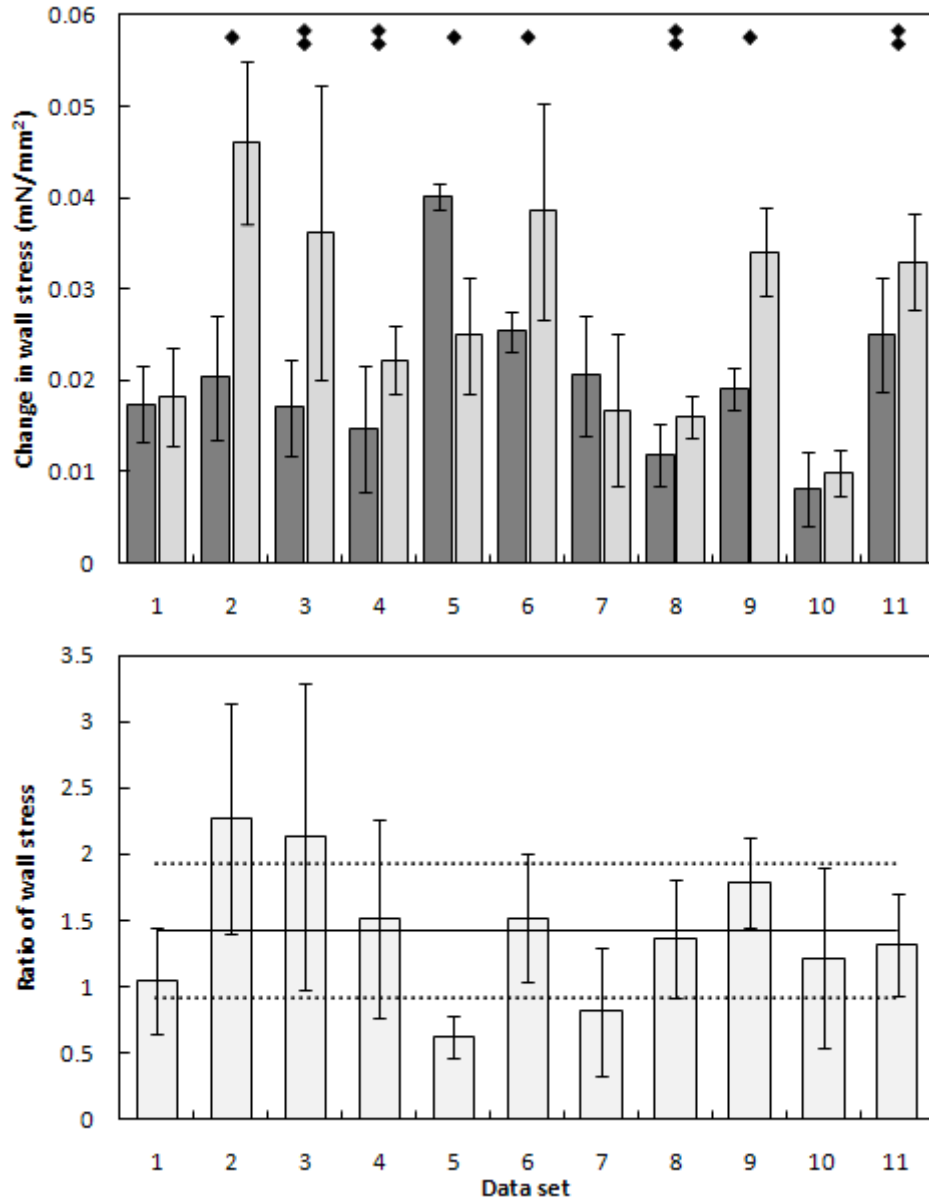
Figure 6.2 Results are shown from 11 out of 12 experiments performed on carotid artery sections; the top graph shows mean response to ultrasound before ■, and after □ the addition of barium chloride for each section; error bars show the standard deviation of the means, ♦ shows a P-value of ≤0.1, ♦ shows a P-value of ≤0.05. The bottom graph shows the ratio of the mean wall stress before and after BaCl₂ addition for each data set; error bars show error computed from the standard deviation of the means shown in the top graph. ▬ shows the mean of the ratios over all data sets; .... shows ± 1 standard deviation of the mean

The increase was 42 % on average, with increases of more than 125% observed in some cases. An increase in the mean response to ultrasound was observed after the addition of $BaCl_2$ in 9 out 11 cases, in 3 of these 9 the increase was not significant. Again there were large variations in the magnitude of the response of individual samples with standard deviations up to 50% of the mean in some cases. Student's T-tests were performed on all data sets to confirm the significance of the increases in response; p-values of less than 0.1 were obtained in 8 out of 11 cases (≤ 0.05 in 4 of these).

Mesenteric arteries

Experiments were performed on four artery rings from two mesenteric arteries; of these four data sets three were discarded due to high levels of noise in the data, failure of the artery to relax and reach the required state for exposures or failure of the vessel to respond to ultrasound. In the experiment that yielded useful data, an initial wall stress of 2.7 mN/mm^2 was applied. The wall stress then decayed by 95% over a period of 100 minutes, before steadily increasing while held under constant strain. Exposures to ultrasound were performed during the steady increase in wall stress.
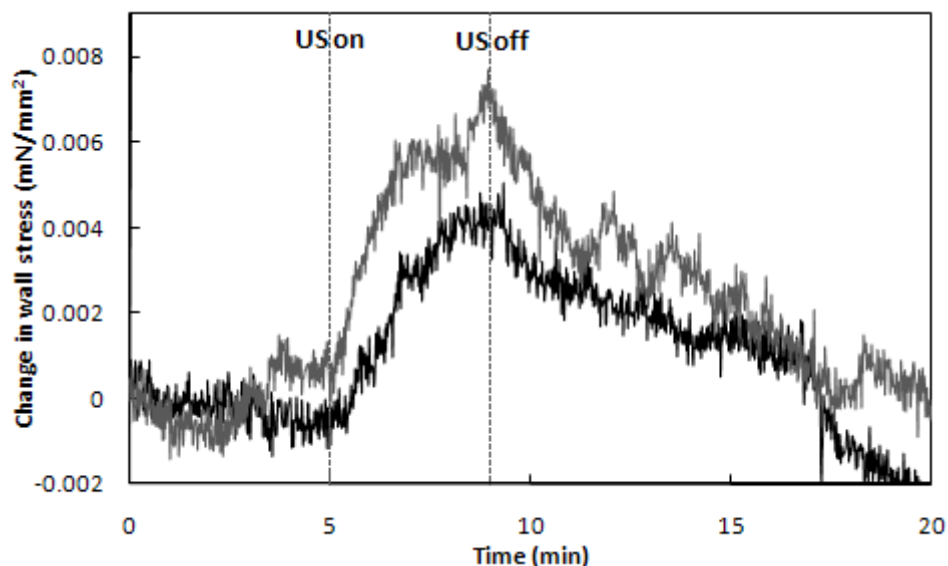
Figure 6.3 Typical response to 4 minute ultrasound exposure before (▬) and after (▬) the addition of $BaCl_2$ to a bath concentration of 4 µM, the dotted lines show the beginning and end of the period of ultrasound exposure. Wall stress increased during ultrasound exposure both before and after the addition of $BaCl_2$; the magnitude of the change was increased in the presence of $BaCl_2$.

Exposure to ultrasound induced contraction of the mesenteric artery ring both before and after the addition of the ion channel blocker; typical responses are shown in Figure 6.3. The addition of $BaCl_2$ had no effect on vessel tone and the behaviour was similar to that of the carotid artery rings. The data obtained from this sample had a much greater level of noise than seen in the carotid artery data; this was characteristic of the data obtained during all of these experiments on mesenteric artery and was one of the reasons that most of the data was not useful.

The data from this experiment is shown in Figure 6.4. On average the increase in response was 47 ± 60 % over all exposures of this artery ring; the error in this figure is very large but a Student's T test showed that the difference between the two groups was significant ($p \leq 0.1$). This result agrees with the results obtained with carotid artery rings, but further data is needed in order to confirm this finding.
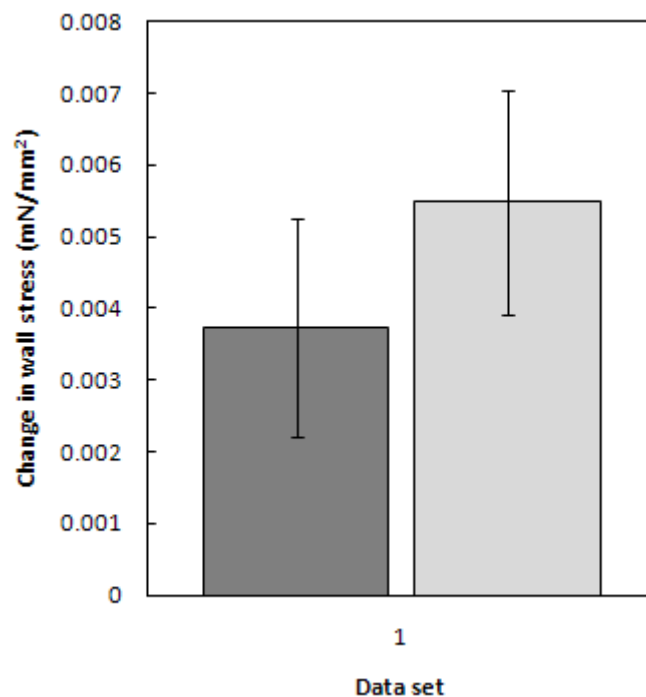
Figure 6.4 Results are shown from 1 out of 4 experiments performed on mesenteric artery sections; the graph shows mean response to ultrasound before ■, and after □ the addition of barium chloride; error bars show the standard deviation of the means.

6.2.3 Discussion

It has been demonstrated that inhibition of inward rectifier channels increased ultrasound induced contraction in the carotid artery. Preliminary results also indicated this effect may be present in the lateral cecal mesenteric artery.

The major effect of ion channel inhibition was to increase the magnitude of the response due to increased flow of calcium into the cell during depolarisation of the cell membrane. The inward rectifier channels help to maintain resting membrane potential; by blocking them with $BaCl_2$, the cell was prevented from returning to the rest state by a greater extent than during ultrasound exposure alone. The basal wall stress was not affected by the addition of the ion channel blocker; inhibition of ion channels elicited an effect only in conjunction with ultrasound exposure.

The results presented here agree with the findings of Mustafa and Thulesius (2005). In their study, vasoconstriction was induced by temperature changes and was found to be mediated by inhibition of potassium channel activity in the cell membrane. Inhibition of other potassium ion channels also affected the response in their study; this effect could be explored in further work on the involvement of ion channel activity on the response of artery rings to ultrasound. These results provide further evidence that the response of carotid arteries to ultrasound is thermally mediated. It seems likely that this result will follow in large mesenteric arteries but further investigation is required to confirm this. The results presented for mesenteric arteries here are preliminary and no solid conclusions can be drawn from them. The response of carotid and large mesenteric arteries to ultrasound was similar (Chapter 4); it seems likely that the cellular mechanism would be the same. However, ion channel populations are known to vary between tissue types, and so it is possible that there may be some differences between the ion channel activity involved in the response in the two vessels. Several types of potassium ion channel were implicated in vasoconstriction due to hyperthermia (Mustafa and Thulesius 2005); their relative contributions to the response could differ between vessel types. Further investigation would be required to confirm this effect in other types of blood vessels, from other large conducting arteries down to the resistance arterioles and capillaries.

Further work would be required to investigate the influence of activity of other types of ion channels on the response. This result suggests that it is possible that responses to ultrasound may occur in many cell and tissue types, as potassium ion channels are present in most cells. These responses could manifest themselves in a variety of ways not limited to contraction of smooth muscle. As discussed in Chapter 2, it has been observed in many studies on isolated cells that ultrasound exposure can elicit responses ranging from altered gene expression to increased cell proliferation. The response to ultrasound in this study was thermally mediated, so responses of this type could be similarly induced by heating from sources other than ultrasound, such as microwave and RF radiation. It is not known exactly how temperature influences ion channel activity. One possibility is that the temperature change causes changes in the lipid bilayer of the cell membrane. The membrane lipids exist in a state close to the phase change between liquid and solid under normal conditions. The liquid crystal nature of the lipid bilayer allows movement of the transmembrane proteins and different lipids. The lipids are important in regulation of the functions and conformational changes of the ion channel proteins, which take place during transport of substances and opening and closing of gated channels. If the lipid bilayer were to undergo a phase change then it seems likely that ion channel activity could be affected.

6.3 Experiments on intracellular calcium activity

In order to investigate further the involvement of ion channels in the response of arteries to ultrasound exposure and temperature changes, experiments were performed using a calcium sensitive fluorescent dye. Contraction of blood vessels is instigated by increases in intracellular calcium levels. Using a calcium sensitive fluorescent dye, which became more fluorescent in the presence of calcium, these changes were visualised and recorded. The increases in intracellular calcium concentration associated with contraction of the vessel were expected to result in increased fluorescence intensity.

While ultrasound induced contraction was confirmed in the carotid and large mesenteric arteries, no response was measured in the small mesenteric arteries. The experiments described in this section were performed to help confirm whether the

lack of response was due to lack of heating by ultrasound absorption in these small vessels or because the ion channel population which mediated the response was not present. Intracellular calcium concentration during temperature changes was investigated in the carotid, large lateral cecal mesenteric artery and small 1st order branches of this artery.

For practical reasons, including the short working distance of the microscope lenses, it was not feasible to expose the vessels to ultrasound and perform fluorescent imaging simultaneously. Time constraints prevented the development of more specialised equipment that would have enabled this procedure; this could be achieved using long working distance lenses and a suitable water bath and tissue support system. For this reason, blood vessels were instead exposed to temperature changes since it has been shown in this thesis that the response of blood vessels to ultrasound was thermally mediated.

6.3.1 Experimental set up and methods

Blood vessels were collected as described for the previous experiments. Large blood vessels were dissected away from the surrounding tissue and cut into sections of approximately 1.5 cm in length. Once dissection was complete, the vessels were stored in Krebs-Ringer buffer at 4 ℃ until needed.

The dye used in these experiments was Fluo-4 (AM form, cell permeant; Invitrogen Ltd. Paisley, UK). This dye was chosen as the excitation and emission wavelengths were well matched to one of the filters available on the microscope which was used here and the fluorescence intensity of the dye was relatively high compared to other available dyes at a given concentration or excitation intensity (Molecular-Probes 2010). The dye also did not require calibration; it could be used to obtain relative changes in calcium concentration. Aliquots of Fluo-4 (50 µg) were removed from the freezer and dissolved in a small amount of DMSO which was then diluted with Krebs-Ringer buffer to make a 5 µM solution. Sections of large artery were incubated in this solution for 3.5 hours at room temperature, then transferred to fresh buffer and left for 30 minutes before use. Small vessels were incubated for 1.5 hours at room temperature in Fluo-4 solution then transferred to fresh buffer and left for 30 minutes

before use. A shorter incubation time was sufficient for these vessels due to the much smaller thickness of the vessel wall. This protocol was based on those used by other investigators using this type of dye, such as Lamont et al. (2003; 2006).

Ring sections of carotid and large mesenteric artery with a thickness of approximately 2mm were cut using a razor blade and pinned out on a small cork mount attached to the base of a large Petri dish. Some square sections were cut from the vessel and mounted so the endothelium could be viewed *en face*. It was found that the fluorescence intensity decreased very rapidly in these sections, which may have been due to leaching of the dye from the tissue. For this reason, only ring sections were used in these experiments. Sections of small mesenteric arteries of approximately 4 mm in length were positioned on the cork mount and held in place with pins.
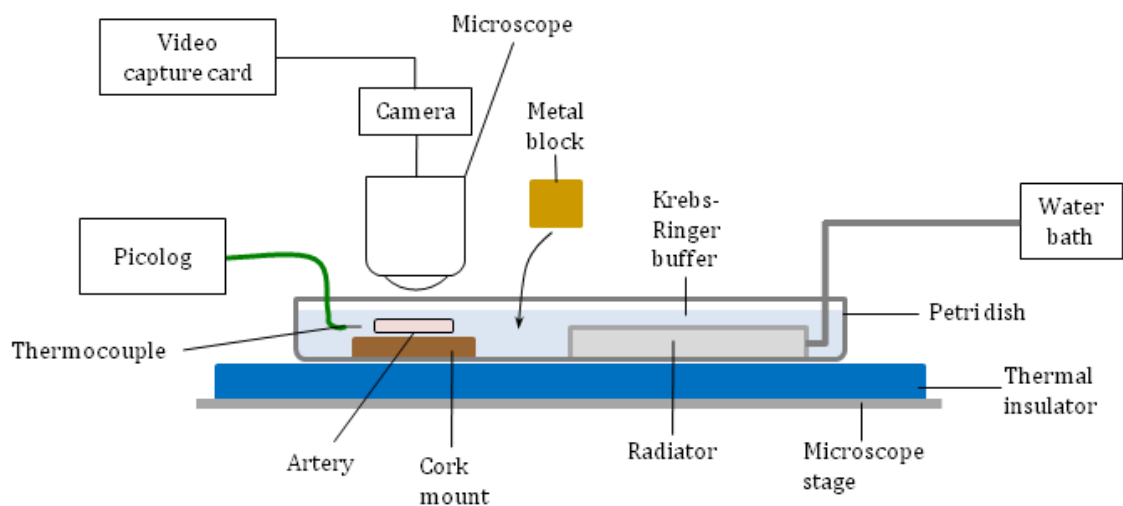
Figure 6.5 Schematic diagram of apparatus used for fluorescent calcium imaging experiments; artery sections were pinned out on a cork mount in a large Petri dish heated by an immersed radiator. Tissue was imaged with a fluorescent microscope and temperature was recorded with a thermocouple placed close to the tissue. A heated metal block was added to the bath to increase temperature rapidly.

The Petri dish was filled with Krebs-Ringer buffer and heated to 37 °C by exchange with a radiator and plastic tubing fed by an external water bath. This assembly was placed on a thermally insulating panel under a Leica fluorescent microscope (DM LFS, Leica Microsystems Wetzlar GmbH, Wetzlar, Germany); a diagram of the apparatus is shown in Figure 6.5. Imaging was performed under a x20 magnification lens with

filters allowing excitation at 450 - 490 nm and emission at 515 nm and above; the absorption and emission wavelengths of Fluo-4 were 488 nm and 520 nm respectively. Images were recorded every 5 seconds with a Moticam 2000 digital microscopy camera and Motic Images Plus digital microscopy software suite (Motic, Barcelona, Spain).

Image capture was initiated once the sections were mounted and visualised; it continued for approximately 10 minutes with a constant temperature before a brass block sealed in clingfilm of approximately 1cm x 1cm x 3cm, heated in boiling water, was added to the dish to induce a temperature increase. Temperature was recorded throughout by a thermocouple placed close to the tissue in the bath. Image capture was continued until the temperature returned to baseline over a period of approximately 15 minutes. After a further few minutes noradrenaline was added to a dish concentration of 1 µM, to check the activity of the vessel and provide a reference change in fluorescence related to calcium concentration. Image capture was ceased approximately 5 minutes after this.

After each experiment, images were post processed using Octave (GNU Octave, released under GNU GPL). The images were imported and stored as a stack in a structured array. Five square regions of interest were defined, a central region and one towards each corner of the image. These regions provided a sample of different regions across the tissue, separated by approximately 100 µm. The average intensity level from each region of interest, from each image was calculated and stored. The mean intensity value over the whole of each image was also calculated and stored. The time course of the mean fluorescence intensity levels was then examined.

This procedure was repeated on 8 carotid artery sections, 8 large mesenteric artery sections and 6 small mesenteric arteries. The procedure was also repeated on undyed tissue to examine the possibility of artefacts in the time course of fluorescence; the time course of fluorescence was observed in tissue held at a constant temperature.

6.3.2 Results

Carotid and large mesenteric arteries

Image capture was initiated soon after the Fluo-4 loaded tissue was mounted and the vessel wall was brought into focus. Fluorescence intensity was initially high but decayed in a logarithmic fashion, rapidly decreasing at first before continuing to fall more slowly. Fluorescence intensity fell by half over the first 5-7 minutes of recording. In control tissue, this decrease in intensity continued throughout recording. Artery rings that were not loaded with Fluo-4 exhibited auto-fluorescence from the elastic tissue, although at a lower level than loaded tissue. The decreases were probably due to photo-bleaching of the Fluo-4 and elastin in the vessels and leaching of the dye from the tissue, which could be significant at these temperatures.

Comparison of the intensities from each region of interest and the image as a whole showed that the time course and magnitude of fluorescence intensity was in most cases similar over the whole image. This confirmed that increases in fluorescence intensity were true, not due to movement of the tissue and the introduction of unbleached areas into the image. This also showed that there were no major differences between calcium activity in different regions of the media of the artery wall within the image (image size approximately 350 x 250 μm).

After the initial fall in intensity at constant temperature, the temperature was raised rapidly by 2.1 ± 0.9 °C in carotid arteries and 2.7 ± 0.9 °C in large mesenteric arteries, which induced a slight increase in fluorescence in most cases, which began at approximately the time when the temperature was at a maximum. When the response had stabilised, noradrenaline was added which caused a much larger increase in fluorescence intensity. The data from an experiment on a carotid artery ring which exhibits this behaviour is displayed in Figure 6.6.

In order to extract a value for the increase in intensity due to each event, a log function was fitted to the initial fluorescence decay. The function was then subtracted from the whole data set to provide a baseline; this would also remove any effect of auto-fluorescence and bleaching on the data. The fluorescence ratio, f/f_0 was then calculated; f is the measured fluorescence intensity at a particular time and f_0 is the

intensity predicted by fitting the initial section of the curve, i.e. the predicted value of intensity if no temperature elevation or noradrenaline induced contraction took place.

Figure 6.6 Typical time course of fluorescence intensity for Fluo-4 loaded mesenteric artery ring during temperature elevation and noradrenaline induced contraction. Temperature increase of approximately 1.5 °C (in this case) was initiated at time **a**, noradrenaline (1 μM) was added at time **b**; the dotted line shows the baseline logarithmic decay. The time course of the temperature rise is shown in the lower graph.

Increases in fluorescence induced by temperature elevation and noradrenaline are then shown by values of f/f_0 greater than 1. Figure 6.7 shows the time course of f/f_0 for the data shown in Figure 6.6; the time course of the bath temperature is also shown here. After the rapid temperature increase, the temperature tended to fall slowly to a lower level than the initial stable temperature. It was extremely difficult to

maintain a very stable temperature in the bath and once the metal block had been added to produce a temperature rise, it could not be removed until the experiment had finished. The presence of the metal block, which would act as a heat sink affected the bath temperature. Any changes in temperature during the periods of 'stable' temperature were much smaller than the large temperature increase created by the metal block.

Figure 6.7 Typical time course of changes in fluorescence intensity in Fluo-4 loaded mesenteric artery ring during temperature elevation by approximately 1.5 ℃ and noradrenaline induced contraction. The time course of the ratio of measured fluorescence intensity to predicted baseline intensity is shown. Temperature increase of approximately 1.5 ℃ was initiated at time a, noradrenaline (1 μM) was added at time b. The time course of the bath temperature is also shown (lower graph).

From the figure, an increase in fluorescence intensity can be observed following temperature elevation. The temperature reached its peak value about 1 minute after the hot metal block was added to the bath. The increase in fluorescence intensity

began at approximately this point and was steady over the next four minutes, during which time the temperature was rapidly changing. Following this, the intensity continued to increase at a slightly lower rate. This period corresponded with cooling of the bath back to the baseline temperature. Noradrenaline (1 μM) was then added (at time **b** in the figure), inducing a rapid increase in fluorescence intensity, which lasted for approximately 2.5 minutes before levelling off.

For carotid artery rings, f/f_0 increased from 1 to 1.4 ± 0.3 on average due to the rise in temperature of 2.1 ± 0.9 °C. Noradrenaline induced a further rise of 0.1 in f/f_0 bringing it to 1.5 ± 0.5 on average. On average, for mesenteric artery rings, f/f_0 increased from 1 to 1.3 ± 0.2 due to the rise in temperature of 2.7 ± 0.9 °C, and by a further 0.8 to 2.1 ± 0.8 on average after noradrenaline induced contraction. The increase in fluorescence due to temperature elevation was similar for carotid and mesenteric arteries. In the mesenteric artery rings the increase in intensity due to noradrenaline was much larger than the increase due to temperature rise, although the results in Chapter 3 indicate that the change in force was similar in both cases.

Small mesenteric arteries

Similarly to experiments on the large arteries, image capture was initiated soon after mounting of Fluo-4 loaded tissue. The fluorescence intensity had a similar time course, with rapid initial decay in a logarithmic fashion. Fluo-4 loaded control curves also exhibited the same time course of fluorescence intensity; un-dyed tissue exhibited auto-fluorescence which also decreased with time.

During the first 10 minutes of image capture, the temperature was held at a constant level, before being increased by 2.6 ± 1.3 ℃, then allowed to cool slowly back to baseline temperature. During this period the intensity continued to decrease. A dose of noradrenaline (1μM) added to the bath induced an increase in fluorescence intensity. A typical time course of fluorescence intensity is shown in Figure 6.8.
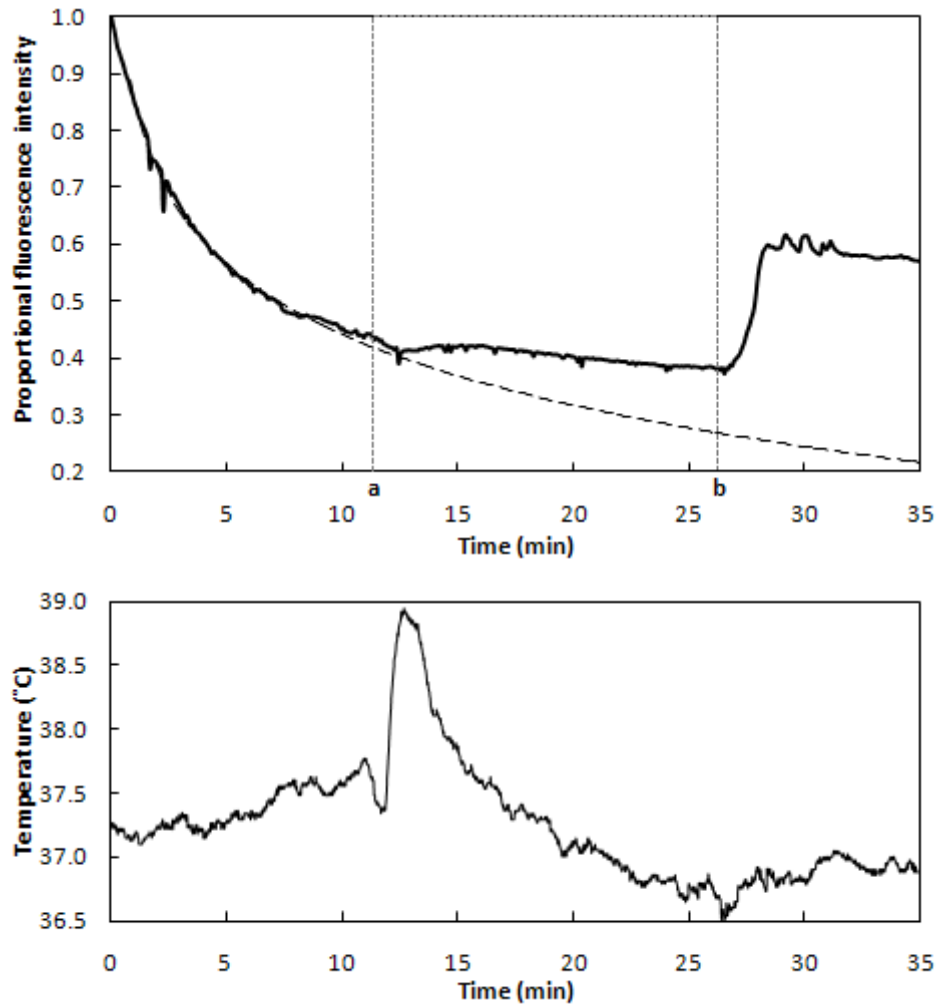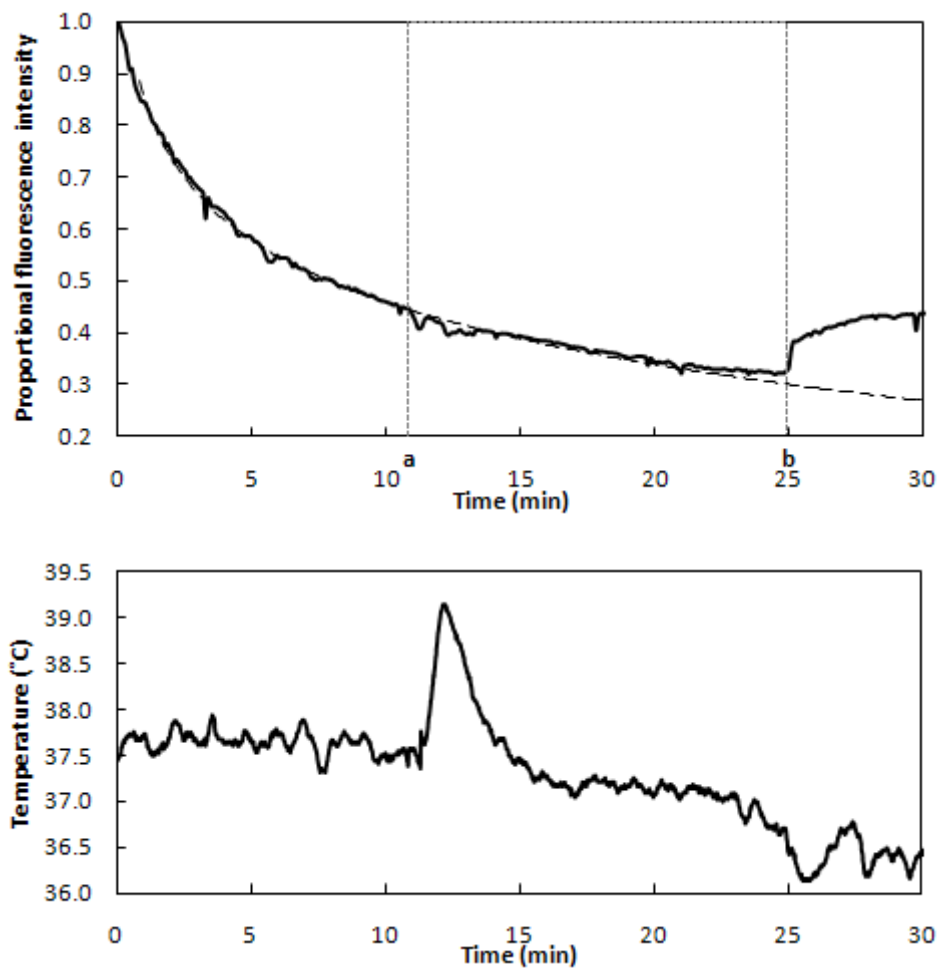
Figure 6.8 Typical time course of fluorescence intensity for Fluo-4 loaded length of small mesenteric artery during temperature elevation and noradrenaline induced contraction. Temperature increase of approximately 1.5 °C was initiated at time **a**, noradrenaline (1 μM) was added at time **b**; the dotted line shows the baseline logarithmic decay. The time course of the bath temperature is also shown (lower graph).

As for the large arteries, a log function was fitted to the initial section of the curve and subtracted from the data to set a baseline. The fluorescence ratio, f/f_0, was calculated as described earlier; the data shown in Figure 6.8 was processed this way and is displayed in Figure 6.9. The temperature during the experiment is shown in the lower graph in the figure. The temperature rise (initiated at time **a**) elicited no change in intensity. The data did not deviate from the function fitted to the initial section of the data. When noradrenaline (1 μM) was added (at time **b**) an increase in fluorescence was observed, from f/f_0 = 1 to 1.3 ± 0.2 on average. Each of the vessels tested

responded to noradrenaline, so their activity was confirmed, but none exhibited changes due to the increase in temperature.
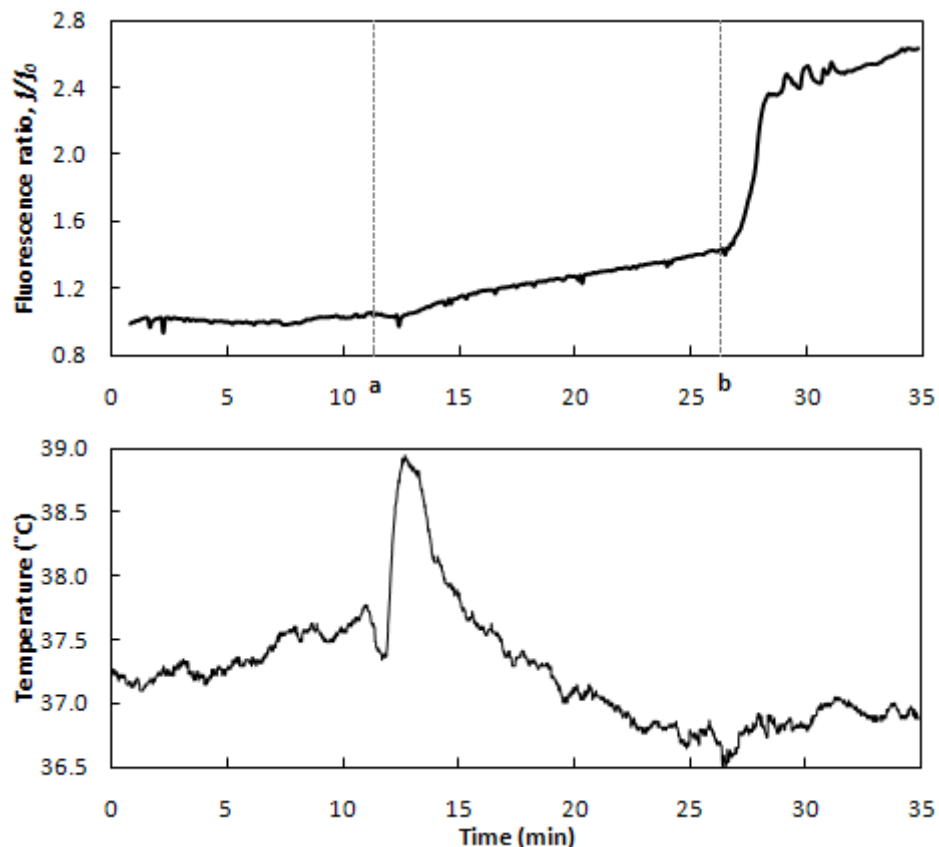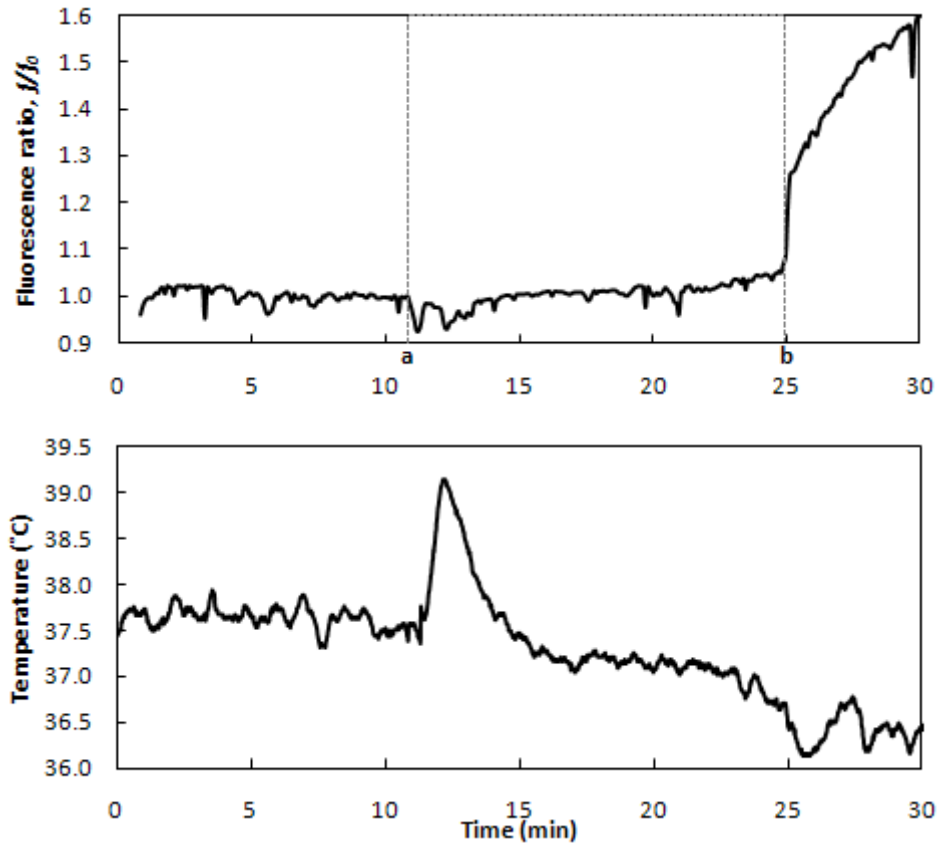

Figure 6.9 Typical time course of changes in fluorescence intensity in Fluo-4 loaded length of small mesenteric artery during temperature elevation by approximately 1.5 ℃ and noradrenaline induced contraction. The time course of the ratio of measured fluorescence intensity to predicted baseline intensity is shown. Temperature increase of approximately 1.5 ℃ was initiated at time **a**, noradrenaline (1 μM) was added at time **b**. The time course of the bath temperature is also shown (lower graph).

These results suggest that ion channel activity is not modified by changes in temperature in these small arteries. This agrees with previous results which showed that the diameter of these vessels is not affected by exposure to ultrasound or temperature changes.

6.3.3 Discussion

Large carotid and mesenteric artery rings exposed to temperature increases exhibited similar increases in intracellular calcium concentration. Calcium concentration measured by fluorescence intensity of a calcium sensitive dye increased during a rapid temperature change and continued slowly following this. The time course was similar in both types of blood vessel and was characterised by a more rapid increase during the first few minutes, as the temperature was increasing, followed by slower increase as the temperature returned to baseline. The magnitude of the changes was similar in both types of vessel on average. As was outlined in the introduction to this chapter, an increase in intracellular calcium ion concentration is associated with contraction of blood vessels. This increase is induced by opening and closing of several types of ion channels in the cell membrane in response to a stimulus. In this case the stimulus was a change in temperature, which affected the activity of some of these ion channels, leading to an influx of calcium into the cells. The results presented in this section therefore provide further evidence that ion channel activity is influenced by changes in temperature, leading to vasoconstriction. In these experiments a relatively large temperature change was employed, mainly to ensure an easily measureable response was elicited. It seems likely that similar changes but on a smaller scale could be induced by smaller temperature changes, of the sort induced by exposure to ultrasound.

There were large variations between the responses of different artery rings, which were expected in light of the variation in previous results. Some variation may have been due to differences in the location of the imaged area with respect to the luminal surface; however, no large differences were observed between locations. For some rings, this region may have been further into the media than for others. Movements of the vessel wall after mounting, as the rings acclimatised to the bath temperature prevented observation of regions very close to the luminal surface and also made precise positioning difficult. There were also difficulties in focusing, as at the magnification used it was difficult to find recognisable features. Other variations originated from differences in the state of the rings, for example, the length of time between harvesting the tissue, dissection, Fluo-4 loading and mounting. The Fluo-4

loading procedure was standardised as much as possible to reduce differences and the data was processed in a way that would eliminate dependence on background fluorescence intensity.

The images were analysed using five regions of interest, as well as the whole image. The time course of intensity from each region and the whole image was compared and found to be very similar. Errors in the results due to significant movement of the vessel were therefore unlikely as the introduction of unbleached areas into the image would affect the time course of each region differently.

No significant changes in intracellular calcium concentration were detected in small vessels during a temperature change, but an increase was induced by noradrenaline, demonstrating cellular viability. The temperature change was of a similar magnitude to that used in the myograph experiments in Chapter 5. The preparation used here was also the same but mounting was different, in this case the vessels were not pressurised. The factors which may underlie the lack of response of these vessels discussed in relation to the experiments in Chapter 5, such as the preparation, wall stiffness and ion channel populations, also apply here. If the ion channel population that is sensitive to temperature changes is not present, then there would be no effect on intracellular calcium concentration. In Section 6.2.2, results were presented that showed that the response of large arteries to ultrasound was mediated by inhibition of inward rectifier potassium channels. It is possible that these ion channels do not exist in these smaller vessels. These ion channels help the cell membrane to return to resting potential after depolarisation. They are inhibited during exposure to ultrasound, by some thermal mechanism. This leads to an influx of calcium into the cell, hence we can measure increased intracellular calcium concentration. If these ion channels are not present then ultrasound exposure or thermal stimulation may not lead to an influx of calcium into the cell.

It was shown in this chapter that the response of carotid and large mesenteric arteries to ultrasound was mediated by inhibition of inward rectifier potassium channels. In carotid and large mesenteric arteries it was also found that an increase in temperature caused changes in ion channel activity that led to increases in intracellular calcium concentration. In smaller mesenteric arteries, no such change in intracellular calcium

was observed during periods of elevated temperature. This finding agreed with the results obtained using these vessels in Chapter 5, which showed that exposure to ultrasound and temperature changes did not induce vasoconstriction.

7 Discussion, conclusions and further work

The results presented in this thesis have shown that in rings of carotid and large lateral cecal mesenteric artery *in vitro*, exposure to both pulsed and continuous wave 3.2 MHz ultrasound at acoustic powers up to 145 mW induced contraction. Wall stress in the arteries increased by up to 1.5% in carotid arteries, by up to 2% in mesenteric arteries during the exposure and returned to baseline approximately 10 minutes after the exposure period. The response was reproducible over a period of several hours. The response was not endothelium-dependent and was not significantly different when induced by pulsed ultrasound at the same total acoustic power. The mechanism of this response was thermal in nature and was associated with inhibition of inward-rectifier potassium ion channels in the cell membrane, channels that would otherwise help to return the cell to resting membrane potential. The thermal nature of the response was confirmed by investigation of the response of artery rings to increases in temperature above baseline; this also induced contraction. Intracellular calcium activity was observed during temperature increases; increases in intracellular calcium corresponding with these temperature elevations were observed. This confirmed that increases in temperature stimulated changes in ion channel activity, which led to increased intracellular calcium and contraction of the muscle fibres.

The response of smaller arteries to ultrasound exposure was investigated using 1st order branches of the lateral cecal mesenteric artery. These arteries were selected to have diameters of between 0.5 and 1 mm, as such they were perhaps slightly larger than the true resistance arteries. Exposure to continuous wave 3.2 MHz ultrasound at an acoustic power of 145 mW did not induce contraction in an open field. Neither was a response induced when an absorbing panel was situated close to the vessel to

increase heating during exposure, to a level comparable with that during exposure of large arteries. The response of these arteries to increases in bath temperature above baseline was also investigated; no change in diameter was observed during the periods of temperature increase. Intracellular calcium activity was observed during increases in temperature; no significant increases were observed corresponding with periods of elevated temperature. It therefore appears that these small arteries do not respond to ultrasound, or changes in temperature, in the same way as the carotid and large mesenteric arteries.

In this section, these results will be discussed in several different contexts and further research possibilities will be highlighted. First, the thermal nature of the response and the interaction with tissue function will be discussed. This will be followed by a discussion of the cellular processes involved in the response, mainly ion channel activity in the cell membrane. The presence of the response in different arteries *in vitro*, the possibility of *in vivo* effects and the likelihood of a similar response occurring during diagnostic ultrasound examinations will be discussed.

Thermal nature of the response

The response of the large arteries to ultrasound was thermal in nature. The exact mechanism of the thermal interaction with the cells is not known, other than that the increase in temperature affects the activity of the ion channels. Increases in temperature will increase the rate of diffusion of substances and the rate of biochemical reactions, which could alter ion channel activity. As the temperature increases further, biochemical reactions will be impaired as enzymes and other molecules begin to break down. The action of vasoactive drugs is temperature dependent, as their function depends on binding of ligands to receptors and other chemical reactions. So at slightly elevated temperatures, normal physiological functions may become exaggerated. Changes in temperature may also affect the cell membrane, altering the mechanical properties of the lipid bilayer and the function of proteins with it.

During exposure of arteries to ultrasound in this study, the cross section of the ultrasound beam at the focal region was smaller than the tissue cross section. The whole tissue sample was not insonated. From the heating profiles measured using the thermal test object in Chapter 3, it can be seen that there was some heating for a few

millimetres either side of the beam axis, which could have provoked a response. It is not known whether only the insonated or heated parts of the artery ring produced a response during ultrasound exposure and whether the response in each area was proportional to the temperature rise there, or whether stimulation in one area caused a signal cascade to produce a response in the whole tissue. It is known that the cells in visceral smooth muscle tissue can communicate with each other; they transmit nerve signals between them, so could transmit other signals. It is also possible in this isometric configuration that contraction of some parts of the tissue could place other parts under strain, inducing further changes in tone due to a stretch-activated response. This may be more likely in small arteries and arterioles which exhibit myogenic tone, where stretching caused by increased blood pressure induces increased muscle tone and contraction. The spatial pattern of the response could be examined by mapping the intracellular calcium activity over the tissue during exposure to ultrasound, where the beam area is contained within the tissue. If the response was localised, then the calcium concentration would be higher close to the beam axis. If a response was induced in the whole tissue by a second signal transmitted from the insonated area, the intracellular calcium concentration would appear constant over the whole tissue.

Involvement of ion channels

It was shown that exposure to ultrasound caused inhibition of the inward rectifier potassium channels, but it is not known which other channels, if any, are also affected. Mustafa and Thulesius (2005) showed that the activity of other types of potassium channels were also affected during contraction of the carotid artery by mild hyperthermia. It therefore seems likely that other potassium ion channel populations would be involved in the response to ultrasound. Further investigation is required to determine which ion channel populations are affected and how this affects the resulting membrane potential.

All cell membranes contain ion channels, which are necessary for cell function. Potassium ion channels are common to all cells, but the populations are likely to vary in type and proportion. In Chapter 2, evidence from the literature was presented on the effects of ultrasound on many different cell types; some of these were related to ion channel activity. Although the mechanisms were not specified as thermal in many

of these studies, small temperature rises may have been possible. It is therefore possible that ultrasound may interact with cell types other than smooth muscle and tissue types other than arteries, to produce responses by similar pathways. These responses could be many and varied and would require wide ranging investigation. The response of smooth muscle to ultrasound was relatively easy to measure, as the cell functions to control vascular tone. Other cell types may not exhibit such obvious and easily measurable transient changes. In many cases, more subtle and longer term changes may be of interest, the nature of which may not be immediately obvious. It could however, be argued that important responses to ultrasound would be changes in the function of cells that have a specific purpose, such as osteoblasts in bone formation, or cells from organs such as the liver, and that investigations should focus on these. A range of intracellular signalling pathways are instigated by ion channel activity and the activity of other membrane proteins. One example of this is the calcium pathway leading to smooth muscle contraction. In different cell types, changes in membrane protein activity could lead to a variety of different signalling cascades and there is much scope for investigation of these pathways.

Response in different arteries

Although it may be possible that some of the effects observed in cells due to ultrasound have similar mechanisms to the responses measured in this study, no response to ultrasound was observed in this study in small arteries, which were branches of the large lateral cecal mesenteric artery. There are physiological differences between the large elastic arteries, conducting arteries and small arteries. The flow in small arteries, resistance arteries and arterioles is more tightly controlled, to regulate local blood flow, than the flow in the large conducting arteries. The response of the true resistance arteries and arterioles may also be different to the response of the 1st order branches from the lateral cecal artery used here. Different responses to some vasoactive substances have been observed between the two vessel populations; this provides evidence that they may respond differently to the same stimuli. The response measured in large arteries was shown to be related to the activity of inward rectifier potassium channels in the cell membrane. If the ion channel population differs in these small vessels, then the mechanism which mediates the response may be absent and no change in diameter would be induced. It is known that vessels from different locations in the circulation have different functions and

have varying amounts of control over local blood flow. These vessels may simply not have the sensors which provoke the response. Arteries of different sizes may be controlled differently by nerves, neurotransmitters and hormones. It may therefore be interesting to investigate the response of small arteries in a small animal *in vivo* preparation, where these control systems are intact.

The results shown here really relate only to the preparations used in these experiments; other vessels may behave similarly, but further investigation is required to confirm this. The two large artery preparations used in this study exhibited similar responses to ultrasound. Herrera et al. (2000) observed different responses due to cooling in the aorta and the renal artery, so it may also be possible that some arteries will respond differently to ultrasound than others. It is also known that smooth muscle found in different tissues can react differently to a given agonist; a substance which induces relaxation in vascular tissue may produce contraction in gastric tissue. Smooth muscle cells in different vascular beds, vessels of different sizes, or even different parts of the same vessel may also respond differently to a particular stimulus. The reason for these differences could be related to ion channel populations, agonist receptors or other components of signal transduction further along the pathway (Somlyo and Somlyo 1994). Because of these differences between tissues, it would be interesting to conduct a wide ranging investigation into the effect of ultrasound on arteries of different sizes and types, from different locations and from different animals. This may be especially interesting and relevant in the arterioles and capillary beds, where changes in vascular tone could have greater physiological significance; a response in these tissues would be important where highly vascularised tissue is exposed to ultrasound. The thermal nature of the response also makes it important to investigate the effects on tissue which is poorly perfused, where heat may not be dissipated effectively.

Clinical implications

It has been shown here that ultrasound in the diagnostic frequency and acoustic power range can cause contraction of blood vessels *in vitro*. Further investigation is required to establish whether this effect would occur *in vivo*, during examinations such as peripheral vascular Doppler flow studies, in which blood vessels are placed at the focus of the beam. The reversible nature of the contractions produced in this

study, suggest that the effect does not cause lasting damage to insonated blood vessels. As the increase in tension continues over several minutes, this may be another indication that exposure to ultrasound in diagnostic applications should be kept to a minimum and that the probe should not be held still for long periods of time. However, as the effect was found to be thermal in origin, heat dissipation by perfusion will diminish or prevent the response. Conversely, vessels situated close to a strong absorber such as bone may be affected. Temperature rises induced by exposure to ultrasound in this case are small and would be quickly dissipated in the body without raising the temperature of the body or organs within it. Core body temperature is controlled remotely by the brain; it seems unlikely that the feedback mechanisms involved in this would be capable of responding to temperature changes on such small scales. However, the effects of this response *in vivo*, where feedback systems are intact can not be determined from these results. As previously mentioned, some insight into the effect of nervous control and hormones on the response may be gained from investigation of the response in an *in vivo* small animal preparation. Another *in vivo* investigation that would be easy to perform, would be to measure blood flow in the capillaries in the nail bed. The capillaries could be easily imaged using a long working distance light microscope. For other *in vivo* studies, a method of measuring vascular tone and blood flow that wouldn't affect the response is required; laser Doppler is a possibility.

Large variations in the magnitude of the response were seen between artery rings. There were many factors that may have contributed to this variation, as discussed in Section 4.7. Another factor which may have contributed could have been the age of the animal, which was not controlled in this study. It is known that the arteries become stiffer with age; the tension applied by the connective tissue will be higher, so for a given change in smooth muscle tone, the vessel will contract less. This factor would be important if a response was observed *in vivo*; the effects in a foetus where the blood vessels have a lower stiffness may be different to the effects in the elderly.

The response of arteries to ultrasound was dependent on acoustic power and in this study, was within the range of acoustic powers used for diagnostic ultrasound. If a response was to occur *in vivo*, in theory it could be induced by diagnostic exposures. However, in this study the positions of the tissue and focal region were fixed with

respect to each other and exposures lasted for 4 minutes. In most diagnostic examinations, the transducer would not be stationary for long periods in this way, so contraction would not continue to any significant level.

As discussed in Chapter 2, the FDA states that during diagnostic ultrasound examinations, the Thermal Index should not exceed 6 without justification. Theoretically, at this limit the acoustic power would be enough to raise the temperature of the tissue by 6 °C. This is much larger than the temperature rise measured in the focal region in this study and it is possible that ultrasound equipment is being used in this way. From measurements of the time course of heating and of the response in this study, it can be seen that the initial rate of temperature rise is high and the time over which this initial rate occurs is not dependent on the final temperature. Where equipment is used with a TI of 6, the initial temperature rise could be of the order created in these experiments even when exposure time is short.

7.1 Novel outcomes from this thesis

This thesis has presented evidence of an effect of ultrasound on carotid and mesenteric arteries that was previously unknown. Exposure to both continuous and pulsed wave ultrasound induced reversible vasoconstriction, the magnitude of which was dependent on acoustic power and was due to a thermal mechanism. The response occurred by an endothelium-independent mechanism and was due to changes in ion channel activity in the cell membrane. Inhibition of inward-rectifier potassium ion channels played a part in the response; fluorescent imaging of intracellular calcium confirmed that small temperature rises could influence ion channel activity. Increases in intracellular calcium levels were induced leading to contraction of the arteries.

8 References

Aaronson PI, Ward JPT and Wiener CM (2004). The Cardiovascular System at a Glance. Oxford, UK, Blackwell Publishing Ltd.

AIUM/NEMA (1992). Standard for real-time display of thermal and mechanical acoustic output indiceson diagnostic ultrasound equipment. Laurel, MD, American Institute of Ultrasound in Medicine Publications.

Al-Karmi AM, Dinno MA, Stoltz DA and Crum LA (1994). "Calcium and the Effects of Ultrasound on Frog Skin." Ultrasound in Medicine and Biology **20**(1): 73-73.

Apfel RE and Holland CK (1991). "Gauging the likelihood of cavitation from short-pulse, low-duty cycle diagnostic ultrasound." Ultrasound in Medicine & Biology **17**(2): 179-185.

Aziba PI and Okpako DT (2003). "Effects of Chloroquine on Smooth Muscle Contracted with Noradrenaline or High-Potassium Solutions in the Rat Thoracic Aorta." Journal of Smooth Muscle Research **39**(3): 31-37.

Basta G, Venneri L, Lazzerini G, Pasanisi E, Pianelli M, Vesentini N, Del Turco S, Kusmic C and Picano E (2003). "In vitro modulation of intracellular oxidative stress of endothelial cells by diagnostic cardiac ultrasound." Cardiovascular Research **58**(1): 156-161.

Bertuglia S, Giusti A and Picano E (2004). "Effects of diagnostic cardiac ultrasound on oxygen free radical production and microvascular perfusion during ischemia reperfusion." Ultrasound in Medicine & Biology **30**(4): 549-557.

BMUS (2009). Guidelines for the safe use of diagnostic ultrasound equipment, Safety Group of the British Medical Ultrasound Society.

Bohr DF, Somlyo AP and Sparks HV, Eds. (1980). Section 2: The Cardiovascular System: Volume II: Vascular Smooth Muscle. The Handbook of Physiology. Bethesda, MD, USA, The American Physiological Society.

Bryan RM, Jr., Steenberg ML and Marrelli SP (2001). "Role of Endothelium in Shear Stress-Induced Constrictions in Rat Middle Cerebral Artery." Stroke **32**(6): 1394-1400.

Chang WH-S, Sun J-S, Chang S-P and Lin JC (2002). "Study of thermal effects of ultrasound stimulation on fracture healing." Bioelectromagnetics **23**(4): 256-263.

Choi BH, Woo J-I, Min B-H and Park SR (2006). "Low-intensity ultrasound stimulates the viability and matrix gene expression of human articular chondrocytes in alginate bead culture." Journal of Biomedical Materials Research Part A **79A**(4): 858-864.

Church CC (2002). "Spontaneous homogeneous nucleation, inertial cavitation and the safety of diagnostic ultrasound." Ultrasound in Medicine and Biology **28**(10): 1349-1364.

Claes L and Willie B (2007). "The enhancement of bone regeneration by ultrasound." Progress in Biophysics and Molecular Biology **93**(1-3): 384-398.

Crisci AR and Ferreira AL (2002). "Low-intensity pulsed ultrasound accelerates the regeneration of the sciatic nerve after neurotomy in rats." Ultrasound in Medicine & Biology **28**(10): 1335-1341.

da Costa Gonçalves A, Barbieri CH, Mazzer N, Garcia SB and Thomazini JA (2007). "Can Therapeutic Ultrasound Influence the Integration of Skin Grafts?" Ultrasound in Medicine and Biology **33**(9): 1406-1412.

Dalecki D, Keller BB, Raeman CH and Carstensen EL (1993). "Effects of Pulsed Ultrasound on the Frog Heart: I. Thresholds for Changes in Cardiac Rhythm and Aortic Pressure." Ultrasound in Medicine and Biology **19**(5): 385-385.

Davies PF (1995). "Flow-mediated endothelial mechanotransduction." Physiol. Rev. **75**(3): 519-560.

Davros WJ, Garra BS and Zeman RK (1991). "Gallstone lithotripsy: relevant physical principles and technical issues." Radiology **178**(2): 397-408.

Dinno MA, Crum LA and Wu J (1989). "The effect of therapeutic ultrasound on electrophysiological parameters of frog skin." Ultrasound in Medicine & Biology **15**(5): 461-470.

Dobrin PB (1973). "Isometric and isobaric contraction of carotid arterial smooth muscle." American Journal of Physiology **225**(3).

Dobrin PB (1978). "Mechanical properties of arteries." Physiol. Rev. **58**(2).

Dobrin PB and Rovick AA (1969). "Influence of vascular smooth muscle on contractile mechanics and elasticity of arteries." American Journal of Physiology **217**(6).

Docker MF and Duck FA, Eds. (1991). The Safe Use of Diagnostic Ultrasound. London, British Institute of Radiology.

Doody C, Duck FA and Humphrey VF (2000). "Comparison of finite element and heated disc models of tissue heating by ultrasound." Ultrasound in Medicine & Biology **26**(8): 1347-1355.

Drury R and Wallington E (1967). Carleton's Histological Technique. London, Oxford University Press.

Duck F (2009). "Acoustic Dose and Acoustic Dose-Rate." Ultrasound in Medicine & Biology **35**(10): 1679-1685.

Duck FA (1990). Physical Properties of Tissue. London, Academic Press.

Duck FA (2002). "Nonlinear acoustics in diagnostic ultrasound." Ultrasound in Medicine & Biology **28**(1): 1-18.

Duck FA and Martin K (1991). "Trends in diagnostic ultrasound exposure." Physics in Medicine and Biology **36**(11): 1423-1432.

Duck FA and Starritt HC (1984). "Acoustic shock generation by ultrasonic imaging equipment." Br J Radiol **57**(675): 231-240.

Duck FA and Starritt HC (1986). "The locations of peak pressures and peak intensities in finite amplitude beams from a pulsed focused transducer." Ultrasound in Medicine & Biology **12**(5): 403-409.

Dunn F (1985). "Cellular inactivation by heat and shear." Radiation and environmental biophysics **24**: 131-139.

Edmonds PD and Sancier KM (1983). "Evidence for free radical production by ultrasonic cavitation in biological media." Ultrasound in Medicine & Biology **9**(6): 635-639.

FDA (1997). Information for manufacturers seeking marketing clearance of diagnostic ultrasound systems and transducers. administration FaD, Center for Devices and Radiological Health.

Furchgott RF and Zawadzki JV (1980). "The obligatory role of endothelial cells in the relaxation of arterial smooth muscle by acetylcholine." Nature **288**(5789): 373-6.

Geiger RV, Berk BC, Alexander RW and Nerem RM (1992). "Flow-induced calcium transients in single endothelial cells: spatial and temporal analysis." Am J Physiol Cell Physiol **262**(6): C1411-1417.

Harle J, Salih V, Mayia F, Knowles JC and Olsen I (2001). "Effects of ultrasound on the growth and function of bone and periodontal ligament cells in vitro." Ultrasound in Medicine & Biology **27**(4): 579-586.

Herrera B, Eisenberg G, Holberndt O, Desco MM, Rábano A, García-Barreno P and Del Cañizo JF (2000). "Paradoxical Effects of Temperature on Vascular Tone." Cryobiology **41**(1): 43-50.

Hildebrandt B, Wust P, Ahlers O, Dieing A, Sreenivasa G, Kerner T, Felix R and Riess H (2002). "The cellular and molecular basis of hyperthermia." Critical Reviews in Oncology/Hematology **43**(1): 33-56.

Hoskins P, Thrush A, Martin K and Whittingham T, Eds. (2003). Diagnostic Ultrasound: Physics and equipment. London, Greenwich Medical Media Limited.

Hrazdira I, Skorpíková J and Dolníková M (1998). "Ultrasonically induced alterations of cultured tumour cells." European Journal of Ultrasound **8**(1): 43-49.

Huang H, Kamm RD and Lee RT (2004). "Cell mechanics and mechanotransduction: pathways, probes, and physiology." Am J Physiol Cell Physiol **287**(1): C1-11.

Huang T-H, Tang C-H, Chen H-I, Fu W-M and Yang R-S (2008). "Low-Intensity Pulsed Ultrasound-Promoted Bone Healing Is Not Entirely Cyclooxygenase 2 Dependent." J Ultrasound Med **27**(10): 1415-1423.

Hwang JH, Tu J, Brayman AA, Matula TJ and Crum LA (2006). "Correlation between inertial cavitation dose and endothelial cell damage in vivo." Ultrasound in Medicine and Biology **32**(10): 1611-1619.

IEC (2007). IEC 60601: Part 2-37: Medical Electrical Equipment: Particular requirements for the basic safety and essential performance of ultrasonic medical diagnostic and monitoring equipment. Geneva, International Electrotechnical Commission.

IEC (2009). Medical electrical equipment - Part 2-5: Particular requirements for the basic safety and essential performance of ultrasonic physiotherapy equipment. Part 2-5: Particular requirements for the basic safety and essential performance of ultrasonic physiotherapy equipment, International Electrotechnical Commission. **IEC 60601-2-5**.

Ito M, Azuma Y, Ohta T and Komoriya K (2000). "Effects of ultrasound and 1,25-dihydroxyvitamin D3 on growth factor secretion in co-cultures of osteoblasts and endothelial cells." Ultrasound in Medicine & Biology **26**(1): 161-166.

Iwabuchi S, Ito M, Hata J, Chikanishi T, Azuma Y and Haro H (2005). "In vitro evaluation of low-intensity pulsed ultrasound in herniated disc resorption." Biomaterials **26**(34): 7104-7114.

James NL, Harrison DG and Nerem RM (1995). "Effects of shear on endothelial cell calcium in the presence and absence of ATP." FASEB J. **9**(10): 968-973.

Kass M, Witkin A and Terzopoulos D (1988). "Snakes: Active contour models." International Journal of Computer Vision **1**(4): 321-331.

Kobayashi Y, Sakai D, Iwashina T, Iwabuchi S and Mochida J (2009). "Low-intensity pulsed ultrasound stimulates cell proliferation, proteoglycan synthesis and expression of growth factor-related genes in human nucleus pulposus cell line." Eur Cell Mater **17**: 15-22.

Kondo T and Yoshii G (1985). "Effect of intensity of 1.2 MHz ultrasound on change in DNA synthesis of irradiated mouse L cells." Ultrasound in Medicine & Biology **11**(1): 113-119.

Korstjens C, van der Rijt R, Albers G, Semeins C and Klein-Nulend J (2008). "Low-intensity pulsed ultrasound affects human articular chondrocytes in vitro." Medical and Biological Engineering and Computing **46**(12): 1263-1270.

Korstjens CM, Nolte PA, Burger EH, Albers GHR, Semeins CM, Aartman IHA, Goei SW and Klein-Nulend J (2004). "Stimulation of bone cell differentiation by low-intensity ultrasound - a histomorphometric in vitro study." Journal of Orthopaedic Research **22**(3): 495-500.

Lamont C, Vainorius E and Wier WG (2003). "Purinergic and adrenergic Ca2+ transients during neurogenic contractions of rat mesenteric small arteries." The Journal of Physiology **549**: 801.

Lamont C, Vial C, Evans RJ and Wier WG (2006). "P2X1 receptors mediate sympathetic postjunctional Ca2+ transients in mesenteric small arteries." Am J Physiol Heart Circ Physiol **291**(6): H3106-3113.

Lehoux S and Tedgui A (2003). "Cellular mechanics and gene expression in blood vessels." Journal of Biomechanics **36**(5): 631-643.

Liu Y, Cho C-W, Yan X, Henthorn TK, Lillehei KO, Cobb WN and Ng K-y (2001). "Ultrasound-Induced Hyperthermia Increases Cellular Uptake and Cytotoxicity of P-Glycoprotein Substrates in Multi-Drug Resistant Cells." Pharmaceutical Research **18**(9): 1255-1261.

Liu Y, Yang H, Takatsuki H and Sakanishi A (2006). "Effect of ultrasonic exposure on Ca2+-ATPase activity in plasma membrane from Aloe arborescens callus cells." Ultrasonics Sonochemistry **13**(3): 232-236.

Lu H, Qin L, Cheung W, Lee K, Wong W and Leung K (2008). "Low-Intensity Pulsed Ultrasound Accelerated Bone-Tendon Junction Healing Through Regulation of Vascular Endothelial Growth Factor Expression and Cartilage Formation." Ultrasound in Medicine & Biology **34**(8): 1248-1260.

Lu H, Qin L, Lee K, Cheung W, Chan K and Leung K (2009). "Identification of genes responsive to low-intensity pulsed ultrasound stimulations." Biochemical and Biophysical Research Communications **378**(3): 569-573.

MacRobbie AG, Raeman CH, Child SZ and Dalecki D (1997). "Thresholds for Premature Contractions in Murine Hearts Exposed to Pulsed Ultrasound." Ultrasound in Medicine and Biology **23**(5): 761-766.

Malek A and Izumo S (1992). "Physiological fluid shear stress causes downregulation of endothelin-1 mRNA in bovine aortic endothelium." Am J Physiol Cell Physiol **263**(2): C389-396.

Malek AM and Izumo S (1996). "Mechanism of endothelial cell shape change and cytoskeletal remodeling in response to fluid shear stress." J Cell Sci **109**(4): 713-726.

Malizos KN, Hantes ME, Protopappas V and Papachristos A (2006). "Low-intensity pulsed ultrasound for bone healing: An overview." Injury **37**(1, Supplement 1): S56-S62.

Maxwell L, Collecutt T, Gledhill M, Sharma S, Edgar S and Gavin JB (1994). "The augmentation of leucocyte adhesion to endothelium by therapeutic ultrasound." Ultrasound in Medicine & Biology **20**(4): 383-390.

Miller DL (1998). "The relationship of scattered subharmonic, 3.3-MHz fundamental and second harmonic signals to damage of monolayer cells by ultrasonically activated Albunex." The Journal of the Acoustical Society of America **103**(2): 1183-1189.

Miller DL and Quddus J (2000). "Diagnostic ultrasound activation of contrast agent gas bodies induces capillary rupture in mice." Proceedings of the National Academy of Sciences of the United States of America **97**(18): 10179-84.

Miller MW and Ziskin MC (1989). "Biological consequences of hyperthermia " Ultrasound in medicine and biology **15**(8): 707-722.

Miyamoto T, Neuman Y, Luo H, Jeon D-S, Kobal S, Ikeno F, Horzewski M, Honda Y, Mirocha JM, Iwami T, Echt D, Fishbein MC and Siegel RJ (2003). "Coronary vasodilation by noninvasive transcutaneous ultrasound: An in vivo canine study." Journal of the American College of Cardiology **41**(9): 1623-1627.

Mizrahi N, Seliktar D and Kimmel E (2007). "Ultrasound-Induced Angiogenic Response in Endothelial Cells." Ultrasound in Medicine and Biology **33**(11): 1818-1829.

Molecular-Probes. (2010, 18/05/2010). "Fluo Calcium Indicators." Product Information Retrieved June, 2010, from http://probes.invitrogen.com/media/pis/mp01240.pdf.

Morris H, Rivens I, Shaw A and ter Haar G (2008). "Investigation of the viscous heating artefact arising from the use of thermocouples in a focused ultrasound field." Physics in Medicine and Biology **53**(17): 4759.

Morrissey JJ, Higashikubo R, Goswami PC and Dixon P (2009). "Mild hyperthermia as a potential mechanism to locally enhance cell growth kinetics." Journal of Drug Targeting **17**(9): 719-723.

Mortimer AJ and Dyson M (1988). "The effect of therapeutic ultrasound on calcium uptake in fibroblasts." Ultrasound in Medicine & Biology **14**(6): 499-506.

Mostafa NZ, Uludag H, Dederich DN, Doschak MR and El-Bialy TH (2009). "Anabolic effects of low-intensity pulsed ultrasound on human gingival fibroblasts." Archives of Oral Biology **54**(8): 743-748.

Mulvany MJ and Aalkjaer C (1990). "Structure and function of small arteries." Physiol. Rev. **70**(4): 921-961.

Mustafa S and Thulesius O (2005). "Hyperthermia-Induced Vasoconstriction of the Carotid Artery and the Role of Potassium Channels." Journal of Stroke and Cerebrovascular Diseases **14**(3): 122-126.

Mustafa S, Thulesius O, Elgazzar AH and Ismael HN (2007). "Synergistic effects of ethanol and hyperthermia on carotid artery vasoconstriction." Clinical Physiology and Functional Imaging **27**(3): 185-190.

Naruse K, Miyauchi A, Itoman M and Mikuni-Takagaki Y (2003). "Distinct Anabolic Response of Osteoblast to Low-Intensity Pulsed Ultrasound." Journal of Bone and Mineral Research **18**(2): 360-369.

NCRP (1992). Exposure criteria for medical diagnostic ultrasound:1. Criteria based on thermal mechanisms. Report No. 113. Bethesda, MD, National Council for Radiation Protection and Measurements.

Nelson MT, Patlak JB, Worley JF and Standen NB (1990). "Calcium channels, potassium channels, and voltage dependence of arterial smooth muscle tone." Am J Physiol Cell Physiol **259**(1): C3-18.

Nelson MT and Quayle JM (1995). "Physiological roles and properties of potassium channels in arterial smooth muscle." Am J Physiol Cell Physiol **268**(4): C799-822.

Ng GYF and Fung DTC (2007). "The Effect of Therapeutic Ultrasound Intensity on the Ultrastructural Morphology of Tendon Repair." Ultrasound in Medicine and Biology **33**(11): 1750-1754.

Nishikori T, Ochi M, Uchio Y, Maniwa S, Kataoka H, Kawasaki K, Katsube K and Kuriwaka M (2002). "Effects of low-intensity pulsed ultrasound on proliferation and chondroitin sulfate synthesis of cultured chondrocytes embedded in Atelocollagen® gel." Journal of Biomedical Materials Research **59**(2): 201-206.

Noble JG, Lee V and Griffith-Noble F (2007). "Therapeutic ultrasound: The effects upon cutaneous blood flow in humans." Ultrasound in Medicine & Biology **33**(2): 279-285.

Noris M, Morigi M, Donadelli R, Aiello S, Foppolo M, Todeschini M, Orisio S, Remuzzi G and Remuzzi A (1995). "Nitric Oxide Synthesis by Cultured Endothelial Cells Is Modulated by Flow Conditions." Circ Res **76**(4): 536-543.

O'Brien WD (2007). "Ultrasound-biophysics mechanisms." Progress in Biophysics and Molecular Biology **93**(1): 212-255.

Oo AY, Conant AR, Chester MR, Dihmis WC and Simpson AWM (2007). "Temperature Changes Stimulate Contraction in the Human Radial Artery and Affect Response to Vasoconstrictors." Ann Thorac Surg **83**(1): 126-132.

Park HG, Han SI, Oh SY and Kang HS (2005). "Cellular responses to mild heat stress." Cellular and Molecular Life Sciences **62**(1): 10-23.

Parvizi J, Parpura V, Greenleaf J and Bolander M (2002). "Calcium signaling is required for ultrasound-stimulated aggrecan synthesis by rat chondrocytes." J Orthop Res **20**: 51 - 57.

Parvizi J, Wu CC, Lewallen DG, Greenleaf JF and Bolander ME (1999). "Low-Intensity Ultrasound Stimulates Proteoglycan Synthesis in Rat Chondrocytes by Increasing Aggrecan Gene Expression." Journal of Orthopaedic Research **17**(4): 488-494.

Perkins MA (1989). "A versatile force balance for ultrasound power measurement." Physics in Medicine and Biology **34**(11): 1645-1651.

Preston RC (1988). "The NPL ultrasound beam calibrator." Ultrasonics, Ferroelectrics and Frequency Control, IEEE Transactions on **35**(2): 122-139.

Ramirez A, Schwane JA, McFarland C and Starcher B (1997). "The effect of ultrasound on collagen synthesis and fibroblast proliferationin vitro." Medicine & Science in Sports & Exercise **29**(3): 326-332.

Raso VVM, Barbieri CH, Mazzer N and Fasan VS (2005). "Can therapeutic ultrasound influence the regeneration of peripheral nerves?" Journal of Neuroscience Methods **142**(2): 185-192.

Raz D, Zaretsky U, Einav S and Elad D (2005). "Cellular Alterations in Cultured Endothelial Cells Exposed to Therapeutic Ultrasound Irradiation." Endothelium **12**(4): 201-213.

Robinson S and Buono M (1995). "Effect of continuous-wave ultrasound on blood flow in skeletal muscle." Physical Therapy **75**(2).

Rutten S, Nolte PA, Korstjens CM, van Duin MA and Klein-Nulend J (2008). "Low-intensity pulsed ultrasound increases bone volume, osteoid thickness and mineral apposition rate in the area of fracture healing in patients with a delayed union of the osteotomized fibula." Bone **43**(2): 348-354.

Saito M, Fujii K, Tanaka T and Soshi S (2004). "Effect of Low- and High-Intensity Pulsed Ultrasound on Collagen Post-translational Modifications in MC3T3-E1 Osteoblasts." Calcified Tissue International **75**(5): 384-395.

Schatzmann HJ and Vincenzi FF (1969). "Calcium movements across the membrane of human red cells." The Journal of Physiology **201**(2): 369-395.

Selemidis S and Cocks T (2007). "Smooth muscle mediates circumferential conduction of hyperpolarization and relaxation to focal endothelial cell activation in large coronary arteries." Naunyn-Schmiedeberg's Archives of Pharmacology **375**(2): 85-94.

Sena K, Leven RM, Mazhar K, Sumner DR and Virdi AS (2005). "Early gene response to low-intensity pulsed ultrasound in rat osteoblastic cells." Ultrasound in Medicine and Biology **31**(5): 703-708.

Shaw A, Pay NM, Preston RC and Bond AD (1999). "Proposed standard thermal test object for medical ultrasound." Ultrasound in Medicine & Biology **25**(1): 121-132.

Somlyo AP and Somlyo AV (1994). "Signal transduction and regulation in smooth muscle." Nature **372**(6503): 231-236.

Song CW, Shakil A, Osborn JL and Iwata K (2009). "Tumour oxygenation is increased by hyperthermia at mild temperatures." International Journal of Hyperthermia **25**(2): 91-95.

Speden RN (1960). "The effect of initial strip length on the noradrenaline-induced contraction of arterial strips." The Journal of Physiology **154**: 15-25.

Starritt HC, Duck FA and Humphrey VF (1989). "An experimental investigation of streaming in pulsed diagnostic ultrasound beams." Ultrasound in Medicine & Biology **15**(4): 363-373.

Starritt HC, Duck FA and Humphrey VF (1991). "Forces acting in the direction of propagation in pulsed ultrasound fields." Physics in Medicine and Biology **36**(11): 1465-1474.

Starritt HC, Hoad CL, Duck FA, Nassiri DK, Summers IR and Vennart W (2000). "Measurement of acoustic streaming using magnetic resonance." Ultrasound in Medicine & Biology **26**(2): 321-333.

Steffen W, Cumberland D, Gaines P, Luo H, Nita H, Maurer G, Fishbein MC and Siegel RJ (1994). "Chrome congestive heart failure: Catheter-delivered high intensity, low frequency ultrasound induces vasodilation in vivo." Eur Heart J **15**(3): 369-376.

Suchkova VN, Baggs RB and Francis CW (2000). "Effect of 40-kHz Ultrasound on Acute Thrombotic Ischemia in a Rabbit Femoral Artery Thrombosis Model : Enhancement of Thrombolysis and Improvement in Capillary Muscle Perfusion." Circulation **101**(19): 2296-2301.

Suchkova VN, Baggs RB, Sahni SK and Francis CW (2002). "Ultrasound improves tissue perfusion in ischemic tissue through a nitric oxide dependent mechanism." Thrombosis and haemostasis **88**: 865-70.

Sun J-S, Tsuang Y-H, Lin F-H, Liu H-C, Tsai C-Z and Chang WH-S (1999). "Bone defect healing enhanced by ultrasound stimulation: An <I>in vitro</I> tissue culture model." Journal of Biomedical Materials Research **46**(2): 253-261.

Takahashi M, Chiba K and Li P (2007). "Free-Radical Generation from Collapsing Microbubbles in the Absence of a Dynamic Stimulus." J. Phys. Chem. B **111**(6): 1343-1347.

Takeuchi R, Ryo A, Komitsu N, Mikuni-Takagaki Y, Fukui A, Takagi Y, Shiraishi T, Morishita S, Yamazaki Y, Kumagai K, Aoki I and Saito T (2008). "Low-intensity pulsed ultrasound activates the phosphatidylinositol 3 kinase/Akt pathway and stimulates the growth of chondrocytes in three-dimensional cultures: a basic science study." Arthritis Research & Therapy **10**(4): R77.

ter Haar G (2007). "Therapeutic applications of ultrasound." Progress in Biophysics and Molecular Biology **93**(1-3): 111-129.

ter Haar G and Duck FA, Eds. (2000). The safe use of ultrasound in medical diagnosis. London, The British Medical Ultrasound Society/ The British Institute of Radiology.

Tien Y-C, Lin S-D, Chen C-H, Lu C-C, Su S-J and Chih T-T (2008). "Effects of Pulsed Low-Intensity Ultrasound on Human Child Chondrocytes." Ultrasound in Medicine and Biology **34**(7): 1174-1181.

Tortora G and Grabowski S (2000). Principles of Anatomy and Physiology. New York, John Wiley & Sons, Inc.

Unsworth J, Kaneez S, Harris S, Ridgway J, Fenwick S, Chenery D and Harrison A (2007). "Pulsed Low Intensity Ultrasound Enhances Mineralisation in Preosteoblast Cells." Ultrasound in Medicine & Biology **33**(9): 1468-1474.

van der Wouw PA, Brauns AC, Bailey SE, Powers JE and Wilde AAA (2000). "Premature Ventricular Contractions During Triggered Imaging with Ultrasound Contrast." Journal of the American Society of Echocardiography **13**(4): 288-294.

VanBavel E (2007). "Effects of shear stress on endothelial cells: Possible relevance for ultrasound applications." Progress in Biophysics and Molecular Biology **93**(1-3): 374-383.

Wang R, Karpinski E and Pang PKT (1991). "Temperature dependence of L-type calcium channel currents in isolated smooth muscle cells from the rat tail artery." Journal of Thermal Biology **16**(2): 83-87.

Wells PNT (1977). Biomedical Ultrasonics. London, Academic Press.

Winlove CP, Bishop JE, Chambers RC and Laurent GJ (1995). The structure and function of extracellular matrix in the pulmonary vasculature. <u>Pulmonary Vascular Remodelling</u>. J.E. Bishop JTR, G.J. Laurent. London, Portland Press.

Wu J and Nyborg WL (2008). "Ultrasound, cavitation bubbles and their interaction with cells." <u>Advanced Drug Delivery Reviews</u> **60**(10): 1103-1116.

Zatzman M, Stacy RW, Randall J and Eberstein A (1954). "Time course of stress relaxation in isolated arterial segments." <u>American Journal of Physiology</u> **177**: 299-302.

Zecchin HG, Priviero FBM, Souza CT, Zecchin KG, Prada PcO, Carvalheira JBC, Velloso LA, Antunes E and Saad MJA (2007). "Defective Insulin and Acetylcholine Induction of Endothelial Cellâ€"Nitric Oxide Synthase Through Insulin Receptor Substrate/Akt Signaling Pathway in Aorta of Obese Rats." <u>Diabetes</u> **56**(4): 1014-1024.

Zhai B-J, Shao Z-Y, Zhao C-L, Hu K, Shen D-M and Wu F (2008). "Optimization of ultrasound-mediated in vitro reversal of multidrug resistance in human hepatocarcinoma cell line HEPG2." <u>Ultrasound in Medicine & Biology</u> **34**(10): 1697-1702.

Zhang H, Lin X, Wan H, Li J-H and Li J-M (2009). "Effect of low-intensity pulsed ultrasound on the expression of neurotrophin-3 and brain-derived neurotrophic factor in cultured Schwann cells." <u>Microsurgery</u> **29**(6): 479-485.

Zhou S, Schmelz A, Seufferlein T, Li Y, Zhao J and Bachem MG (2004). "Molecular Mechanisms of Low Intensity Pulsed Ultrasound in Human Skin Fibroblasts." <u>J. Biol. Chem.</u> **279**(52): 54463-54469.